Role and properties of the confined amorphous phase of polymers

Malgorzata Walczak

ParisTech
INSTITUT DES SCIENCES ET TECHNOLOGIES
PARIS INSTITUTE OF TECHNOLOGY

ARTS ET MÉTIERS ParisTech

CMMS PAS, Lodz, Poland

PhD Thesis

in co-supervision to obtain the degrees of

Docteur de l'École Nationale Supérieure d'Arts et Métiers

Spécialité: "Mécanique et Matériaux"

École doctorale n° 432 : Sciences des Métiers de l'Ingénieur - 2012-ENSAM-0042

and

Doctor of Chemistry

Specialty: "Chemistry and Physics of Materials"

Centre of Molecular and Macromolecular Studies, PAS, Lodz, Poland

presented and defended publicly by

Małgorzata WALCZAK

November 21th 2012

Role and properties of the confined amorphous phase of polymers

Directors of Thesis : **Andrzej GALESKI and Gilles REGNIER**

Jury

M. Marek POTRZEBOWSKI, prof. dr hab., NMR chemistry, CMMS PAS	President
M. Andrzej BUDKOWSKI, prof. dr hab., Physics, Jagellonian University	Reviewer
M. François RIBOT, dr hab., Chimie de la matière condensée / Univ. Pierre et Marie Curie	Reviewer
Mme. Maria KOZIOLKIEWICZ, prof. dr hab., biochemistry, Technical University of Lodz	Examiner
Mme. Barbara NAWROT, prof. dr hab. biochemistry, CMMS PAS	Examiner
M. Stanisław SLOMKOWSKI, prof. dr hab. polymer chemistry and physics, CMMS PAS	Examiner
M. Jacek ULANSKI, prof. dr hab. molecular physics, Technical University of Lodz	Examiner
M. Wlodzimierz STANCZYK, prof. dr hab. silicon and liquid crystal chemistry, CMMS PAS	Examiner
M. Piotr GUGA, prof. dr hab. biochemistry, CMMS PAS	Examiner

THESIS

Arts et Métiers ParisTech - Centre de Paris
PIMM UMR CNRS 8006 and
Centre of Molecular and Macromolecular Studies PAS, Lodz, Poland

I would like to THANK a lot to both of my supervisors, Prof. Galeski and Prof. Regnier for helping me during preparation of this thesis. I am also grateful to all of my friends from Łódź and Paris. Thanks for all those years together.
Co-tutelle grant from French Ministry of Foreign Affairs is greatfully acknowledged.
Eric Baer and Anne Hiltner from Case Western Reserve University, Cleveland, Ohio, for producing multilayered films designed for the purpose of this thesis and Michael Wuebenhorst from Katholike Universitet Leuven for allowing me to participate in dielectric measurements that are a part of the thesis, are greatfully acknowledged.
I am grateful to Prof. Marek Potrzebowski and his team for help with SS NMR study too.

TABLE OF CONTENTS:

Introduction

Polymer based products are used for large consumption applications (automotive industry, domestic and electric applications, toys, etc.) but also for sophisticated high technology products (electronic devices, biomedical implants, etc.) as they are easy to process and form and also due to their functionality. Wide range of polymer properties results from a great variety of chemical structure and supermolecular structure complexity that can be relatively easy modified by tuning conditions of phase transitions such as crystallization and phase separation. These material properties are mainly determined by the structure, at a nanoscale; during forming, stretching or shearing of a semi-crystalline polymer melt followed by rapid cooling the specific morphologies of thin crystalline lamellae interspersed with thin amorphous layers are generated. Also other higher hierarchical structures arise such as deformed spherulites, shish–kebab or more complex crystalline macrostructure with a high anisotropy of molecular orientation.

For engineering applications, there is an industrial need for the prediction of those induced mechanical properties in order to determine many functional properties, for example the strength of blown bottles or the shrinkage and the warpage of injected parts. Despite extensive research the prediction of those macroscopic mechanical properties of nanostructured polymers is still a bottle neck. Four main problems remain very tough to solve:

a) The precise knowledge and description of the topology of the microstructure,
b) The multiscale modelling,
c) The modelling of the interfaces between constituents or interphases between phases,
d) The determination of the mechanical properties of confined phases.

The objective of my research is to go deeper into the two last previous points. As technological trends tend to master systems of nanometer size, it becomes imperative to gain a complete understanding of how the properties of such small material systems might differ from those of bulk systems. An example of such an area where the properties at the nanometer length scale exhibit significant deviations from bulk properties is the study of thin polymer films with at least one free surface [1]. But these studies are not sufficient to understand the behavior of

nanostructured materials, nanocomposites and semicrystalline materials, which can be also considered as nanocomposites from a mechanical point of view, because interfaces and interphases play a major role. The idea is to determine the properties of a nanostructured model material: a multilayer film in which one material could be confined in a large number of nanolayers. This technique has been developed for years by Baer [2] who gave us the opportunity to manufacture these specific films for the study.

CMMS Polish Academy of Sciences in Lodz (Poland), which has a excellent experience of studying material at a nanoscale and PIMM at Arts et Métiers ParisTech (France), which has already done some encouraging works based on micromechanical modelling technique to predict the elastic and viscoelastic properties of semi-crystalline polymers and nanocomposites, are associated in this study; therefore this PhD thesis is a joined work from the two laboratories.

The first chapter aims to summarize the state of art on confined polymer layers. Fisrtly it deals with the well-known but not well understood amorphous confined phase met in semicrystalline polymers. The complex morphology around crystalline lamellae reduces chain mobility in the amorphous phase and more rigid amorphous phase has been highlighted in some crystalline polymers. Predicting the mechanical properties of semicrystalline polymers by taking into account this morphology is important to understand the role of crystalline lamellae and amorphous phase, but it requires strong assumptions on the mechanical properties of this amorphous phase.
Then, the variation of T_g in amorphous phase will be discussed when its thickness approaches to nanoscale. These variations seem to depend on the chemical nature of the material, but also if a free surface exists or if the amorphous material is fully confined.
Finally, dynamics and chain motions in polymers in amorphous polymers will be described to better understand the major role of interfaces, The main physical means of characterisation of polymer chain mobility will be presented and discussed.

In the second chapter experimental part of the work is presented.
Firstly preparation of the multilayered films by special way of coextrusion process is shown in details. Informations about applications of those films, prepared by coextrusion process from different polymers, in the past and now, in microscale and the same in nanoscale is presented. Further advantages of choosing PS and PC for preparation of our multilayerd films are discussed. Also the relative compositions of our films, with different thicknesses of each layers and with overall thicknesses 25 and 125 μm are demonstrated. After we can find here information about physico-chemical analyses used in these studies. Details concerning each experimental technique are available here too.

Results of the experimental part of the study and discussions concerning the properties of confined amorphous phase will be presented in the third chapter.
The third chapter is divided into four subsections. First of them is focused on the physico-chemical characterization of multilayered films with density measurements, atomic force microscopy and differencial scanning calorimetry. Second relates to the dynamics of the chains in the vicinity of PS/PC interface. This phenomenon was investigated by Solid State Nuclear Magnetic Resonance and Dielectric Relaxation Spectroscopy.
Third subsection tells about viscoelastic properties of multilayered films measured by rheology the same as by modelling. Subsequently variation of PS mechanical properties with layer confinement is discussed.

The work will end with general conclusions derived from the study, the summary of the study and with references helpful in preparing of this thesis.

1. Confined polymer medium: state of knowledge.

1.1. The confined amorphous phase in semi-crystalline polymers.

1.1.1. Morphology of semi-crystalline polymers.

Polymers with regular structure of macromolecules are able to crystallize partially during cooling from molten state. Semi-crystalline polymers have complicated morphology consisting of crystalline lamellae separated by thin amorphous region schematically presented in Figure 1.1.

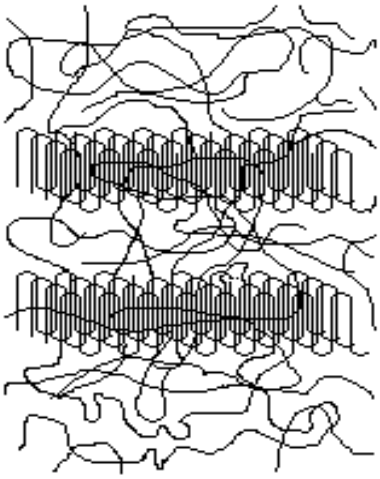

Figure 1.1. Scheme of crystalline lamellae separated by amorphous layers in semi-crystalline polymer.

The crystalline lamellae have thicknesses varying typically from several nanometers to several tens of nanometers. The fusion temperature is directly linked to their thicknesses according to Gibbs-Thomson equation. But, different conformational possibilities in the amorphous region of the semi-crystalline polymers has implications on melting temperature and the processes involved in phase transformation from ordered to disordered. Fully melting behavior cannot be explained just by Gibbs –Thomson equation, as is proved by Pandey et al. [3] after experiments on ultra high molecular weight polyethylene, where the topological constraints are tailored by adopting a different synthesis route. In semi-crystalline polymers we can find dependence of crystal thickness and topological constrains residing in the amorphous phase on the melting behavior of the crystalline phase. Of course with changing the heating rate we are changing the mechanism involved in melting behavior of polymer. For example in disentangled polyethylene below the heating rate 1ºC/min. melting occurs by successive detachment of chains from side surface, while above 1ºC/min. melting can proceed from the side and inside the crystallites. The number of chain segments involved in the melting process also increases with the increasing heating rate. There is a discrete change in slope with the heating rate too. This slope increases with increasing entanglement density in amorphous region and with the increasing number of shared chains among many crystallites. At low heating rates melting by successive detachment of the chain stems is impossible when the same chain is shared among many crystallites and demands co-operative conformational transformation at larger length scales.
The melting time, which is characteristic for a material in nascent disentangled samples, decreases with increasing molecular weight due to lower entanglement density in amorphous region of higher molecular weight samples.

An amorphous component consists of highly entangled chains forming a continuous network. The entanglements and crystallites adjacent to the amorphous layers constitute physical cross-links of that network. The entanglements existing in a

molten polymer are usually not resolved by the crystallization process. What is important, most of them is just shifted into amorphous interlamellar layers [4]. This means redistribution, typically on the length scale of about 10 nm and modification of the local network density, but generally, the isotropic entangled network of the melt is kept after crystallization. That network should manifest itself in high reversibility of the deformation, which in fact, is frequently observed experimentally. The number of entanglements persisting in the amorphous phase after sample crystallization depends on the conditions of crystallization process and, therefore, can be modified in a certain range. The number of entanglements in solidified semi-crystalline polymer usually remains high, while the local density of entanglements inside amorphous layers can be similar to or even higher than the respective density in the melt. This is especially true for fast-crystallized samples of polymers of moderate or high molecular weight, in which the rate of disentanglement driven by crystallization is usually much lower than the overall rate of crystallization. At such conditions nearly all pre-existing entanglements are only rejected by growing crystallites into surrounding amorphous layers rather than being resolved. Modification of the local entanglement density resulting from crystallization process leads to an essential difference between the molecular network within amorphous layers of semi-crystalline polymers and that present in amorphous polymers, in which the entanglement density depends only on the properties of the chains, and depends neither on their length nor thermal history of the sample [5]. On the contrary, the density of the network in a solid semi-crystalline polymer is expected to vary with both molecular weight and conditions of its crystallization.

The goal of investigations presented in the paper of Bartczak and Kozanecki [6] was to study the high-strain deformation behavior of semi-crystalline polymers with special attention given to the role of the amorphous phase and its topological structure. For this purpose materials demonstrating a notable variation in the amount and properties of the amorphous phase were studied, yet a similar structure of the crystalline component and supermolecular structure were needed as the object of studies. Results of the reported study demonstrate that the deformation behavior at low strains, including the yield range, is governed by the properties of the crystalline phase. The key parameter controlling the yield is most likely the length of crystalline stem determining the rate of nucleation of dislocations, which are elementary carriers of plastic deformation by crystallographic slip mechanisms. The amorphous layers,

although more compliant than crystallites, are intimately connected to and strongly constrained by adjacent lamellae and can deform only cooperatively with them to accommodate the strain. Thus, the role of the amorphous component at this stage of deformation is limited to transfer the load to and between crystallites. The situation changes at higher strains, when stresses generated by stretching of the network of entangled chains within the sheared amorphous layers become higher than those accompanying deformations of the crystalline component. Consequently, the stage of strain hardening is a property of the amorphous component. The obtained results confirm that the strain hardening stage is controlled primarily by the properties of the network of entangled chains of the amorphous component. The rubber-elasticity of the molecular network, manifesting itself in the strain hardening behavior, is determined by the density of cross-links, produced by chain entanglements and chains immobilized on the crystal-amorphous interface. These in turn, as demonstrated by model calculations, appear to depend on molecular weight, crystallization kinetics and resultant crystallinity of the sample. The higher molecular weight and/or crystallization rate, the larger density of the entanglements. Also the chain architecture, i.e. the presence of long or short branches or comonomer units, modifies the density of the network, which is finally shaped upon crystallization. All that makes the amorphous component of semi-crystalline polymers significantly different than amorphous polymers, where the density of chain entanglements depends neither on molecular weight nor thermal history of the sample.

Typically, the lengths of the polymer chains are many times greater than the lamellar thickness. Hence, each molecule must pass through the same or different lamellae many times. The manner in which this requirement is met is obviously of the foremost importance in regard to the molecular morphology of the crystal-amorphous interphase. Transition from the virtually perfect order of the crystal to the isotropy and randomness of the amorphous or liquid state cannot suddenly occur.

It is well known that the reduction of surface chain density in lamellar semi-crystalline polymers due to tilting of the interfacial plane from orthogonality to the chain sequences within the crystal allows the incidence of adjacent folds to decrease highly. The tilt angle of 34.5º was determined for linear PE by Basset and Hodge [7].

In the case of others polyethylenes, authors found the tilt angle in the range 18-45º,

depending on the crystallization conditions [7,8]. Only ~17% of all the chain sequences within the crystal are involved in adjacent folds in the first layer. Approximately 32% of the chain sequences emanating from the crystal return in the second layer, forming loops of two horizontal bonds. The remaining ~51% of chain sequences return in the third layer. Therefore, most of the reentry loops comprise two or three horizontal bonds.

Chain configurations in the noncrystalline region between two lamellar crystallites are little affected by the entry of chain sequences from the more remote surface if the interlamellar separation is greater than 4-5 lattice layers, or length around 20 Ä.
In lamellar single crystals, the sites of chain reentry are separated predominantly by two or three lattice steps. For polymer melts bounded by a hard wall, we have narrow interphase comprising no more than two lattice layers. The chain sequences tend to orient along the surface in the first layer adjoining the wall, whereas in the second layer they exhibit a slight preference for orientation normal to the surface.

1.1.2. The rigid amorphous phase.

Early investigations on semi-crystalline polymers based their description on a two-phase model, where the two phases, one amorphous and one crystalline, have nanometer dimensions in one or more directions. Actually it is known that the decoupling between crystalline and amorphous phases is in general incomplete, due to the length of the polymer molecules that are much longer than the dimensions of the nanophases, and due to possible geometrical constraints. Therefore a more detailed analysis must consider also an intermediate nanophase that is located at the interface between the crystalline and amorphous phases [9]. So to describe the semi-crystalline polymers we should notice that there is the coexistence of the mobile

(traditional) amorphous phase, the crystal – amorphous transition layer (rigid amorphous phase) and the crystalline fraction.

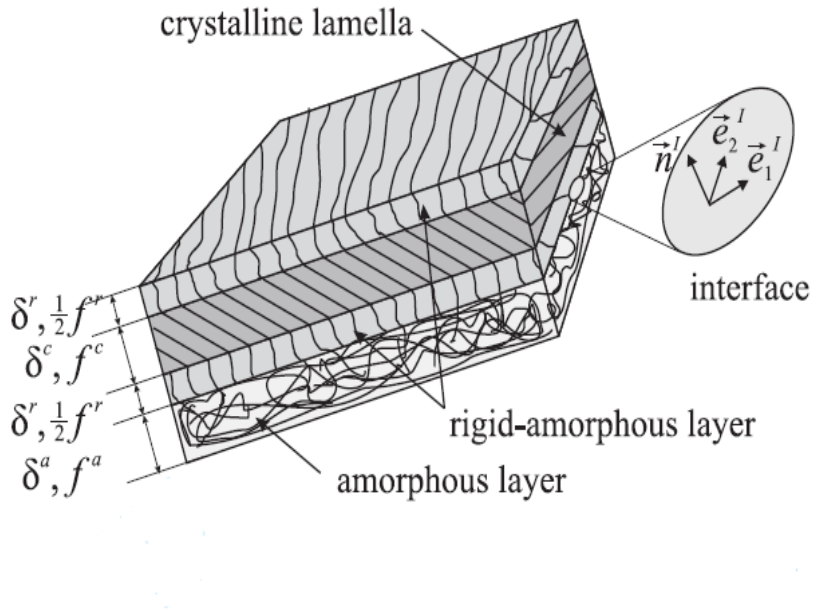

Figure 1.2. Schematic drawing of a three phase composite inclusion.

The intermediate phase is non-crystalline and originates from the continuation of the partially crystallized macromolecules across the phase boundaries. Since it includes amorphous portions of macromolecules whose mobility is hindered by the near crystalline structures, this in-between phase is generally named ‘‘rigid amorphous fraction” (RAF), its mobility being lower than that of the unconstrained amorphous phase, which is usually addressed as ‘‘mobile amorphous fraction” (MAF).

The reason of the formation of the RAF is the difference of the density between crystalline and amorphous phases. This density paradox was studied by Hoffman and Frank. They found that in melt-crystallized polymers some folding is required. Alternatively, the crystals must have the chains at a slope angle to the crystal surface. If neither condition is met, a serious density anomaly at the crystalline-amorphous interface is predicted: the density is too high. These workers pointed out that the difficulty can be soften by interspersing some tight folds between (or among) longer loops in the amorphous phase.

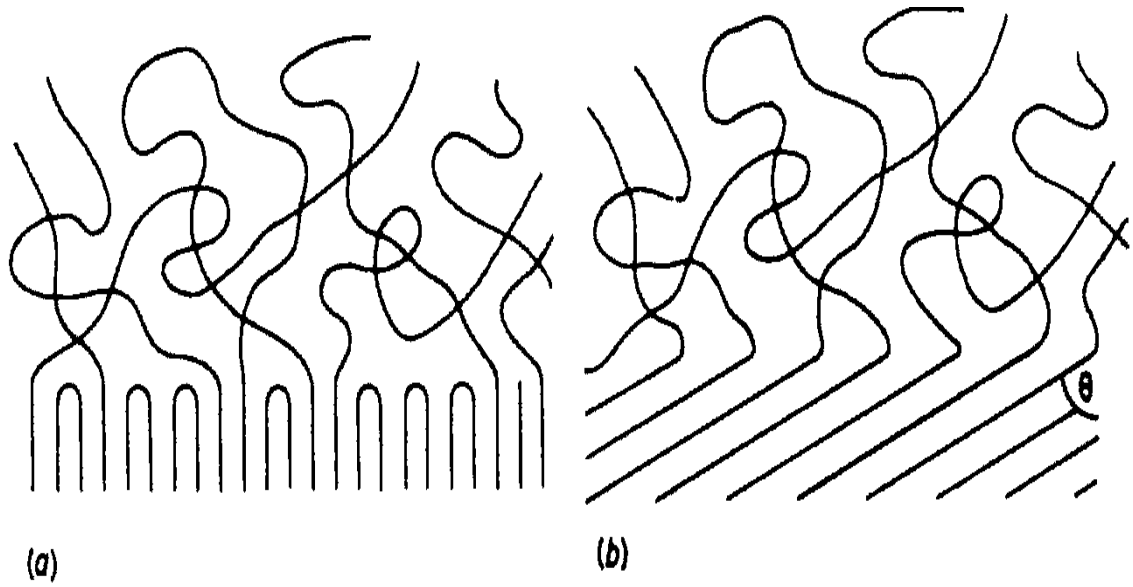

Figure 1.3. Alternative resolutions of the density paradox:
(a) increased chain folding beyond critical value,
(b) oblique angle crystalline stems to reduce amorphous chain density at interface[10].

Frank [11] derived a general equation that combines the probability of back folding, p, and the slope angle, θ, with the crystalline stem length, l, and the contour length of the chain, L, to yield the minimum conditions to prevent an anomalous density in the amorphous region:

$$\left(1 - p - \frac{2l}{L}\right)\cos\theta \leqq \frac{3}{10} \qquad (1.1.)$$

Hoffman [12] showed that the density of the amorphous phase is better accounted for by having at least about 2/3 adjacent reentries, which he calls the variable cluster model. An illustration of how a chain can crystallize with a few folds in one lamella, then move on through an amorphous region to another lamella, where it folds a few more times and so on, is illustrated in Figure 1.4 :

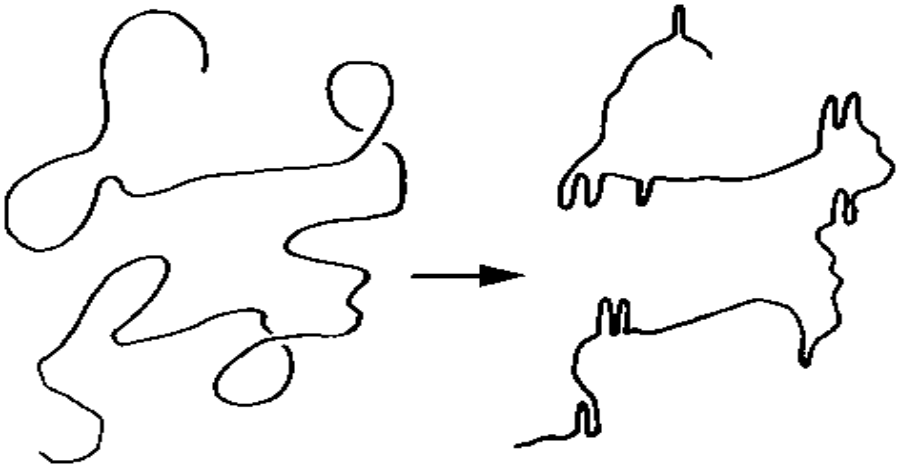

Figure 1.4. The variable cluster model, showing how a chain can crystallize from the melt with some folding and some amorphous portions and retain, substantially, its original dimensions and its melt radius of gyration [13].

If both the tilt angle of chains at the interfaces and density of adjacent chain reentry are sufficient to prevent for packing anomaly then no RAF is formed. An example of such polymer is linear polyethylene with large chain tilt [9]. Otherwise the coupling between crystalline and amorphous phases as a rule produces a broadening of the glass transition to higher temperatures. In some polymers the presence of the RAF may cause a separate glass transition, but the temperature at which the rigid amorphous fraction loses its solid character is a question still widely debated: the process can be located between the T_g of the unconstrained amorphous phase (bulk T_g) and the melting point [9,14] and/or occur simultaneously with fusion [15].

Since the RAF immobilizes the amorphous fraction, its presence must change the properties of the polymers. With changing the structure and content of the RAF we will change the mechanical properties of semi-crystalline polymer. We are able to use the knowledge about RAF to modify polymer properties and to control the failure mechanism in semi-crystalline polymers. In semi-crystalline polymers the behavior of the nanoscale phase is important for mechanical, thermal, optical and other macroscopic properties.

The first experimental evidence of the existence of the rigid amorphous fraction (RAF) was reported by Menczel and Wunderlich for several semi-crystalline polymers

[16, 17, 18]. It was observed that the hysteresis peak at the glass transition was absent when these polymers were heated much faster than they had previously been cooled. In the glass transition behavior of poly(ethylene terephthalate) (PET), the hysteresis peak gradually disappeared as the crystallinity increased. At the same time, it was noted that the ΔC_p of higher crystallinity PET samples was much smaller than could be expected on the basis of the crystallinity calculated from the heat of fusion. It was also observed that this behavior was not unique to PET only, but is characteristic of most semi-crystalline polymers: the sum of the crystallinity calculated from the heat of fusion and the amorphous content calculated from the ΔC_p at the glass transition is much less than 100% (a typical difference is about 20–30%). This 20–30% difference was attributed to the existence of the ‘‘RAF’’ which has lower heat capacity due to limited chain mobility. The presence of the RAF also affected the unfreezing behavior of the ‘‘mobile’’ (or traditional) amorphous fraction. As a consequence, the phenomenon of the enthalpy relaxation diminished with increasing rigid amorphous content. It was suggested that the disappearance of the enthalpy relaxation was caused by the disappearance or drastic decrease of the time dependence of the glass transition.

Enthalpy relaxation near the glass transition is nonexponential and nonlinear. Nonexponential relaxation is very common in almost all types of condensed matter, but nonlinearity is unusual because for enthalpy relaxation it becomes significant at small departures from equilibrium (typically about 2 K in the temperature domain). Only nonlinear viscoelasticity in polymers is comparably important for such small and practically significant perturbations.

In the work of Menczel [19] after the cooling calibration was accomplished, the cooling glass transition experiments indicated that the glass transition in semi-crystalline polymers is not completely time independent, because its width depends on the ramp rate. However, it was shown that the time dependence is drastically reduced, and the midpoint of the glass transition seems to be constant which can explain the absence of the enthalpy relaxation.

The RAF can be determined if the fraction of the traditional amorphous phase is determined from the heat capacity jump at the glass transition, and the crystallinity is calculated from the heat of fusion.

It is known that the following techniques could be used to characterize the RAF in semi-crystalline polymers:

- DSC, MTDSC, DEA
- TEM
- WAXD
- SS NMR
- Density measurements.

Also using quasi-isothermal (QI) heat capacity measurements Cebe et al. [20] investigated the formation behavior of the crystalline, mobile amorphous and rigid amorphous fractions in poly(trimethylene terephthalate), PTT. For PTT most of the RAF vitrifies between 451K and T_g step by step during QI cooling after the crystal have formed. The constraints imposed by the crystal surface reduce the mobility of the entangled polymer chains attached to the lamellae. They suggested that this vitrification of the RAF have place outward away from the lamellar surface in a step by step way during QI cooling. Because of the effect of densification brought by physical aging during the long time of quasi-isothermal treatment, after reheating, devitrification of RAF takes place at a temperature above its previous vitrification temperature. In the work of Cebe et al. [20] a large amount of rigid amorphous fraction was formed at temperatures above T_g . Mobility of the chains located farther from the crystal surfaces is restricted little by little during QI cooling. Due to the successive vitrification the layers which constitute RAF are formed one after another. After crystallization, when the temperature decreases, the rate of RAF formation increases. It means that at lower temperatures the density increases, thermal motion of the molecules decreases and the vitrification is faster. When the material passes through the glass transition temperature and the rest of the mobile amorphous phase vitrifies into the glassy state, the process stops. When the material is reheated, the process of devitrification occurs firstly for the MAF and after for the RAF. There are suggestions that by physical aging MAF and RAF can undergo densification and this is the reason why the devitrification temperature is higher than the previous

vitrification temperature and why we observe larger amount of solid fraction during heating than during cooling.

RAF does not have the properties of the bulk material while MAF posses those properties. It means that MAF is able to undergo its liquid to solid transition at T_g even if there are no crystals. But if we want to form RAF we need some kinds of barriers, like constraints of the crystal or particles of some additives inside the material.

Also the group of Hong [21] described the structural formation of PTT at various crystallization conditions. They used the differencial scanning calorimetry and small angle X-ray scattering analysis to discover the dependence of the crystallization temperature (T_c) and crystallization time (t_c) on the variation in thickness and fraction of each phase (RAF, MAF and crystalline phase). It was found that interphase thickness and rigid amorphous fraction linearly increase with T_c . The crystallization time effect on the RAF formation is leading to increase of the interphase thickness and rigid amorphous fraction too, but after the t_c = 3h it becomes unobvious. The long period and crystal thickness does not change a lot with changing of the T_c in that paper. Broadening and shift of the T_g is the obvious result of the RAF formation.

In the work of Righetti and all [22] a new and simple method to monitor the development of crystalline, MAF and RAF during cooling from the melt is applied to isotactic polystyrene. It was found that the RAF of this polymer starts to vitrify at the end of the non-isothermal crystallization and the vitrification is finished during subsequent cooling to room temperature. The kinetics of vitrification of the RAF in isotactic polystyrene is not exactly simultaneous with the non-isothermal crystallization. So the conclusion is that for iPS crystallized during non-isothermal crystallization the limitation of crystal growth because of the complete vitrification of the amorphous phase next to the crystal is impossible.

1.1.3. Mechanical properties of isotropic semi-crystalline polymers.

The behaviour of confined amorphous phase in semi-crystalline polymers is very important for both basic science and technology. Several theories were proposed to explain what kind of properties the confined amorphous phase has.
Considering the elastic properties of blown materials we can observe that there is very important influence of crystallinity content and molecular orientation [23].
Also during injection of semi-crystalline polymers the thickness of the sample plays very important role. Properties of injected materials depends on the thickness of the sample, what is related to big difference in modulus and microstructure.
It is shown that there is very important influence of orientation and crystallinity surface on those properties too [24].
There is another question: should we consider semi-crystalline materials as composite materials? Using such approach we can find the order of magnitude of elastic properties taking into account the properties of each phase [25].One can also consider the problem as an isotropic case [26]. The difficulty is which scale one has to use. It is known that bounded amorphous phase, which is oriented and adjacent to the crystal, has properties with a very high gradient. In some aspects the properties of the amorphous phase (such as folds, chain ends, dangling chains, macromolecules connecting at least two different lamellae and numerous chains knots connected with crystals in a permanent way) present in the interlamellar regions inside the spherulites and localized on the interspherulitic boundaries, are similar to the properties of low molecular liquids at the temperature above its glass transition temperature. A significant difference, among others, is the presence of physical constraints in the amorphous phase structure, reversible chain entanglements and fragments of macromolecules spanning interfacial boundaries of crystallites, which markedly decrease the mobility of macromolecules.

There are some indications in literature that suggest that the amorphous layers may be stiffer than purely bulk amorphous material due to the confinement of amorphous layers between thick crystalline lamellae [27]. Boyd [28] showed that for the

amorphous phase, the relaxed modulus associated with the glass-rubber relaxation (β process) is very high due to the constraints by the neighboring lamellae, leading to the immobilization of amorphous segmental reorientation.

Several schemes of modelling were proposed to show the contents and construction of semi-crystalline materials:

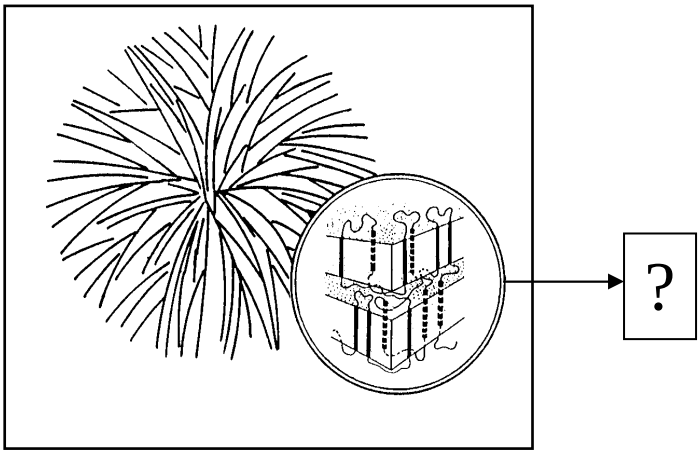

Figure 1.5. Scheme of semi-crystalline medium.

Homogenization schemes:

- self-consistent method [29],
- hybrids methods: U-inclusion and S-inclusion [30].

Regnier et al. chose two micromechanical models to represent semi-crystalline polymers [31]. One is the differential scheme in which ellipsoidal crystallites are randomly dispersed in amorphous phase as it is seen in Figure 1.6 and the second is a self-consistent scheme where the material is considered as an aggregate of

randomly oriented two layered-phase composite inclusions, crystalline and amorphous.

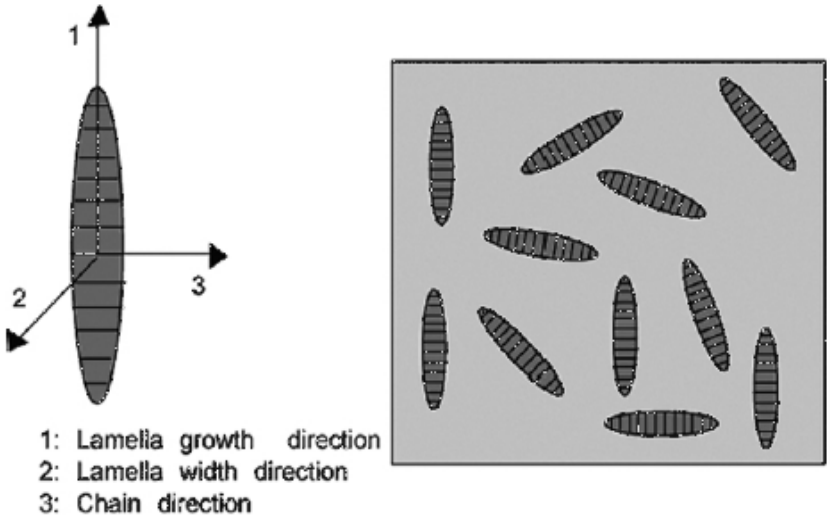

Figure 1.6. Schematic drawing of crystalline lamellae dispersed in crystalline matrix.

Nicolov and Doghri [32] proposed the structure of semi-crystalline high density polyethylene (HDPE) as a closely packed crystalline lamellae separated by layers of amorphous polymer. In their work a semi-crystalline polymer is modelled as an aggregate of randomly oriented composite inclusions, each consisting of a stack of parallel lamellae with their adjacent amorphous layers. They modelled the viscoelastic constitutive behaviour for the amorphous phase assuming a polydomain liquid- crystal-like structure. The intermediate phase linking the crystalline lamellae and the amorphous phase is assumed to form a surface layer around each lamellae:

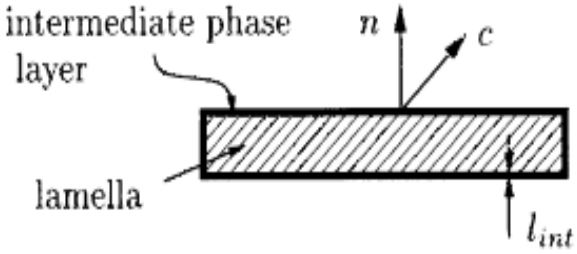

Figure 1.7. Intermediate phase layer in PE.

The free energy of the intermediate layer for a given lamellae is a function of the density difference between two phases, the intermediate layer volume and the thickness of the layer. The intermediate phase volume fraction changes with crystallinity as it was stated by Mandelkern [33]. The role of the intermediate phase in this case is to maintain homogeneous slip in the lamellae and prevent them from localization of deformation. Introduction of those intermediate phase explains us the double yield phenomena in HDPE. At the first yield point the role of that phase is to prevent the lamellae from localization of deformation and the second yield point corresponds to the failure of the intermediate phase membrane.

A yield point in polymers usually is accepted as the point where a local maximum is shown in the stress-strain curve. For samples which initially deform homogeneously this maximum occurs as a result of the internal plastic strain rate of the material increasing to a point where it becomes equal to the applied strain rate. In some cases a maximum in force also relates to the onset of necking, where strain hardening of the necked materials is not sufficient to counteract the reduction of the cross-sectional areas, leading to a reduction in load.

In general, considering semi-crystalline polymers, the yielding phenomena is associated with a change in the morphology of the material where spherulitic structures transforms into fibrillar structures. Those changes occur by shearing and fragmentation of the crystalline lamellae into blocks that rearrange into parallel microfibrils. Seguela et al. [34] have pointed out that the two yield points are due to the slip of the crystal blocks past each other in the mosaic crystalline structure

(heterogenous slip) and the homogeneous shear of the crystal blocks (homogeneous slip).

In the past it has been thought that the double yield phenomenon is a characteristic of semi-crystalline polymers but recently the existence of double yielding in nanostructured amorphous polymer was reported [35]. Subsequently, Li et al. [36] had also reported the morphology-dependent double yielding behavior in injection molded polycarbonate/polyethylene blend, which is a typical incompatible blending system.

In the work of Manzur and Rivas [37] the double yielding phenomenon was observed in specimens of LLDPE. The stress–strain curves confirmed that this phenomenon was in correlation with the stretching rate and showed that it occurred much more easily and distinctly at lower stretching rates. The authors of that paper determined crystallinity degree of deformed samples from WAXS experiments in a wrong way. They were not aware of the fact that only crystals fulfilling Braggs law contribute to WAXS patterns, while other crystals are not contributing. For isotropic samples with uniform spatial distribution of crystals WAXS pattern is representative for the whole population of crystals, however, when crystalline material becomes oriented then the fraction of crystals fulfilling the Braggs law in WAXS pattern is not representative for the whole sample. Sample should be rotated and positioned at various Euler angles in order to obtain information about other fractions of crystals. Incorrect data interpretation led authors of [38] to many false conclusions about crystal sizes, crystallinity, orientation and their changes during drawing such as crystal melting and recrystallization. We can't base further reasoning on such an experimental work.

Findings of Brooks et al. [38] showed that the first yield point is associated with low stress and strain values and that it is not associated with necking. Authors think that it is partially or even totally recoverable. The second yield point occurs at higher stress and strain values and it is associated with necking of the material and is irrecoverable.

By thermal treatment, the effect of the crystallinity level on the double yielding behavior was studied in some detail by Shan et al. [39]. The results showed that the second yield stress becomes larger than the first after the thermal treatment, which is contrary to the case without thermal treatment. With the annealing time decreasing and the annealing temperature increasing, the percentage crystallinity becomes higher, and the second yield point is much more apparent with a decrease of crystallinity of the specimens. These results with PA6 indirectly showed us also that

the second yield point is not only associated with the deformation of the crystalline region.

Drozdov and Gupta described the semi-crystalline polymer as an assemblies of meso-regions, each one being an equivalent network of chains connected by temporary junctions [40].

In the paper of van Dommelen et al. [41] a multiscale numerical model is used to investigate the mechanism of intraspherulitic deformation of semi-crystalline polyethylene. This model goes through microscopic, mesoscopic and macroscopic levels. Properties of the crystalline and amorphous regions are identified. In this work twisted lamellar structure of spherulitic material was represented by an aggregate of preferentially oriented two-phase composite inclusions within each material point of macroscopic finite element models of a spherulitic structure. Deformations were found to initiate in the centre, spreading out in the approximate equatorial region for uniaxial loading conditions and in inclined directions for plane strain loading. While inhomogeneous deformations developed mainly as a consequence of the anisotropic structure of each spherulite and due to interactions between irregularly distributed spherulites.

The amorphous phase in semi-crystalline polymers consist mainly of an assembly of disordered macromolecules, which are morphologically constrained by the neighboring crystalline lamellae. Plastic deformation in these domains occurs by the thermally activated rotation of segments.

The mechanical behavior at the mesoscopic level is often modeled by an aggregate of layered two-phase composite inclusions as was first proposed by Lee et al. [42,43] for rigid/viscoplastic material behavior. Each separate composite consists of a crystalline lamella which is mechanically coupled to its corresponding amorphous layer as is seen on the Figure 1.8:

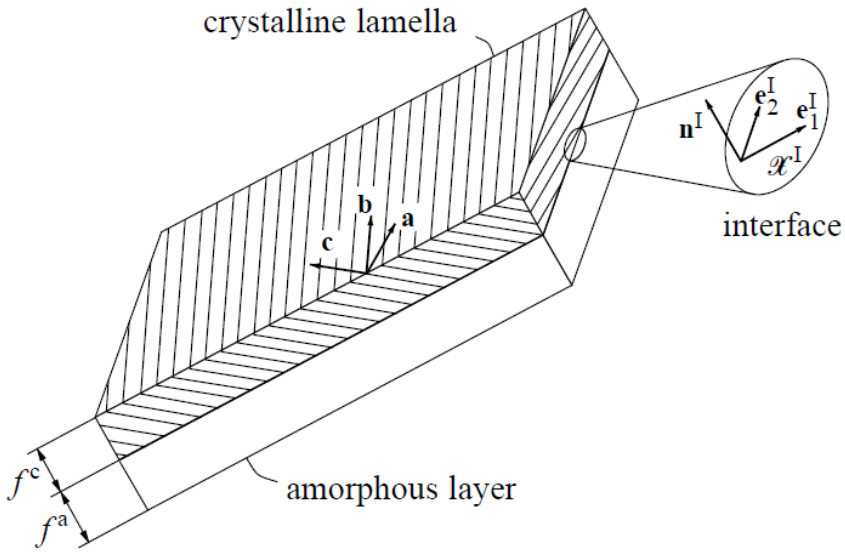

Figure 1.8 . Schematic illustration of a layered two-phase composite inclusion.

From the experimental point of view the micro-mechanical characterisation of the semi-crystalline polymers presents lots of restraints due to the fine scale of the morphological constituents.

The amorphous layers' microstructure is not fully understood at present, mainly because of the experimental difficulties stemming from the fact that it cannot be isolated and studied separately from the bulk material.

In general in semi-crystalline polymers the amorphous phase can be defined as an assembly of disordered macromolecules. The presence of the crystalline lamellae affects strongly the behaviour of these amorphous ones, what can restrain the deformation. The amorphous phase can be divided into the inter-lamellar where the chains are typically constrained by the crystalline lamellae and the rubber like usually located around the spherulitic structures and less conditioned by the crystalline lamellae. That is why the amorphous phase presents a heterogeneous strain evolution during deformation. To understand better the mechanism of the deformation inside the amorphous phase and the influence of the crystalline phase on the amorphous phase deformation Pinto et al. [44] used a simple stack model for

different loading paths and types as a preliminary stage before the complete analysis for the LLDPE under tensile tests. Results obtained by them showed that during the relaxation stage, the variance values drop more intensively down to a stabilization regime in the shear case than in the transversal tensile test. The field fluctuations are more important for the transversal tensile loading than for the shear loading too.

1.2. Variation of T_g at the interface of an amorphous domain.

Many important polymers do not crystallize. They form glasses at low temperatures. At higher temperatures they form viscous liquids. The transition that separates the glassy state from the viscous state is known as the glass–rubber transition. According to theories this transition attains the properties of a second-order transition at very slow rates of heating or cooling. Often the glass transition temperature is defined as the temperature where the thermal expansion coefficient undergoes a discontinuity. Qualitatively, the glass transition region can be interpreted as the onset of long-range, coordinated molecular motion, the beginning of reptation. Rather than discontinuities, in enthalpy, andvolume, their temperature derivatives, heat capacity, and coefficients of expansion exhibit jumps. By difference, melting and boiling are first-order transitions, exhibiting discontinuities in enthalpy and volume, with heats of transition.

The glass transition temperature of amorphous polymers, T_g, is their most important property. In fact, upon synthesis of a new polymer, the glass transition temperature is among the first properties measured.

While only 1 to 4 chain atoms are involved in motions below the glass transition temperature, some 10 to 50 chain atoms attain sufficient thermal energy to move in a

coordinated manner in the glass transition region. The number of chain atoms, 10–50, involved in the coordinated motions was deduced by observing the dependence of T_g on the molecular weight between cross-links, M_c. When T_g became relatively independent of M_c in a plot of T_g versus M_c, the number of chain atoms was counted.
In fact the term “glass transition” refers to the temperature at which ordinary glass softens and flows. A criterion sometimes used for T_g for both inorganic and organic polymers is the temperature at which the melt viscosity reaches a value of 10^{12} Pa·s on cooling.
The glass transition and other transitions in polymers can be observed experimentally by measuring any one of several basic thermodynamic, physical, mechanical, or electrical properties as a function of temperature. Details about the transitions is available for example through dynamic mechanical measurements, sometimes called dynamic mechanical spectroscopy (DMS). Measurements by DMS refer to any one of several methods where the sample undergoes repeated small-amplitude strains in a cyclic manner.

In Figure 1.9 we can see the dependence of T_g on several factors. There is no discontinuity in the V–T or H–T plots, only a change in slope. This is characteristic of a second-order transition. First-order transitions include melting, boiling, and changes in crystalline structure with temperature, these are characterized by discontinuities in V–T and H–T plots.

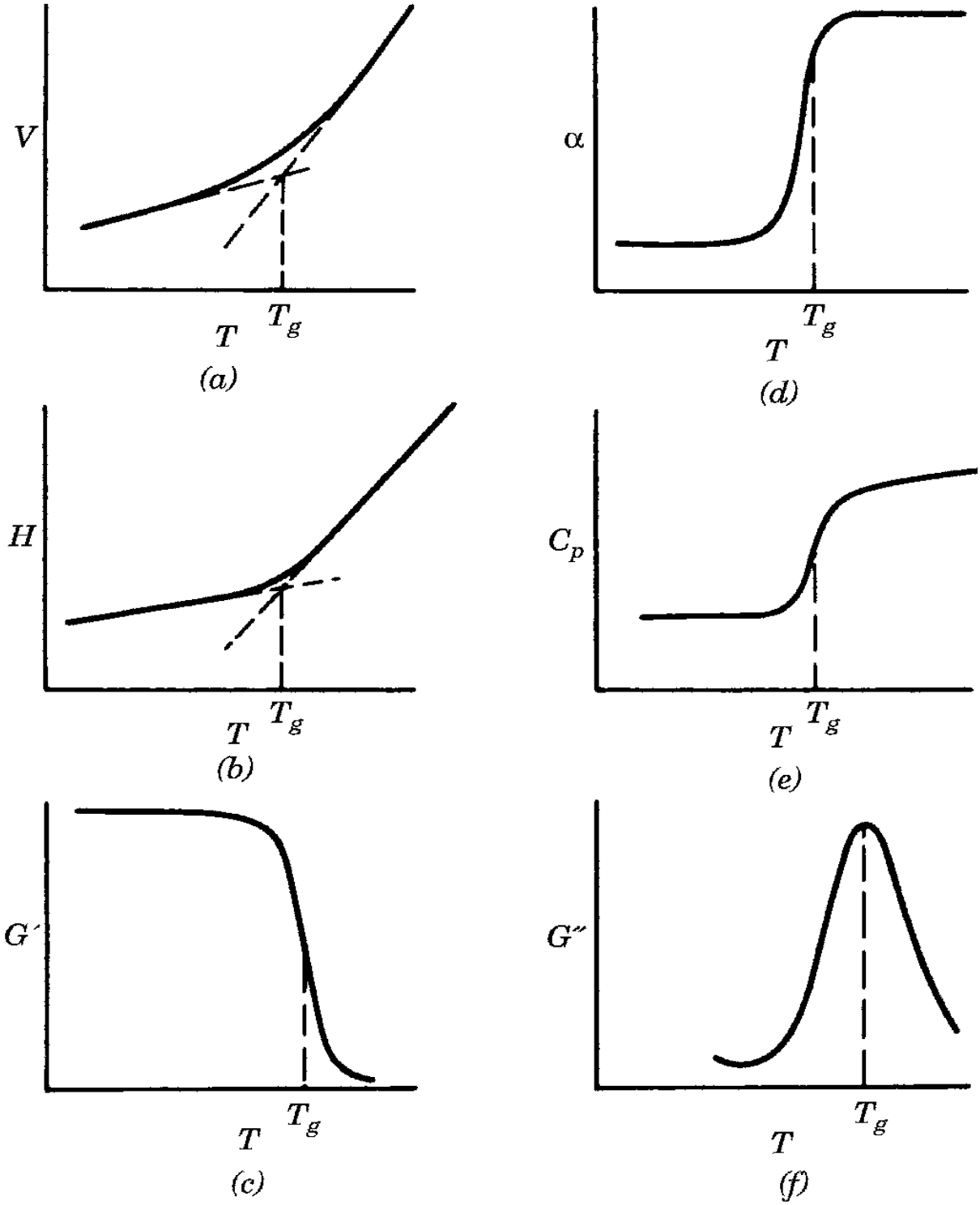

Figure 1.9. Idealized variations in volume - V, enthalpy -H, storage shear modulus - G', α - the volume coefficient of expansion, C_p - the heat capacity, and the loss shear modulus - G'', as a function of temperature [45].

The glass transition temperature can increase, decrease or remain constant depending on the way we are carrying out the measurements. The change in glass transition temperature can be controlled by tuning strength of interfacial interactions and the dynamics of the confining medium as hard or soft.

1.2.1. Variation of T_g in the case of the existence of a free surface.

Ellipsometry is the first technique that was used to investigate the dependence of the glass transition temperature on the thickness of polymer films. In this technique, the quantity measured is the ellipticity induced upon the reflection of polarized light from a bare or film-covered surface. The glass transition of the film is determined by measuring the temperature dependence of the refractive index or thickness of the film.

The early work reported on thin polymer films was performed primarily using a pseudo-thermodynamic mode. More recently dynamic measurements and measurements of the rheological responses have been performed.

The glass transition temperature is determined from a change in the slope of a property of the film, such as thickness and Brillouin frequency, with temperature.

The Positron Annihilation Lifetime Spectroscopy (PALS technique) was also used [[46]] to study the near surface region of thin PS films. In that work, a surface glass transition was found to be the same as the bulk glass transition of PS. Meanwhile in other papers we can find significant surface effect, for example in the work of Jean et al. [[47]] where the surface T_g values were measured as a function of the surface depth probed and found to decrease from the bulk value for a probe depth larger than 40 nm to a value 57 K less than the bulk T_g.

It is difficult to explain this disagreement.

From work of Efremov et al. [[48]] where authors used three thin polymer films of PS, PMMA and poly(2-vinyl pyridine) PVP of different molecular weights and where the

heat capacities C_P (T) of the films were measured upon reheating at a heating rate of 30–40 K.ms^{-1} we can see that the absence of confinement or size effects on T_g for the films could be related to the high heating and cooling rates used in the experiments. However, the results for all polymers studied showed both broadening and loss of transition contrast effects with decreasing film thicknesses. In addition, no significant effect of molecular weight on T_g was observed.

Free standing polystyrene films are said to be a model to show reduced glass transition [[49]]. Very large decrease in T_g has been observed for free standing thin polystyrene films in the following papers [[50], [51], [52]].

Molecular chemistry and the molecular architecture have a strong influence on the T_g depression in thin polymer films. For example when we look on results of the measurements of T_g of thin free standing films of PMMA the T_g is only depressed by 10 K for thicknesses about 40 nm. This is different from what is observed for free standing PS films where a reduction of 40 K in T_g was reported for similar thickness films.

There is also large molecular weight effect on the T_g in free standing PS films. We observe a decrease of the T_g with decreasing molecular weight and film thickness. In the case of PS with lower molecular weights, it was suggested [[76]] that the finite size effects are dominant in determining the change in T_g. Taking into account high molecular weights PS molecular weight play dominant role.

Dutcher and co-workers [[50]] were the first who measured the glass transition in free standing thin polymer films using the BLS technique (Brillouin Light Scattering). In this technique, we measure the frequency shift of light, which is inelastically scattered from thermally excited acoustic phonons.

Thin PS films were also studied by several other scientists [[53], [54], [55]]. Chain confinement effect was claimed to play a dominant role, resulting in a linear dependence of $T_g(h)$ for high molecular weights polystyrene (M_w > 300kg/mol) and for lower molecular weight polystyrene films the concept of finite size effect was put forward.

Reichert [[56]] presented novel experiments in which the confinement of an interface zone between solids and liquids was investigated. He was using water or metals and

he found that the interfacial confinement can lead even to 30% densification of the liquid phase.

It is evident that there must be surface or other effects on so called size effect. In the following references [[57], [58], [59]] surface effect is discussed. The glass transition temperature depression is related to the ratios of surface to volume.

Serghei [[60]] showed thanks to dielectric measurements that for isotactic PMMA we are not observing a change of T_g with changing the thickness of the film. But when we use hyper-branched PMMA we can see decreasing of T_g with decreasing of film thickness. Also the dynamic spectrum changes its shape with decreasing film thickness.

1.2.2 . T_g in confined medium.

It is known that confinement effect is related to isochoric glass formation. The surface of a rigid matrix is constraining a high T_g layer of fluid that surrounds a low T_g core of lower density. There should not be a size effect as the hydrostatic constraints are independent of the size except for cavitation, failure of the liquid, glass or interface become important.

There may be other effects than confinement, size effect or surface effect. Also the specific molecules studied in confinement may be important. Taking into account blends or copolymers we can find thermodynamic effects related to polymer mixing.

It is known that the glass transition temperature of thin supported polymer films $T_g(h)$ differs a lot from that of the bulk polymer $T_g(bulk)$. Beaucage et al. [[61]] and Keddie et al. [[60]] were the firsts, who showed by ellipsometry that polystyrene films of thicknesses less than 40 nm exhibited $T_g(h) < T_g(bulk)$. The modification of the glass transition temperature, influenced by the surface treatment which leads to silanised silicon surfaces, have been reported by several workers [[50], [62], [63], [64], [65]].

The thickness of the polymer thin film dependence of the glass transition temperature $T_g(h)$, using ellipsometry at variable temperature, for poly(methyl-methacrylate) (PMMA) of various tacticity in confined geometry was measured in the work of Grohens et al. [66]. They pointed several factors that significantly affects $T_g(h)$:

- polymer microstructure (stereoregularity of PMMA) related to local dynamics;
- interfacial interactions;
- conformation of the polymer chains.

In the work of Mataz Alcoutlabi and Gregory B McKenna [49] the effects of size and confinement at the nanometer size scale on both the melting temperature, T_m , and the glass transition temperature, T_g, are reviewed. They present in details the dynamic, thermodynamic and pseudo-thermodynamic measurements reported for the glass transition in confined geometries for both small molecules confined in nanopores and for ultrathin polymer films. The glass transition temperature decreases, increases, remains the same or even disappears depending upon details of the experimental (or molecular simulation) conditions. Although there is an accepted thermodynamic model (the Gibbs–Thomson equation) for explaining the shift in the first-order transition, T_g , for confined materials, the depression of the glass transition temperature is still not fully understood and clearly requires further investigation.

Smaller decrease and even increases in T_g have been reported for supported polymer thin films [63,67,68]. It appears that interactions between the substrate and the constrained thin films contribute to the contradictory results found in thin free standing polymer films. Also the treatment of the substrate can have an important role in the T_g behavior in supported thin polymer films.

Ellipsometric measurements performed by de Pablo and coworkers on supported thin poly(4-hydroxystyrene) films [69] show an increase or decrease in T_g relative to the bulk that depends on the type of the substrate and the surface energy of the substrate. In these studies, the effect occurs only for film thicknesses of less than 50 nm.

Recent measurements of the glass transition in block copolymers on substrates using spectroscopic ellipsometry show different results depending on the interaction with the substrate [70]. The copolymers used by Pham and Green [71] were PS and

tetramethylbisphenol-A polycarbonate (TMPC) on SiO_x/Si substrates. Authors examined the influence of film thickness and composition on the effective T_g of compatible thin film mixtures. Measurements revealed that while the T_g of TMPC films increased with decreasing film thickness, h, the effective T_g of thin film mixtures of PS and TMPC decreased with decreasing film thickness. In these mixtures, T_g was independent of film thickness at large h. They also found that while the T_g of bulk mixtures of TMPC/PS exhibited large negative deviations from additivity with composition, such deviations were negligible in the thin film mixtures. In this work the thickness dependence of T_g is compared with the theory. The authors used a model based on a free volume theory [71] to explain the decrease in T_g observed in the supported PS/TMPC films.

The x-ray reflectivity technique gives better determination of the film thickness than that determined by ellipsometry because it is not convoluted with the film density through the index of refraction. Orts et al. [72] were among the first to use x-ray reflectivity to measure the thermal expansion in thin polymer films. The samples were polystyrenes supported on silicon. The sample was first annealed for 1 h at 90ºC and then the x-ray reflectivity scan started at 30ºC. In that work, contractions of the thin films below the glass transition (negative coefficient of thermal expansion) were observed and an indication of a decrease in T_g relative to the bulk one was reported.

For monodisperse polystyrene on hydrogen terminated silicon surfaces Wallace et al. [63] showed a dramatic increase in the glass transition of the films. According to the authors, these results showed that the substrate has a large effect on the change in T_g for supported films where the experiments were carried out under vacuum. Thermal expansion of thin PS films in the glassy state is found to be independent of the film thickness, whereas for the rubbery state, the thermal expansion is found to decrease with decreasing film thickness.

Positron Annihilation Lifetime Spectroscopy (PALS) has been used to study the thermal expansion coefficients and T_g for thin polymer films too [73]. DiMaggio et al. used this technique to measure the glass transition in supported thin PS films. The results showed a decrease in the glass transition with decreasing film thickness, which is consistent with results obtained by using other techniques. The results also showed that the thermal expansion coefficient of the PS films in the glassy state was independent of the film thickness and that in the liquid state was found to decrease

with decreasing film thicknesses what is not consistent with results obtained by ellipsometry.

The BLS technique was also used by Dutcher et al. to study the elastic properties of polystyrene/polyisoprene multilayered thin films [74].The results showed that the Brillouin frequency response of thin polymer layers is similar to that of the bulk materials (high frequency elasticity remains unchanged even when the polymer is confined to ultrathin films).

Mechanical measurements of the thermoviscoelastic response have been performed to investigate confinement effects on the T_g in thin polymer films too, using dewetting dynamics methods [75] and also by atomic force microscopy (AFM) measurements [76].

Reiter [76] suggested that the shift in T_g was due to the decrease in density of the thin films but he did not confirm this result by using other experimental techniques.

The change of T_g in the amorphous phases between crystalline lamellaes in semi-crystalline polymers was reported in several papers [77, 78, 79, 80].

In the work of Liu et al. [81] workers proposed that when the layer thickness becomes comparable to the interphase dimension, the layers lose their identity and a new composition is created that is totally interphase. To test this possibility, they chose an immiscible glassy polymer pair, polycarbonate (PC) and poly(methyl methacrylate) (PMMA) for forced-assembly into nanolayers, and used thermal analysis, gas transport, and positron annihilation lifetime spectroscopy to probe the effect of layer thickness. DSC thermograms of films with layers thicker than 100 nm contain two inflections in heat capacity at 112ºC corresponding to the T_g of PMMA and at 144ºC corresponding to the T_g of PC (Figure 10). However the glass transition temperatures gradually shift closer together as layer thickness decreases below100 nm. When the layer thickness is 10 nm or less the two inflections merge into a single inflection at a temperature that is intermediate between the glass transition temperatures of PC and PMMA. The breadth of the glass transition, measured as DT between the onset and finish of the heat capacity inflection, is about 8ºC for the individual constituents but broadens considerably to about 15ºC when a single inflection is observed.

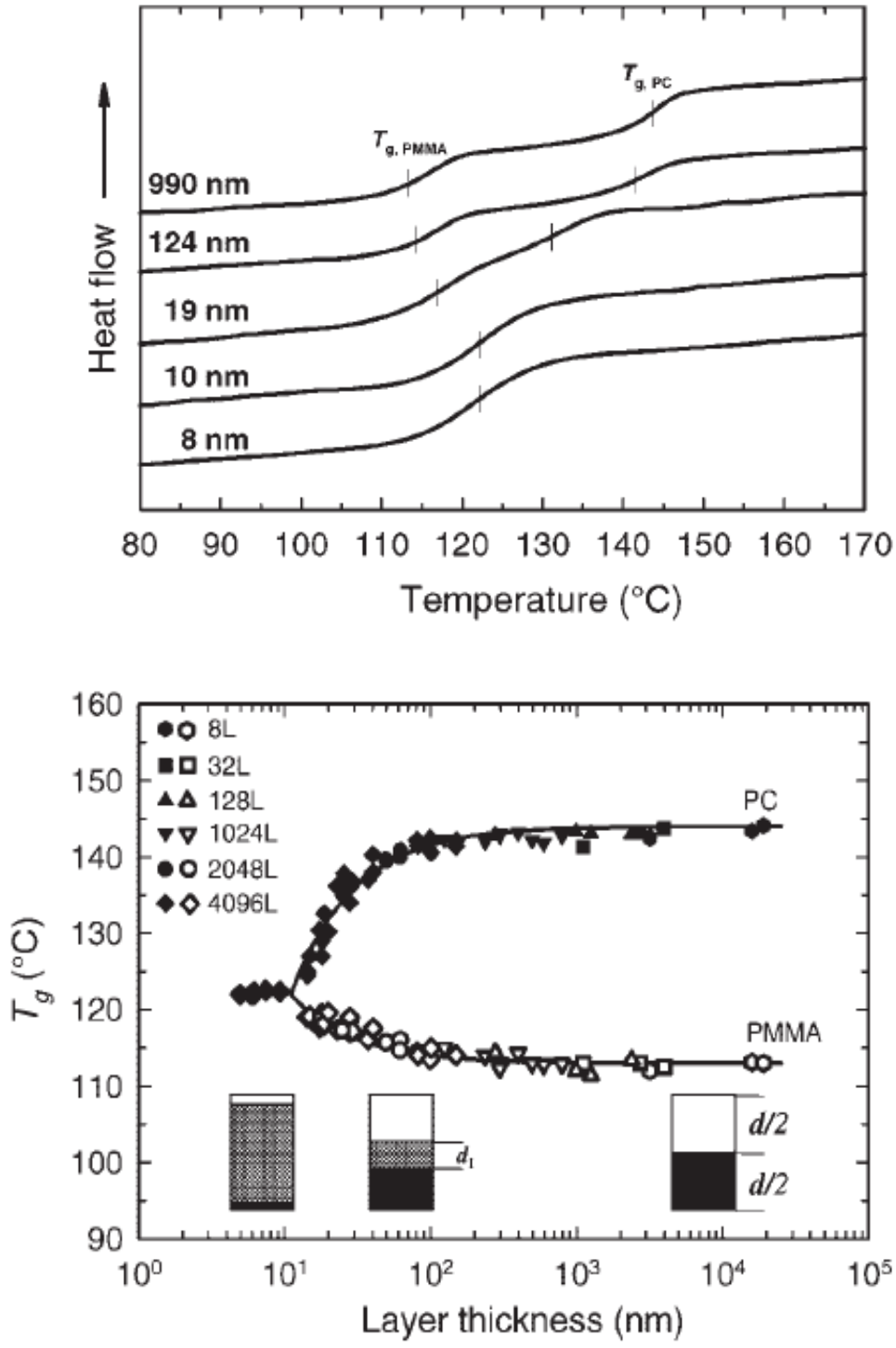

Figure 1.10. Glass transition behavior of PC/PMMA nanolayer films. In the upper plot, heating thermograms show convergence of the heat capacity inflections corresponding to T_gs of the constituent polymers into a single inflection as the layers become thinner. In the lower plot, the dependence of T_g on layer thickness is described by the three-layer interphase model as illustrated schematically in the figure [82].

The convergence to a single glass transition is not symmetrical (Figure 1.10). The T_g of PMMA increases only about 10ºC, whereas the T_g of PC decreases by 22ºC. In nanolayers the glass transition temperatures of PC and PMMA converge asymmetrically to 122ºC.

The conclusion is that when the layer thickness in nanolayer films becomes comparable to the interphase dimension, the layers lose their integrity as constituent layers, and the film becomes essentially totally interphase. The composition profile is not homogeneous, but rather undulating with a period that is twice the layer thickness. For the PC/PMMA pair, nanolayers with average layer thickness of 10 nm or less present properties of the interphase.

Also a change of T_g in glass forming microemulsions was investigated [[82], [83], [84]].

Results reported for molecular simulations for both small molecules confined in nanopores and thin polymer films [[85], [86], [87]] also indicate that the interaction between the wall and confined liquid can play an important role in determining the sign of the shift in T_g of the confined liquid compared with the bulk.

1.3. Dynamics at the interface.

1.3.1. Chain motion.

In the amorphous state the position of one chain segment relative to its neighbors is comparatively disordered. In the relaxed condition, polymer chains making up the amorphous state form random coils. The chains are highly entangled one with another, with physical cross-links appearing at about every 100 to 600 backbone atoms. In a particular polymers this value is different, it depends on chain flexibility. For predicting entanglement density there is a purely topological model saying that chain is divided into rotational rigid units with unconstrained rotation. The length between entanglement knots is given by:

$$M_e = 3M_vC^2 \qquad (1.2)$$

Where M_v is the length of a skeletal unit which is an elementary rotational unit, and

$$C = < R^2_0 > / n < l^2_v > \qquad (1.3)$$

is a measure of chain intrinsic flexibility [88].

Such a model predicts that in a molten state there is an equilibrium density of entanglements independent of temperature and pressure. It is valid only for unperturbed chains and assuming no dependence of chain flexibility on temperature and pressure [89].

Small molecules move primarily by translation. A simple case is of a gas molecule moving in space, following a straight line until hitting another molecule or a wall. In the liquid state, small molecules also move primarily by translation, although the path length is usually only of the order of molecular dimensions.

Polymer motion can take two forms:

- the chain can change its overall conformation, as in relaxation after strain,
- the chain can move relative to its neighbors.

Both motions can be considered in terms of self-diffusion. All such diffusion is a subcase of Brownian motion, being induced by random thermal processes. For center-of-mass diffusion, the center-of-mass distance diffused depends on the square root of time. For high enough temperatures, an Arrhenius temperature dependence is found. Polymer chains find it almost impossible to move “sideways” by simple translation, for such motion is exceedingly slow for long, entangled chains. This is because the surrounding chains that block sideways diffusion are also long and entangled, and sideways diffusion can only occur by many cooperative motions. Thus polymer chain diffusion demands separate theoretical treatment.

The first molecular theories concerned with polymer chain motion were developed by Rouse [90] and Bueche [91] (Figure 1.11):

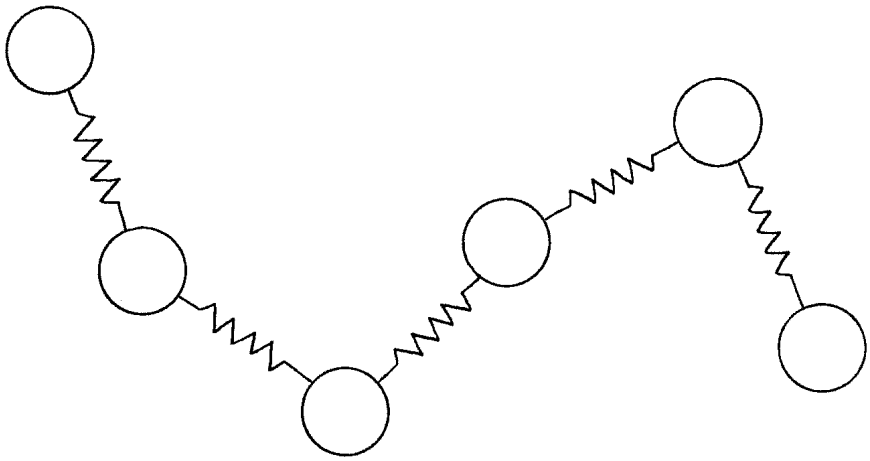

Figure 1.11. Rouse–Bueche bead and spring model of a polymer chain.

After it was modified by Peticolas [92]. This theory begins with the notion that a polymer chain may be considered as a succession of equal submolecules, each long enough to obey the Gaussian distribution function. That is, they are random coils in their own right. This model resembles a one-dimensional crystal. The segments move through a viscous medium (other polymer chains and segments) in which they are immersed. This viscous medium exerts a drag force on the system, damping out the motions. It is assumed that the force is proportional to the velocity of the beads, which is equivalent to assuming that the bead behaves exactly as if it were a macroscopic bead in a continuous viscous medium.

Zimm [93] advanced the theory by introducing the concepts of Brownian motion and hydrodynamic shielding into the system. One advantage is that the friction factor is replaced by the macroscopic viscosity of the medium. The Rouse–Bueche theory is useful especially below 1% concentration. However, only poor agreement is obtained on studies of the bulk melt.

The theory describes the relaxation of deformed polymer chains, leading to advances in understanding the creep and stress relaxation. While it does not speak about the center-of-mass diffusional motions of the polymer chains, the theory is important because it serves as a precursor to the de Gennes reptation theory.

De Gennes [94] introduced the theory of reptation of polymer chains. His model consisted of a single polymeric chain, P, trapped inside a three-dimensional network,G, such as a polymeric gel. The gel itself may be reduced to a set of fixed obstacles, O. His model is illustrated in Figure 1.12 .

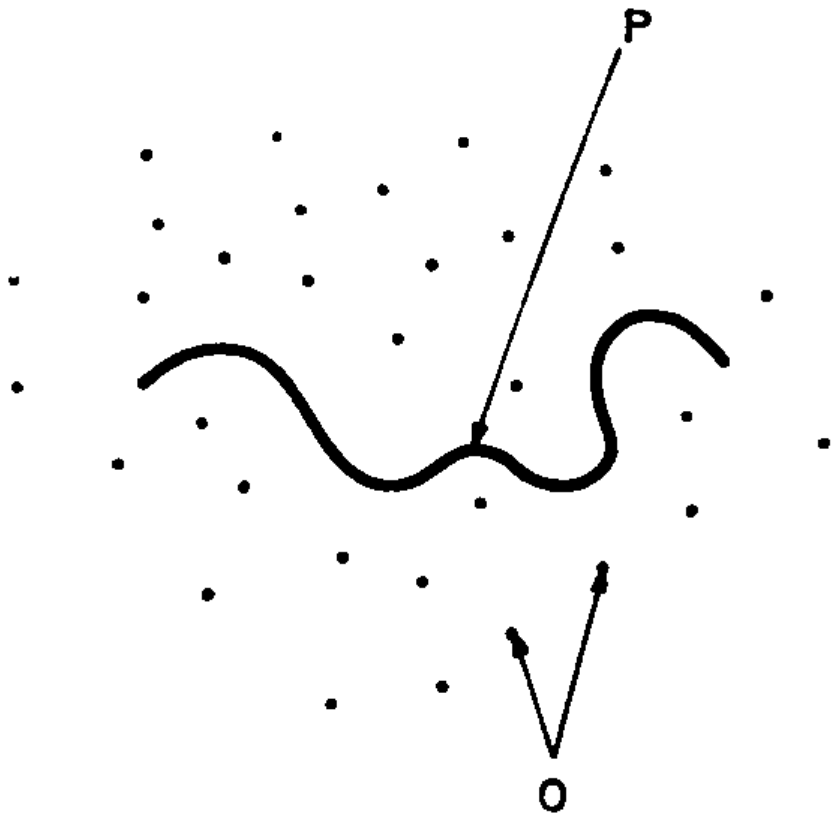

Figure 1.12 . A model for reptation of de Gennes. The chain P moves among the fixed obstacles, O, but cannot cross any of them.

The chain P is not allowed to cross any of the obstacles but it may move in a snakelike fashion among them. The snakelike motion is called reptation. The chain is assumed to have certain “defects,” each with stored length. These defects migrate along the chain in a type of defect current. When the defects move, the chain progresses as shown in Figure 1.13:

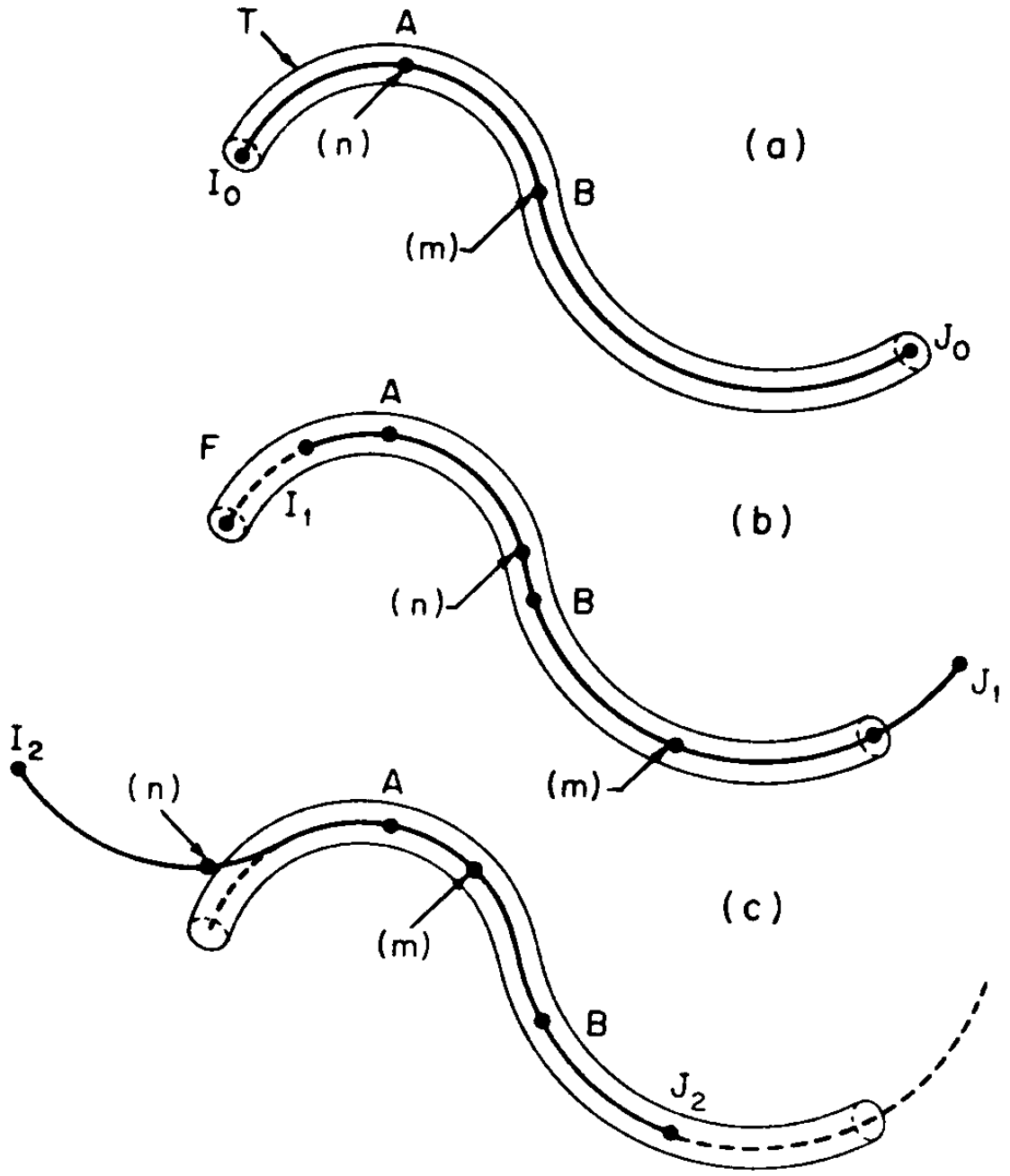

Figure 1.13. The chain is considered within a tube.
(*a*) Initial position.
(*b*) The chain has moved to the right by reptation.
(*c*) The chain has moved to the left, the extremity choosing another path, I_2J_2.
A certain fraction of the chain, I_1J_2, remains trapped within the tube at this stage.

The tubes are made up of the surrounding chains. The reptation motion yields forward motion when a defect leaves the chain at the extremity. The end of the chain may assume various new orientations.
In zoological terms, the head of the snake must decide which direction it will go through the bushes. De Gennes assumes that this choice is at random.
De Gennes found also that the self-diffusion coefficient, D, of a chain in the gel depends on the molecular weight M as:

$$D \propto M^{-2} \qquad (1.4)$$

Numerical values of the diffusion coefficient in bulk systems range from10^{-12} to 10^{-6} cm^2/s. In data reviewed by Tirrell [95], polyethylene of 1 x 10^4 g/mol at 176°C has a value of D near 1 x 10^{-8} cm^2/s. Polystyrene of 1 x 10^5 g/mol has a diffusion coefficient of about 1 x 10^{-12} cm^2/s at 175°C. The inverse second-power molecular weight relationship holds. The temperature dependence can be determined either through activation energies (Ea = 90 kJ/mol for polystyrene and 23 kJ/mol for polyethylene) or through the WLF equation.

The reptation time, T_r, depends on the molecular weight as:

$$T_t \propto M^3 \qquad (1.5)$$

Continuing these theoretical developments, Doi and Edwards [96] developed the relationship of the dynamics of reptating chains to mechanical properties. In brief, expressions for the rubbery plateau shear modulus, G^0_N, steady-state viscosity, η_0, and the steady-state recoverable compliance, J^0_e, were found to be related to the molecular weight as follows:

$$G^0_N \propto M^0 \qquad (1.6)$$

$$\eta_0 \propto M^3 \qquad (1.7)$$

$$J^0_e \propto M^0 \qquad (1.8)$$

An important reason why the modulus and the compliance are independent of the molecular weight (above about 8 M_c) is that the number of entanglements (contacts between the reptating chain and the gel) are large for each chain and occur at roughly constant intervals. But since most of packing and chain arrangement follow from random processes, it is rather average interval possessing wide distribution. Experimentally, the viscosity is found to depend on the molecular weight (M) to the 3.3-3.5 power, when $M > M_c$ (M_c - critical molecular weight, usually around value 10^4). In the case when $M < M_c$ we have linear relationship between viscosity and M.
Value closer to 3.4 was found by Graessley [97] and Doi [98] regarding fluctuations of tube length. Because of those fluctuations they modified the reptation time as:

$$T_r \propto T_s M^3 \left[1 - \left(\frac{M_e}{M} \right)^{1/2} \right]^2 \qquad (1.9)$$

where T_s is the characteristic relaxation time for chain segment, defined in a monomer scale. Estimated T_s for liquid monomer has a value around 10^{-11}s [99].

1.3.2. Characterization of molecular mobility at interface.

a) SSNMR.

To study the dynamics at the interface several experimental methods are used. One of them is Solid State Nuclear Magnetic Resonance (SSNMR).

While dilute solution ^{1}H and ^{13}C NMR spectra measured under classical Fourier transform conditions tend to be sharp and narrow, similar NMR spectra on solid polymers are usually very broad. Recent advances have made solid-state techniques more valuable to polymer science. Improvements include dipolar decoupling, crosspolarization, CP, highpowered decoupling, DD, and magic-angle spinning techniques, MAS, which are often combined. Beyond studies of homopolymers and statistical copolymers, solid-state NMR can characterize polymer blends and composites, which frequently have supermolecular organization that disappears in solution. Since most polymers are used in the solid state, studies showing how the polymer is organized, and how organization changes with processing, provide much needed basic and engineering information. Such studies may combine ^{1}H and ^{13}C spectra to obtain more detailed information.

For example, two-dimensional WISE (WIdeline SEparation) experiments allow information obtained from the isotropic chemical shift in the ^{13}C spectra and the proton line shape in the ^{1}H spectra, respectively, to be displayed. Two-dimensional NMR studies of polymer solutions can also be used to detect and assign NMR resonances from lesser chain structures in polymers (e.g., chain ends, defects, branches, and block junctions), critical in characterizing many synthetic polymers.

Solid-state NMR provides powerful techniques for explaining the segmental dynamics and local conformation in solid materials. These methods allow detailed studies of dynamics occurring over a wide range of frequencies. Fast dynamics (~100 MHz) can be characterized to some extent by NMR relaxation-time measurements [100]. Dynamics occurring within the kHz frequency scale can be studied by line shape analysis [101] or dipolar–chemical-shift correlation methods [102]. Slow dynamics (1 Hz–1 kHz) can be studied by the so-called Exchange NMR experiments, where

relatively slow conformational transitions or segmental reorientations are observed due to changes of orientation-dependent NMR frequencies [103].

The analysis of the behavior of the NMR line shapes as a function of temperature is one of the most traditional procedures for probing molecular dynamics using solid state NMR. The ^{1}H NMR spectrum of rigid materials is characterized by broad lines, usually with Gaussian or Lorentzian shapes due to the strong coupling between the ^{1}H nuclei in the spin network. As in the case of any other anisotropic interaction, molecular motion can induce the averaging of the ^{1}H–^{1}H dipolar interaction, reducing the line widths. Thus, monitoring the line width as a function of temperature and using appropriate models give information about correlation times and activation energies of molecular motions.

Traditionally, NMR spectroscopy gives us dynamics information from relaxation time measurements and from ^{2}H line shape analysis too. The second method is particularly sensitive to the amplitude, geometry, and time scales of motions. So we can't use it for non-deuterated synthetic polymers or proteins.

To extract dynamic amplitudes with site resolution, we can alternatively employ two-dimensional (2D) magic-angle spinning (MAS) NMR. One of the simplest techniques is the 2D wide-line-separation experiment [104] which yields the ^{1}H-^{1}H dipolar couplings in the indirect dimension, separated by the ^{13}C chemical shift of individual sites in the direct dimension.

In the paper of Hong et al. [105] it is shown that also the LG-CP experiment can be used to provide information on the amplitude and geometry of fast segmental motions. Authors demonstrate the using of Lee-Goldburg cross-polarization (LG-CP) NMR under fast magic-angle spinning (MAS) to investigate the amplitude and geometry of segmental motions in biomolecular and polymeric solids. By using a 2D LG-CP technique, they resolved the ^{13}C - ^{1}H or ^{15}N - ^{1}H dipolar couplings according to the ^{13}C or ^{15}N isotropic chemical shift. Applications to systems undergoing 180° phenylene ring flips show spectral line shapes reflecting the geometry of the motion.

An applications of rotor synchronized 2D MAS-Exchange NMR are also known in order to study the conformational dynamics in amorphous and semi-crystalline polymers [106], liquid crystals, and the tautomerism and molecular dynamics in molecular crystals [107, 108].

In the work of Jones et al.[109] proton spin relaxation and molecular motion in a bulk polycarbonate was studied. The proton relaxation times determined in this structurally specific, single type of proton study provide a suitable basis for a quantitative description employing a correlation function-spectral density approach.

Order and Mobility in Polycarbonate-Poly(ethylene oxide) Blends Studied by Solid-State NMR and Other Techniques is the subject of work done by Brus et al. [110]. Solid-state 1D and 2D ^{13}C CP/MAS NMR and ^{1}H CRAMPS (combined rotation and multipulse spectroscopy) and Raman spectroscopy, X-ray scattering, and DSC were used to investigate the structure, morphology, and dynamic behavior of blends of two semicrystalline polymers, polycarbonate (PC) and poly(ethylene oxide) (PEO). The splitting of aromatic carbon signals in the ^{13}C CP/MAS NMR spectra and the absence of spinning sidebands in the ^{1}H dipolar spectra (2D WISE) indicate restricted mobility and hindered cooperative motions of PC chains resulting from blending of PC with PEO and from fixed ordering due to partial crystallinity of PC itself. The observed multiple splittings of the signals of aromatic and carbonate carbons indicate comparable amounts of trans-trans and cis-trans conformational structures of the carbonate group. 2D WISE spectra prove large differences in molecular mobility of amorphous PEO and PC. High mobility of amorphous PEO is not imparted significantly to less mobile PC, despite intimate mixing in the amorphous phase of PC-PEO blends suggested by ^{13}C CP/MAS NMR spectra and CRAMPS ^{1}H-^{1}H homonuclear dipolar dephasing and proved by 2D CRAMPS and WISE spin diffusion measurements. The morphology and domain sizes at the nanometer scale were determined from analysis of spin diffusion processes. Molecular mobility of PC was restricted not only to crystallites, but the presence of crystallites was said to retard the cooperative motions in neighboring amorphous phase (interface) [111].

b) Dielectrical properties.

Dielectrical properties measured over a wide range of frequencies and temperatures gives us valuable information about structure and dynamics of polymeric systems in the rubbery and glassy state too.
The dielectric loss constant, ε'', or its associated tan δ can be measured by placing the sample between parallel plate capacitors and alternating the electric field. Polar groups on the polymer chain respond to the alternating field. When the average frequency of molecular motion equals the electric field frequency, absorption maxima will occur.

In the work of Lupascu et al. [111] dielectric relaxation spectroscopy was applied to study the molecular dynamics of the various PS samples in a wide temperature range concerning the glassy, semicrystalline, or amorphous liquid state. Authors found two relaxation processes β_1 and β_2 not reported before in the literature for both a-PS (atactic PS) and s-PS (syndiotactic PS). These new dynamic processes showed Arrhenius behavior and a common activation energy around 80 kJ/mol, and they crossed the α-relaxation region, indicating the coexistence of an amorphous and nonamorphous phases with specific structural and dynamic properties.

The dielectric properties for thin syndiotactic poly(methyl methacrylate) (s-PMMA) and PVAc films have also been investigated in the frequency range from 0.1 to 1 MHz at temperatures between 263 and 423 K [112]. For both the s-PMMA and PVAc, a broadening of the distribution of the relaxation times was observed and this broadening was more pronounced for the α process than for the β process. The broadening increases with decreasing film thickness indicating a different dynamics for confined thin films to that for the bulk material.
Kremer and co-workers [113] performed dielectric measurements for thin films of isotactic poly(methyl methacrylate) (i-PMMA) of two molecular weights sandwiched between aluminium electrodes. Commercial PMMA used in research and industry is rich in syndiotactic triads, which has a higher T_g than isotactic PMMA. Also, the glass transition of the thin i-PMMA films was determined by temperature-dependent

ellipsometric measurements of the thickness of films prepared on silica. The dynamic results showed a decrease in the glass transition for thin i-PMMA films and a broadening of the relaxation time distribution. Also, a decrease of the dielectric strength with decreasing film thickness was reported.

In addition to being used to study confinement effects on the α relaxation process for thin films, dielectric spectroscopy has also been used to study the secondary β relaxation. Fukao et al [108] found that the dynamics of the β relaxation in atactic poly(methyl methacrylate), a-PMMA, became faster with decreasing film thickness. The authors suggested that there is a strong correlation between the α and β processes despite the fact that these relaxations are located at different temperatures and different frequencies [108]. Dutcher and co-workers [114] observed in the case of thin isotactic PMMA that there was a strong correlation between the relaxation times for both α and β processes. It was also found that the β relaxation of i-PMMA became faster for thicknesses below 10 nm. However, in the Kremer and co-workers work, the β relaxation for PMMA was found to be independent of the film thickness whereas the dynamics of the α relaxation became faster with decreasing film thickness [109].

In the work of Jenczyk et al. [115] molecular dynamics of polyisoprene, polystyrene and poly(styrene-b-isoprene) diblock copolymer has been studied by means of broadband dielectric and magnetic resonance spectroscopies. With these two methods one can selectively study the dynamics of polyisoprene and polystyrene chains in diblock copolymer in wide range of frequency. In the studied systems the Broadband Dielectric Spectroscopy (BDS) allowed to observe very slow motions, while the NMR technique permitted to reach the high frequency limit.

The measurements of dielectric permittivity as well as NMR second moment, spin–lattice relaxation times T_1 and$T_{1\rho}$ in wide range of temperature were performed. It was found that the copolymer exhibits all motions observed in the neat components i.e., three motions connected with polyisoprene blocks (segmental, normal-mode and methyl group rotation) and one (segmental) related to polystyrene blocks. The mutual interaction between polystyrene and polyisoprene chains leads to stiffening of polyisoprene blocks and loosening of polystyrene structure.

The effect of thickness on the glass transition dynamics in ultra-thin polystyrene (PS) films (4 nm < L < 60 nm) was studied by thin film ac-calorimetry (alternating current heating), dielectric spectroscopy (DRS) and capacitive dilatometry (CD) by Lupascu

et al. [116]. In all PS-films, a prominent _α-process was found in both the ac-calorimetric and dielectric response, indicating the existence of cooperative bulk dynamics even in films as thin as 4 nm. Glass transition temperatures (T_g) were obtained from ac-calorimetric data at 40 Hz and from capacitive dilatometry, and reveal a surprising, marginal thickness dependence $T_g(L)$. These results were rationalized by differences in film annealing conditions together with the fact that those techniques probe exclusively cooperative dynamics (ac-calorimetry) or allow the effective separation of surface and "bulk"-type mobility (CD). Two other observations, a significant reduction in *c*p towards lower film thickness and the decrease in the contrast of the dilatometric glass transition, support the idea of a layer-like mobility profile consisting of both cooperative "bulk" dynamics and non-cooperative surface mobility.

c) DMTA.

Dynamic mechanical analysis (DMA, also known as dynamic mechanical spectroscopy) is a technique used to study and characterize materials. It is most useful for studying the viscoelastic behavior of polymers. A sinusoidal stress is applied and the strain in the material is measured, allowing one to determine the complex modulus. The temperature of the sample or the frequency of the stress are often varied, leading to variations in the complex modulus. This approach can be used to locate the glass transition temperature of the material, as well as to identify transitions corresponding to other molecular motions.

Relaxation processes play a dominant role and result in a complex pattern of temperature-dependent and frequency dependent properties of polymers.
In general thermal equilibrium is a dynamical situation where chains change between states activated by thermal energies. The microscopic dynamics shows up in the macroscopic experiments. Relaxation rates observed in certain mechanical or

dielectrical measurements equal the rates of transitions within a certain group of conformations.

The rates of conformational transitions of a chain encompass an enormously wide range. Local rearrangements including only a few adjacent mers are usually rapid and take place with rates similar to those in ordinary liquids. Conformational changes of more extended sequences require much longer times.

The rates of the relaxatory modes in a sample do not cover the whole spectral range homogeneously, but usually one observes a separation into several regions of rates where relaxation is accumulated. Each region belongs to a group of processes with similar roots. It has become a convention to designate these different groups by Greek letters, α, β and γ, and to use the symbol α for the process with the lowest transition rates showing up at the highest temperature.

On the other hand, the symbol γ is used for the processes observed at the low temperature end and this means those with the highest transition rates.

Major groups of relaxation processes in polymers are:

- local processes, observed in the glassy state;
- cooperative processes in longer chain sequences that provide the basis for the elasticity of rubbers and the viscoelasticity of polymer melts;
- chain diffusion, which controls the flow behavior;
- specific processes in partially crystalline states, associated with coupled motions of sequences in the crystallites and the amorphous regions.

Modification of the interface changes the viscoelastic response of crystalline polymer blends. For incompatible systems, usually one or more additional tan δ (mechanical loss) peaks appear which reflect the embrittlement of the material. Upon proper compatibilization, the additional peaks disappear and the material becomes tougher.

In the work of Galeski [117] dynamic mechanical analysis (DMTA) evidenced the occurrence of interactions of the compatibilizer with blend components through temperature shift and intensity change of α, β and γ relaxation processes of polymer components.

The shift is the result of high molecular orientation of the amorphous phase of matrix polymer and of the stabilization effect of unbroken interfaces in compressed samples.

Figure 1.14 illustrates the change of tan δ for amorphous and crystalline phases of polymers.

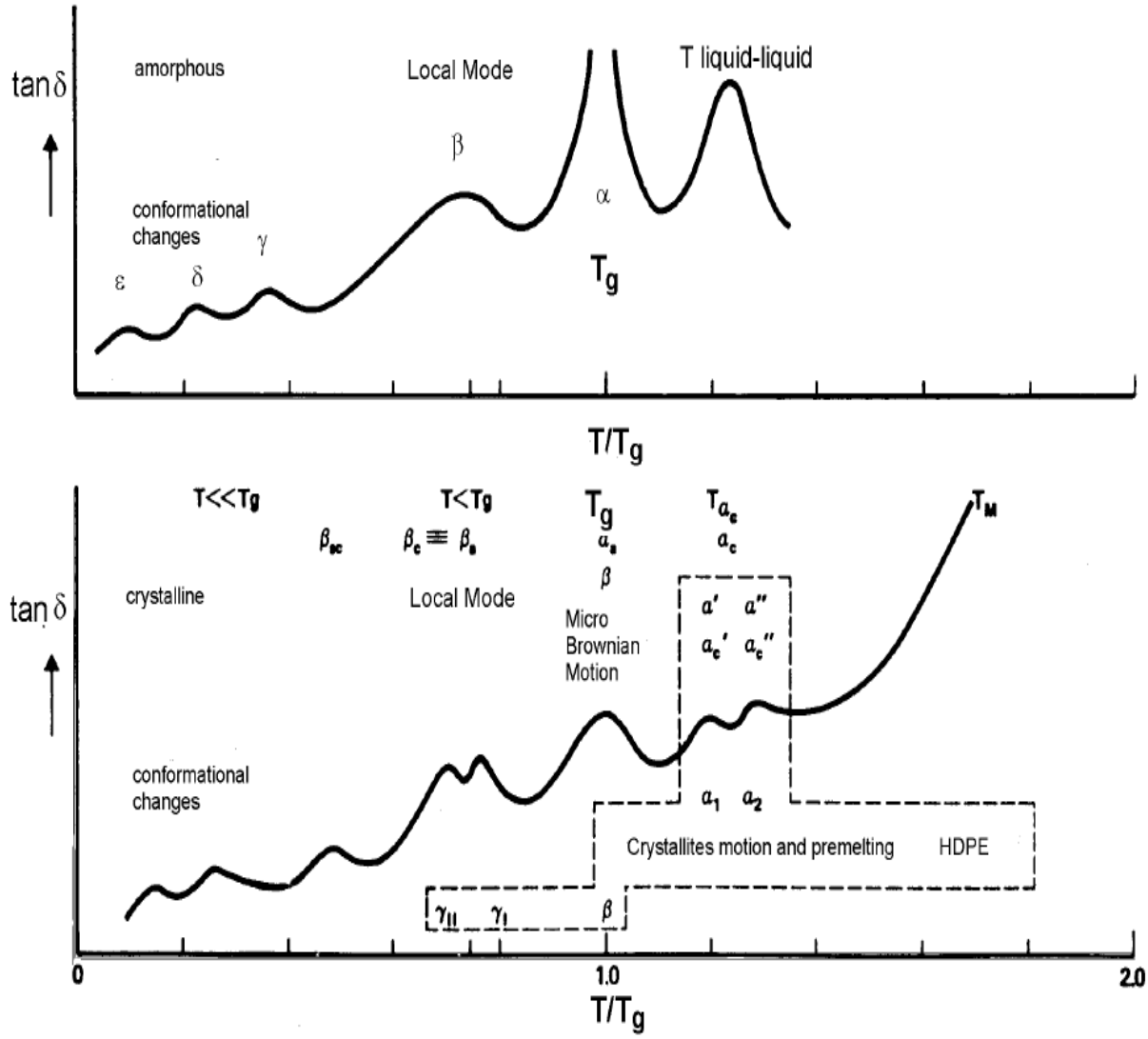

Figure 1.14. Graph of relaxation spectra of amorphous and crystalline phases polymers [[118]].

Divergence from the elastic Hooke law can be of two types: stress induced when the yield point is reached, and time dependence anomalies connected with time and rate dependencies. Time dependence anomalies are characteristic of the materials the behavior of which is a combination of elastic and viscous responses. If stress induced anomalies are not present, e.g. at low strain, the response of the material is linearly viscoelastic. The material response to deformation or stress on the molecular level is, unlike for low molecular weight materials, due to polymer chain displacements or rotations of chain fragments: the higher the temperature the larger elements participate in the motion. If the material is subjected to oscillating sinusoidal stress or strain, the response of the material is delayed by the angle δ, dependent on the activated motions which vary with temperature [118].

In polymer blends the structure is more complicated because usually there is a dispersed phase, a continuous phase and the interface. The applied force is transmitted onto the dispersed inclusions from the matrix via the interface. Therefore, the properties of the interface play a vital role in force transmission and overall behavior of a blend.

2. EXPERIMENTAL OF THE STUDY

2.1. Preparation of the multilayered films.

2.1.1. Principle.

Multilayered films (PC/PS) with 257 alternating layers were extruded from melt on a laboratory scale coextrusion line at Case Western Reserve University that incorporates layer-multiplying technology. The schematic drawing of layer-multiplying coextrusion in Figure 2.1 shows how a series of n multiplying elements combines two dissimilar polymers as $2^{n+1} + 1$ alternating layers. After the polymer melts, materials are combined in the ABA feed block, the melt stream flows through a series of layer-multiplying die elements; each element splits the melt vertically, spreads it horizontally, and finally recombines it with twice the number of layers. After that, the melt is spread in a film die to further reduce the layer thickness.

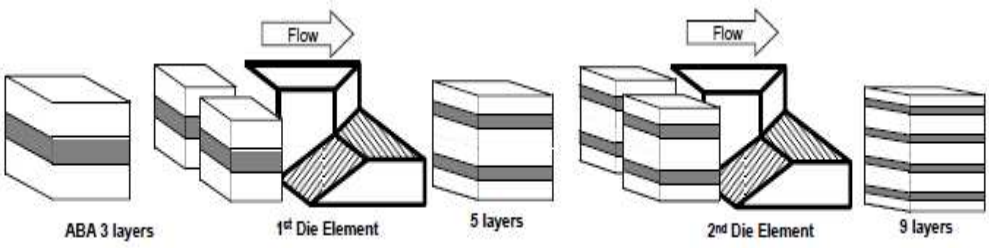

Figure 2.1. Layer-multiplying coextrusion for forced-assembly of polymer nanolayers.

In coextrusion process microlayers are comprised of alternating layers of two or more components with individual layer thicknesses ranging from macroscale to nanoscale. Typically, the total number of layers ranges from ten to thousands. By varying the melt feed ratio, the final sheet or film thickness, and the number of layers, and the individual layer thicknesses can be precisely controlled. The coextrusion system consists of two or more single screw extruders with melt pumps (metering to ensure a regular flow rate), a coextrusion block, a series of layer multiplier elements, and a tape or film die (Figure 2.2).

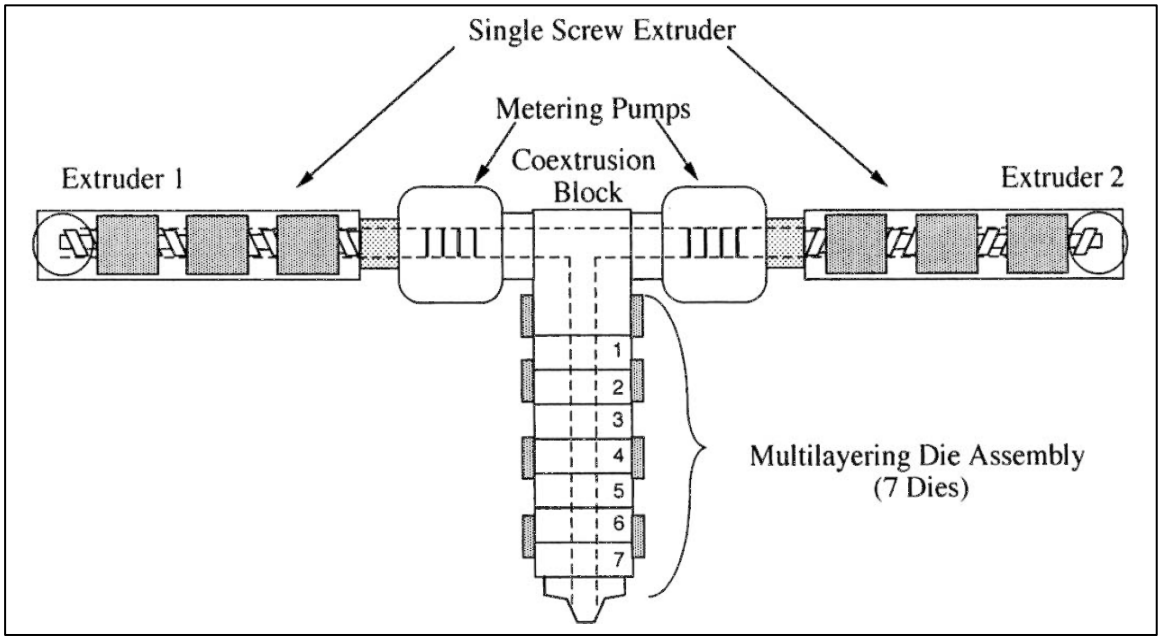

Figure 2.2. Two component microlayer system, showing extruders, pumps, feedblock, multiplier dies and film die [119].

Metering pumps are controlling the two melt streams that are combined in the feedblock as two parallel layers. From the feedblock, the two layers flow through a series of layer multiplying elements. Each element doubles the number of layers. In

each element the melt is first sliced vertically, then spread horizontally and finally recombined.

The quality of coextruded microlayers depends on the viscosity ratio of the components. The material with the lowest viscosity will tend to encapsulate the other so that it forms a slip film between the high viscosity component and the wall [120]. Additionally interfacial instabilities can occur as the melt streams come together when the viscosity mismatch is large. To minimize these effects, the viscosities of the components should be as close as possible. The viscosity of each component should then be determined as a function of temperature before coextrusion process. After, those viscosities must be used to identify the processing temperature where the two polymers have the value of viscosity in the same range.

2.1.2. Applications of multilayered films (microscale).

Films made by coextrusion have several significant applications. Also microlayer systems are very attractive as model systems because of the large specific interfacial area and good layer uniformity.

For example layers may be used to add colors or visual effects, screen ultraviolet radiation, provide barrier properties, and to control surface properties.

Films exhibiting colorful iridescence were produced by alternating two polymers of different refractive indices, such as polypropylene and polystyrene or polycarbonate and poly(methyl methacrylate), and approximately controlling the volume fraction and layer thicknesses [121, 122]. Films which reflect ultraviolet or near infrared radiation have been obtained also by microlayer coextrusion [123]. Water-barrier properties of 128-layer polyethylene/polystyrene films were not affected significantly by crumpling, presumably because the cracks or flaws in the polystyrene were randomized [124]. In the same paper, mutual reinforcement was observed in biaxially oriented microlayer films of polypropylene and polystyrene over a wide range of composition ratios.

Microlayering is an attractive approach for creating designed architectures from particulate-filled polymers too. If the particles are anisotropic, for example tubes or

short fibres, the geometric constrains imposed by layer multiplying ensure orientation of the particles in the plane of the layers. Additionally filled and unfilled layers can be alternated. If, for example, the filler is added in order to reinforcement of the stiffness, the toughness can also be enhanced by alternating a ductile layer to stop cracks. If the objective is to obtain anisotropic electrical properties, conducting layers filled with metallic particles can be alternated with unfilled isolator layers. Additionally, high-melt-strength layers can carry low-melt-strength materials during fabrication. The reduction in thickness of layers from macro to micro scale has a large improvement in the toughness and impact strength of multilayered extrudates.

Coextrusion is also suitable for applying thin multilayer films as coatings on substrates. Growing applications for coextrusion are in automotive, construction, thermoforming operations, to form specific packages or containers. Coextrusion is also used in the profile market, pipes as well as window profiles have been made from coextruded structures.

2.1.3. Down to multinanolayers films.

Forced assembly of two dissimilar polymers using layer multiplying coextrusion makes it possible to fabricate films with thousands of alternating layers with thickness in the nanometer range. The thickness of an individual nanolayer can be even on the size scale of the polymer interphase. The high fraction of interphase makes it possible to probe the interphase with conventional tools of polymer analysis.

In the work of Ma et al. [[125]] an investigation of the effects of layer thickness on the deformation behavior of microlayer composites with alternating PC and SAN layers has been made. Authors conclude that composites with 49, 194, 388 and 776 layers all yield in uniaxial tension with the same yield stress, but the fracture strain, which represents how far the neck propagates, increases with the number of layers. The absence of visible crazing or significant volume change during necking of the 388 and 776 layer composites indicates that in these instances crazing is suppressed. A transition in the microdeformation behavior is observed as the layer thickness decreases. In the 49- and 194-layer composites individual layers exhibit behavior that is characteristic of the bulk. As the number of layers is increased to 388 and 776,

SAN crazing and cracking is suppressed and shear bands are formed. Those shear bands extends through several layers. Shear deformation of the SAN is attributed to the local shear stress concentration at the interface, created by impingement of a PC shear band.

.As the individual layer thickness is about tens of nanometers, it is on the same size scale as the dimension of the polymer molecules. In this case unusual structures can appear, especially if one of the components is crystalizable [126]. Confined, two-dimensional crystallization of polymers presents challenges and opportunities due to the long-chain and covalently bonded nature of the macromolecule. In the paper of Wang et al. [8] authors discovered a morphology that emerges as confined polyethylene oxide (PEO) layers become thinner. They found that when the thickness is confined to 20 nanometers, the PEO crystallizes as single, high-aspect-ratio lamellae that resemble single crystals. Unexpectedly, the crystallization habit imparts also two orders of magnitude reduction in the gas permeability.

If the layers are thin enough, the interfacial regions totally dominate the bulk behavior. The large interface to volume ratio to nanolayered polymers facilitates studies of interfacial phenomena such as adhesion, interdiffusion, interfacial reactions, and surface-nucleated crystallization. It is also possible to produce new classes of materials with unique properties using nanolayering. Two miscible polymers can be in intimate contact with minimal mixing , because coextrusion process requires stringent laminar flow conditions and short processing times. Gradient compositions can be produced by controlled interdiffusion too. Through analysis of the effect of layer thickness and adhesion between layers, further structures and property enhancement can be achieved.

There is also another coextrusion system, that adds a third polymer between layers of polymer A and polymer B. This third polymer may be added for certain properties like barrier, adhesion, strength. Insertion of the tie layer (T) at each interface is accomplished by extruding three polymers into a feedblock that combines the melt into five layers with the sequence ATBTA. Normally the thickness of the tie layer is one tenth that of the A and B layers. The five layer melt goes then into the multiplying elements. As a result a layer sequence $(ATBT)_xA$, is obtained, where x is equal to $(2)^n$ for an assembly with n multiplying elements. The ability to insert a thin tie layer

at each interface between dissimilar polymers A and B creates opportunities for efficient incorporation of compatibilizing agents, what is not so easy using conventional method of blending.

Multilayer co-extrusion has developed into an important polymer fabrication process, providing large growth opportunities for the polymer industry. It is a single-step process starting with two or more polymer materials that are simultaneously extruded and shaped by using a single die to form a multilayered sheet or film. Coextrusion avoids the costs and complexities of conventional multistep lamination and coating processes, where individual plies must be made separately, primed, coated, and laminated. Coextruded multilayered tapes are challenging traditional materials, such as metals, glass, paper, and textiles.

2.1.4. Material choice.

In this study multilayered films consisting of PC and PS were used. Those polymers were chosen due to similar viscoelastic behavior. It makes coextrusion process easy to process. We don't have problems with several parameters connected with special properties of each polymer.

The polycarbonate was Dow Calibre 200-15 with bulk density 1.20 g/cm^3 according to ASTM D792 and melt flow index of 15 g/10 min according to ASTM D1238.

The polystyrene was Dow STYRON 685D with bulk density 1.04 g/cm^3 according to ASTM D 792 and melt flow index of 1.5 g/10 min according to ASTM D1238.

2.1.5. Studied films.

In this study the total film thicknesses were 25μm and 125μm and relative compositions were varied to produce polycarbonate and polystyrene layers of different thicknesses. The weight compositions of multilayered films and thicknesses of PC and PS layers were :

257 Layer PC/PS Multilayered Film: 125 μm Film			
Composition (PC/PS)	Overall Film Thickness (μm)	PC Layer Thickness (nm)	PS Layer Thickness (nm)
100/0	125	125	-
95/5	125	930	50
90/10	125	880	100
85/15	125	830	150
80/20	125	780	195
75/25	125	730	245
70/30	125	680	290
0/100	125	-	125

Table 2.1. Weight compositions and layers thicknesses for multilayered films with the overall thickness 125 μm.

257 Layer PC/PS Multilayered Film: 25 µm Film			
Composition (PC/PS)	Overall Film Thickness (µm)	PC Layer Thickness (nm)	PS Layer Thickness (nm)
100/0	25	25	-
95/5	25	185	10
90/10	25	175	20
85/15	25	165	30
80/20	25	155	40
75/25	25	145	50
70/30	25	135	60
0/100	25	-	25

Table 2.2. Weight compositions and layers thicknesses for multilayered films with the overall thickness 25 µm.

The extruders, multipliers and die temperatures were set to 270°C to ensure matching viscosities of the two polymer melts:

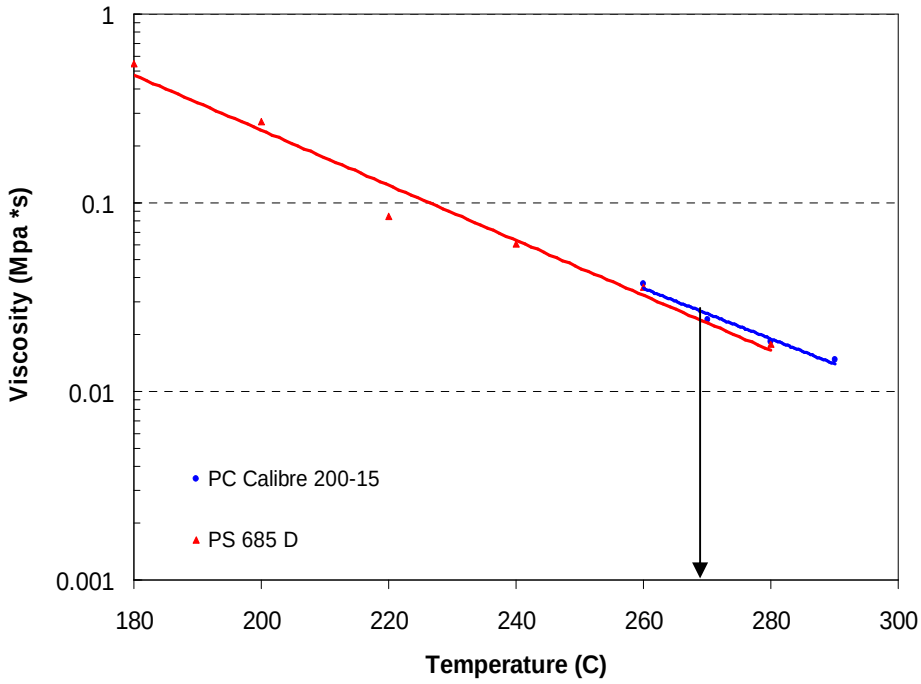

Figure 2.3. Viscosities of PC and PS versus temperature.

In each film we have 257 alternating layers of PC and PS. Polycarbonate is creating the external layers.

2.2. Physico-chemical analysis.

2.2.1. Density measurements.

In order to check the real volume mass of our samples, using a weighing device and water, density measurements of PS and PC in multilayered films PC/PS were done. Samples were weighted in the air (m_{air}) and in the water (m_{water}). Using Archimede's

principle and knowing the volume mass of air ρ_{air} and water,ρ_{water}, volume mass of multilayered films ρ can be determined:.

$$\rho = \frac{m_{air}}{m_{air} - m_{water}} \left(\rho_{water} - \rho_{air} \right) + \rho_{air} \qquad (2.1)$$

2.2.2. Dynamic mechanical properties.

Rheological behavior of multilayered films at 140°C and pure PS was investigated by dynamic mechanical measurements in parallel-plate geometry (diameter 25 mm) using an ARES rheometer machine. Samples were made from disks with a diameter of 25 mm cut in films and stacked on each other to get a total thickness of about 1 mm. Then this assembly was welded at 160°C during one hour in the rheometer under a normal force of 15N. No variation of the thickness of the film stack was noted.

Dynamic Strain Sweep Tests (DSST) were performed to choose proper value of strain for Dynamic Frequency Sweep Tests, in the area, where material is still in linear viscoelastic regime. It was done with a frequency 100 rad/s in the range of strain: 0.01-10% and at the temperature 140°C. After this, storage modulus G', loss modulus G", and dynamic viscosity η* were measured as a function of frequency at the temperature 140°C [Dynamic Frequency Sweep Test (DFST)].

For pure PC, rectangular torsion tests were done using an ARES rheometer machine. The samples were prepared by compression of dried granules at 200°C.

2.2.3. Differential Scanning Calorimetry (DSC).

Thermal properties of the multilayered films were studied by Differential Scanning Calorimetry on a TA Instruments Q series 1000 apparatus. Several disks with a diameter of 6 mm were cut in the films and stacked in aluminum DSC pans. The weight of the small disk stack was about 10 mg. It was heated with a rate of 30˚C/min from 20˚C to 180˚C.

2.2.4. Atomic Force Microscopy (AFM).

The thickness of individual polycarbonate and polystyrene layers was measured by Atomic Force Microscopy (AFM). The film was embedded in epoxy resin (Araldite Resin Mollenhauer Mixture) and cured for 24 hours at 60^{o}C. Cross-sections were microtomed perpendicular to the plane of the film by glass knife and observed. The AFM images were obtained in air with a commercial multimode scanning probe microscope (Nanoscope IIIa, Digital Instruments,) operated in the tapping mode. Measurements were performed at ambient conditions using rectangular type Si probes with a spring constant of 42 N/m and resonance frequencies in the 264-311 kHz range. The tip radius was 10 nm.

2.2.5. Solid State Nuclear Magnetic Resonance (SSNMR).

The solid-state magic angle spinning (MAS) experiments were performed on a BRUKER Avance III 400 spectrometer at 100.613 MHz frequency for ^{13}C, equipped with a MAS probe head using 4 mm ZrO_2 rotors. A sample of glycine was used for setting the Hartmann-Hahn condition, and glycine was used as a secondary chemical shift reference δ=176.04 ppm from external TMS. The conventional spectra were

recorded with a proton 90º pulse length of 4 μs and a contact time of 2 ms. The repetition delay was 6s, and the spectra width was 25 kHz. The FIDs were accumulated with a time domain size of 2K data points. The RAMP shape pulse was used during the cross-polarization and spinal TPPM decoupling. The cross-polarization efficiency was measured with contact times between 10 μs and 12 ms. The spectral data were processed using the TOPSPIN program.

For the LG-CP period, the ^{1}H effective field strength was 50 kHz in all experiments, and the ^{13}C spin-lock field strengths was adjusted to the first-order sideband condition $\omega_{13C} = \omega_{1Heff} - \omega_r$. Spinning speed was 13 kHz and was regulated to ± 3 Hz by a pneumatic control unit. Recycle delays varied from 1.5 s to 4 s. The 2D LG-CP experiments incremented the LG-CP contact time at a step of 16.28 μs. At a spinning speed of 13 kHz, the dwell time for the evolution period was thus 19.23 μs. The maximum t_1 evolution time was typically about 1 ms. Only cosine-modulated data were collected. Thus, a real Fourier transformation was performed on the t_1 data, yielding spectra with a symmetrized ω_1 dimension and showing the dipolar splittings. Since the t_1 time signal increases with increasing LG-CP contact time, the ω_1 dimension was processed using the baseline correction mode “qfil” in the TOPSPIN software. This subtracts a constant intensity from the time signals before Fourier transformation and yields spectra free of a dominant zero-frequency peak giving ^{1}H-^{13}C doublet.

Pieces of films for all polymer systems were rolled and inserted into the 4 mm zirconium rotors.

In our project for analysis of the effect of molecular motion on the line shape of the dipolar spectra we have carried out sensitivity-enhanced LG-CP measurement, employing PILGRIM pulse sequence (phase-inverted LG recoupling under MAS).

2D spectra for the films were recorded with spinning rate 13 kHz at various temperature. The ^{1}H effective field strength, ω_{1Heff}, was matched to the ^{13}C spin-lock field strength δ_{13C}, by $\omega_{1Heff} - \omega_{13C} = \omega_r$ (-1 condition). The LG CP contact time was incremented asynchronously with rotation to yield the heteronuclear dipolar dimension of the 2D experiment. The ^{13}C-spin isotropic chemical shift was detected in the second dimension of the experiment.

1D projections taken from PILGRIM correlations for PC film were recorded at temperatures 296K, 373K and 393K. Similar Variable Temperature (VT) measurements were carried out for PS film, however since the glass transition for PS is in the range of 378K- 383K, we have measured this sample at 296K, 348K , 373K and 388K. The VT LG-CP approach was also employed for PC/PS film, with relative composition 70/30 and total thickness 125µm.

2.2.6. Dielectric Relaxation Spectroscopy.

Dielectric relaxation spectroscopy was done for single component materials (reference materials) as well as for multilayered films PC/PS with total thickness 25µm using a Broadband Dielectric Spectrometer. It was done in Katholieke Universiteit Leuven, Laboratory for Acoustics and Thermal Physics, Department of Physics and Astronomy, thanks to professor M. Wübbenhorst. The complex permittivity was measured versus temperature and frequency. The range of frequency was 10^0 - 10^6[Hz] and the range of temperature was from -100ºC to 200ºC.

To screen the multilayered spectra for features that are beyond an ideal superposition of the pure single polymer samples, modeling of the expected “ideal” multilayer response was performed.

3. PROPERTIES OF CONFINED AMORPHOUS PHASE AND DISCUSSIONS

3.1. Characterization of multilayered films

The required thickness of PS and PC layers was set by the yield of melt pumps mounted and operating on extruders. The expected thickness of layers is calculated from the total thickness of multilayer film, the number of layer multiplications and the ratio of yields of PS and PC pumping (composition of the film).
Firstly we wanted to check the mean thicknesses of PS and PC layers. For these reasons density measurements of the multilayer films have been done.
In order to determine the local variation of the layer thickness in the multilayered films the AFM technique was used.
Finally, the DSC measurements were performed for each multilayer film to determine the variation of glass transition of both amorphous materials in confined layers.

3.1.1. Checking the mean thickness of multilayered films

Volume mass of different composites PC/PS was determined thanks to density measurements according to Equation 2.1 and are given in Table 3.1. Then, knowing the density of bulk PS and PC at ambient temperature, ρ_{PS} and ρ_{PC} respectively, and supposing that the density of confined PS layer and PC layers do not differ significantly from the bulk ones, it was possible to calculate the volume fraction α of PS in the multi-layered films:

$$\alpha = \frac{\rho - \rho_{PC}}{\rho_{PS} - \rho_{PC}} \qquad (3.1)$$

Films PC/PS PS (nm)-PC(nm)	mass in air (g)	mass in water (g)	vol mass (kg/m^3)
PS	0.924	0.031	1031.7
PC	0.730	0.114	1181.5
290-680	0.451	0.056	1138.3
150-830	0.331	0.047	1162.0
100-880	0.610	0.089	1167.3
60-135	0.102	0.012	1136.2
50-145	0.276	0.035	1141.8
40-155	0.188	0.025	1149.9
30-165	0.292	0.041	1159.8
20-175	0.245	0.036	1168.7
10-185	0.234	0.035	1172.3

Table 3.1. Density measurements of the studied multilayered films.

Films PC/PS PS (nm)-PC (nm)	% of PS	% of PC
290-680	0.29	0.71
150-830	0.13	0.87
100-880	0.09	0.91
60-135	0.30	0.70
50-145	0.26	0.74
40-155	0.21	0.79
30-165	0.14	0.86
20-175	0.09	0.91
10-185	0.06	0.94

Table 3.2. Calculated values of the volume fraction of PS in multilayered films PC/PS.

After that, measuring the overall thickness of each film, e, and knowing the number of layers in each composite 2 n+1, the thickness of PS layer and PC layer in the composite can be found (Table 3.3):

$$e_{PS} = \frac{\alpha e}{n} \qquad e_{PC} = \frac{(1-\alpha)e}{n+1} \tag{3.2}$$

Films PC/PS PS (nm)-PC (nm)	1 layer of PS (nm)	1 layer of PC (nm)
290-680	270	662.
150-830	135.	897
100-880	95	898
60-135	59	135
50-145	52	142
40-155	43	159
30-165	29	172
20-175	19	199
10-185	13	204

Table 3.3. Mean values of each layer of PS and PC in multilayerd films PC/PS.

Comparing to the assumed values of the PS and PC fractions given in Tables 2.1 and 2.2, we can see a good agreement between assumed and measured values of the fraction of each films component. Nevertheless, some discrepancies occur on thickness values due to film thickness variations. Those measured values will be used to predict numerically the viscoelastic behaviour of composite films.

3.1.2. Shape of the layers – AFM.

Cross-sections were microtomed by a glass knife normally to layers plane. The direction of the cutting did an angle of approximately 30°C.

The AFM images of cross-sections of multilayered films reveal alternating layers of PS and PC. The border lines between layers can be easily distinguished. It can be noticed also that thicker layers are uniform, continuous and exhibit uniform thickness. Examples of such AFM images are presented in Figure 3.1. Good layer uniformity was clearly evident in the low-resolution images.

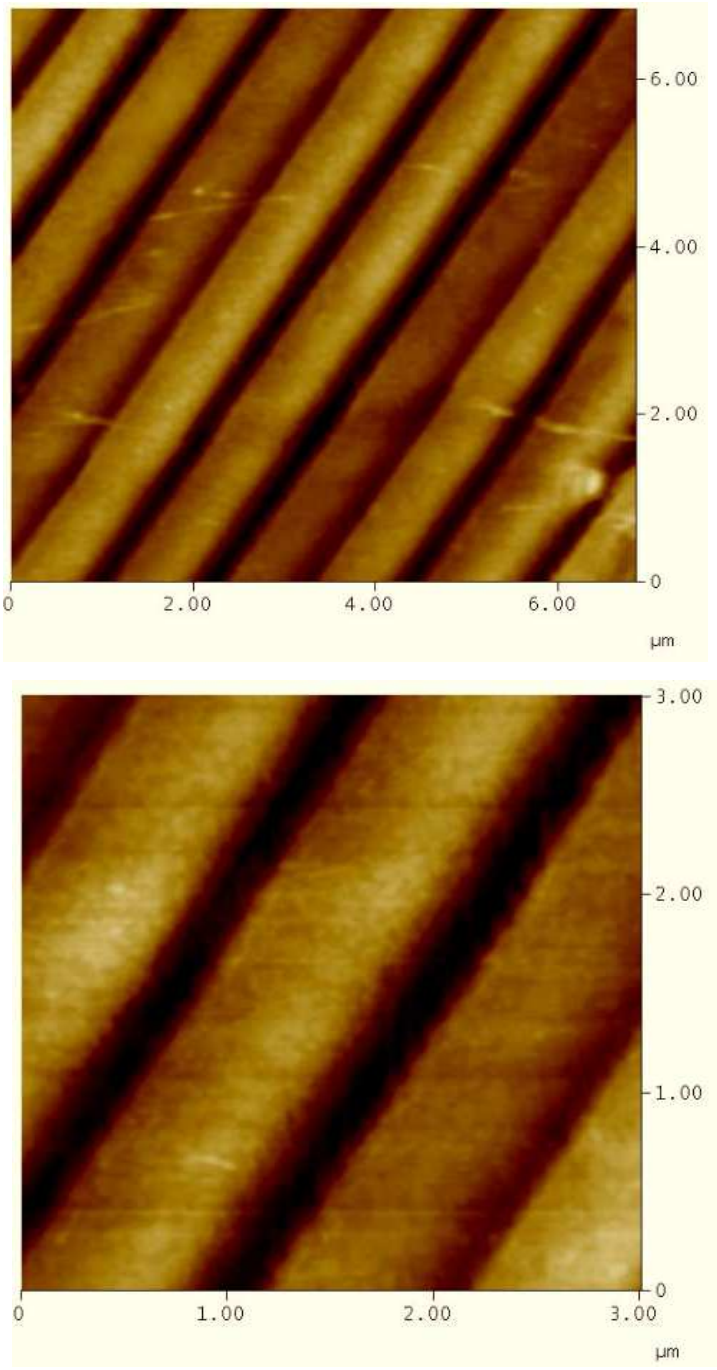

Figure 3.1. AFM images for the film PC/PS, 70/30, 125 µm thick (scale: 6µm - top image and 3µm – lower image). The light bands belong to polycarbonate and the dark ones correspond to polystyrene layers.

Thin layers are less uniform and their thickness varies more from layer to layer (Figure 3.2).

Especially the AFM images for the films with the overall thickness 25µm exhibit less uniformity. Very thin layers in those films lose their continuity as it can be seen in

several locations in cross-sections or even they simply disappear. They also change their thicknesses as we can see in Figure 3.3 where exemplary AFM image of cross-section of worst case of 25 μm thick film PC/PS, 95/5, with expected thickness of PS 10nm is presented:

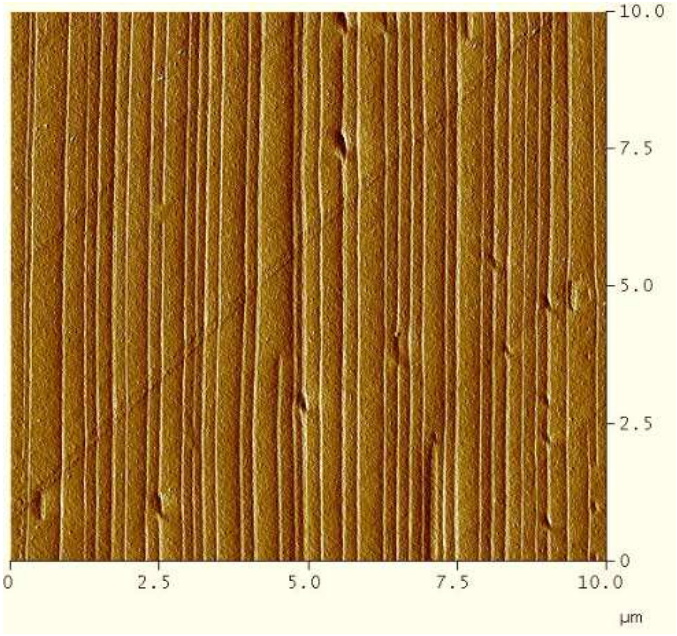

Figure 3.2. AFM images for the film PC/PS, 85/15, 25 μm thick.

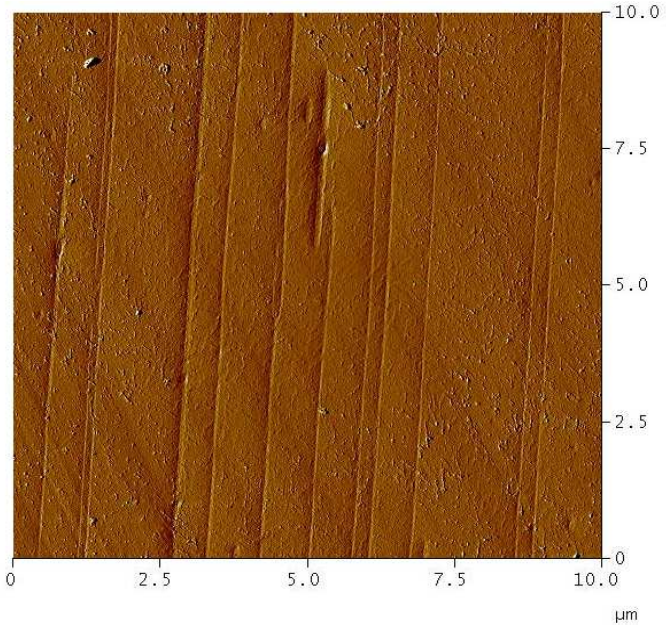

Figure 3.3. Example of the AFM image for the film with the overall thickness 25μm (PC/PS, 95/5, thickness of PS 10nm).

Nevertheless, for most of multilayered films the average thicknesses of PS and PC layers can be measured with a good repeatability. The expected values of the thickness of each layer calculated from processing parameters are listed in Tables 2.1 and 2.2, for two multilayered film thicknesses and for various film compositions. In order to examine those calculated values the cross-sections of multilayered films were observed by AFM technique in a tapping mode. The thickness of each layer was determined from AFM images using the Nanoscope computer program (Figure 3.4).

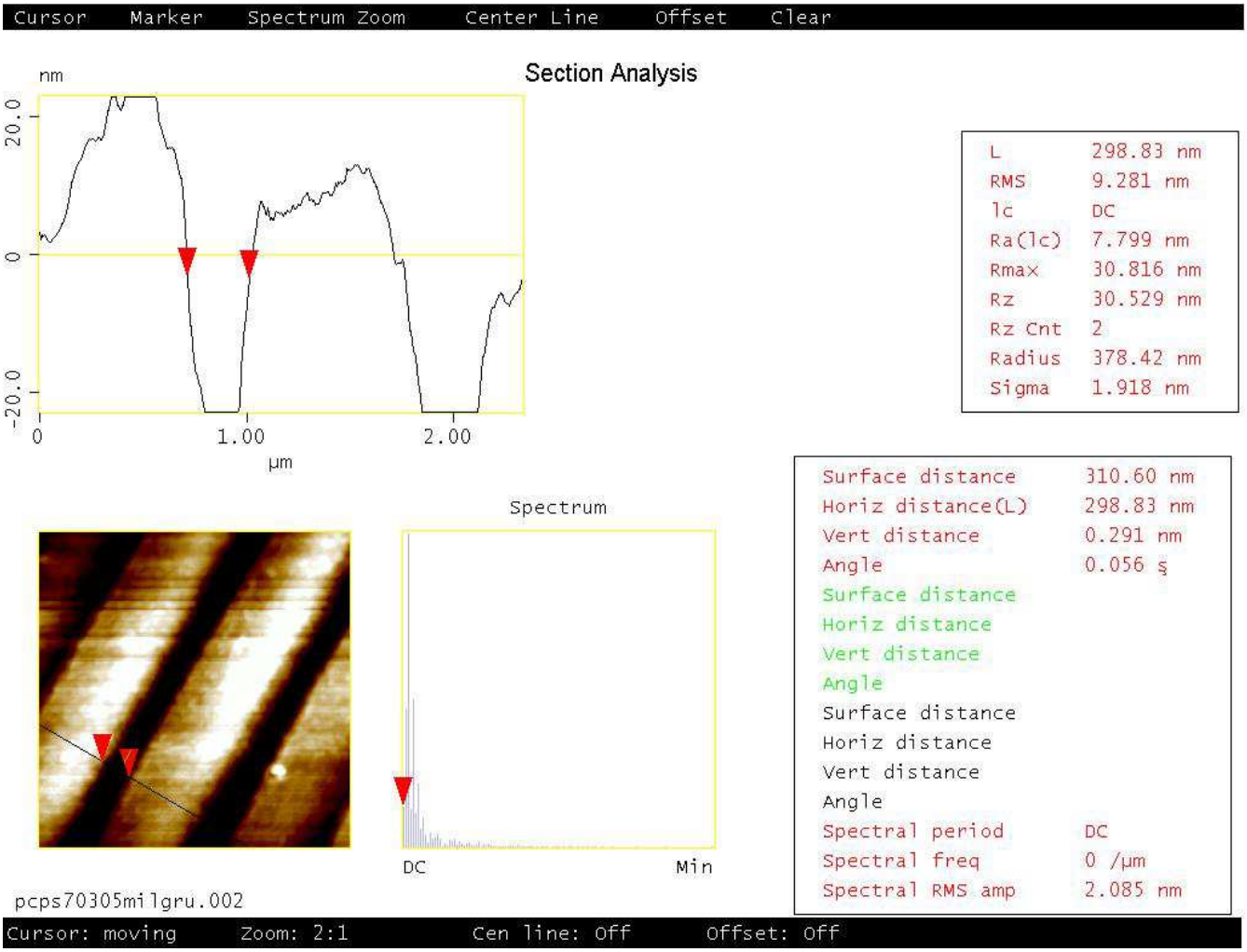

Figure 3.4. Way of measuring thickness of each layer. Example for the film PC/PS, composition 70/30, 125 µm thick (Nanoscope program).

As it can be seen from Table 3.4 the thicknesses of each PC and PS layers determined from cross sections of coextruded films with alternating layers are in reasonably good correlation with the estimated thicknesses determined from the processing parameters:

Multilayered films PC/PS	**Calculated layers thicknesses [nm]**		**Measured by AFM layers thicknesses [nm]**		**Thicknesses from density measurements [nm]**	
	PC	**PS**	**PC**	**PS**	**PC**	**PS**
PC/PS, 70/30, 125μm	680	290	≈ 685	≈ 298	662	270
PC/PS, 95/5, 25μm	185	10	≈ 187	≈ 14	204	13

Table 3.4. Comparison of the calculated and measured layers thicknesses. Example for the films with the thickest (PC/PS, 70/30, 125μm) and the thinnest (PC/PS, 95/5, 25μm) layers of polystyrene.

3.1.3. Thermal properties – T_g versus thickness of PS layer

Polystyrene and polycarbonate exhibit glass transition at around 100-105ºC and 150-155°C respectively. In DSC a glass transition is observed as a change in heat capacity which is lower for PS than for PC. In multilayered films with low concentration of PS it is difficult to resolve clearly a glass transition of PS. Firstly we tried to perform all the thermal measurements on a calorimeter TA instrument DSC Q1000 with a heating rate of 10ºC/min. and a weight of the sample around 10mg. But

as we can see on Figure 3.5 this heating rate was too low to observe the T_g of PS in multilayered films with low concentration of PS. That is why we decided to perform thermal analysis with the higher heating rate of 30ºC/min and a sample weight around 10 mg.

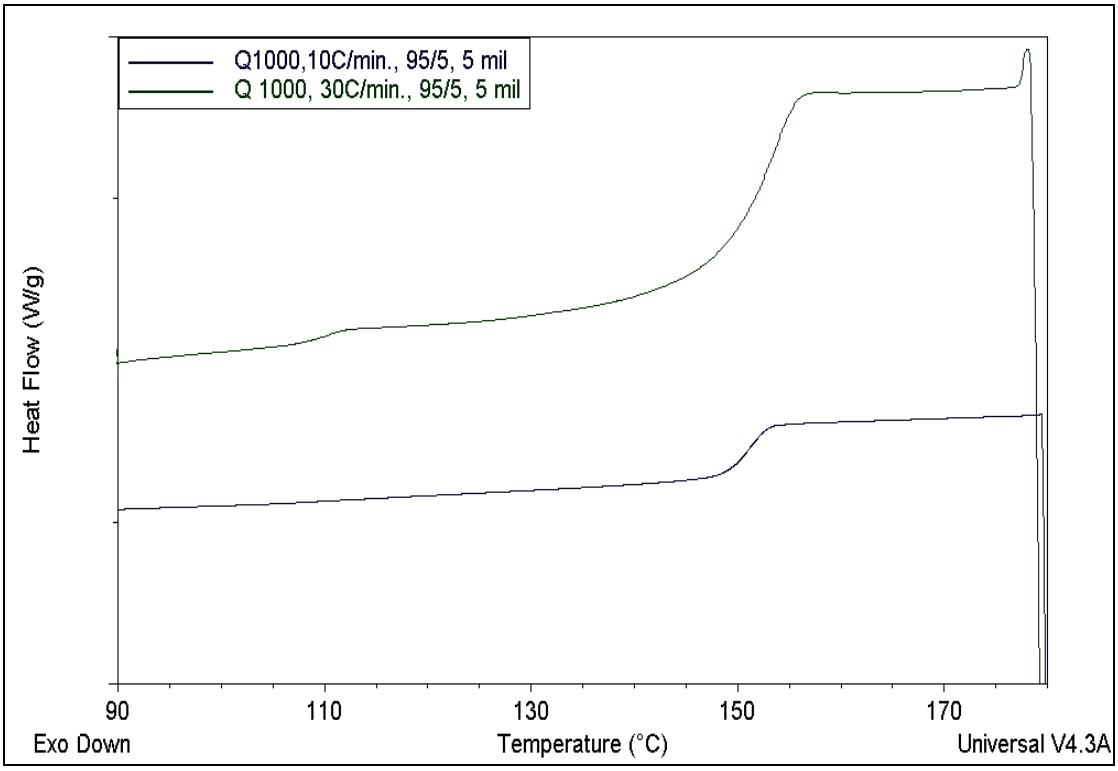

Figure 3.5. Comparison of DSC thermograms for multilayered films having composition PC/PS of 95/5, thickness 125µm and number of layers 257 with different heating rates.

Heating thermograms for pure materials in the form of 257 layered films where PC in multilayers was replaced by PS (for PS) and PS was replaced by PC (for PC) showed the glass transition for PS in the range of 107.6˚C, and for PC we could observe T_g at 154.1˚C. But for example, for 257 layered film PC/PS, 70/30,125µm thick, where the thickness of PS was 290 nm and the thickness of PC was 680 nm

the glass transition temperature is at 109.1 and 151.7^{o}C for PS and PC component respectively (Table 3.5):

Material:	**Q1000, ramp 30˚C/min.**	
	T_g of PS [˚C]	**T_g of PC [˚C]**
PC control, 125 µm	-	154,08
PC/PS, 70/30, 125µm	109,09	151,71
PS control, 125 µm	107,62	-

Table 3.5. Shifts in glass transition temperatures of PC and PS in multilayered film with 257 layers.

In Figure 3.6 we can see heating thermograms for all studied 257 layered films PC/PS with relative compositions and thicknesses of each layers as shown in Tables 2.1 and 2.2:

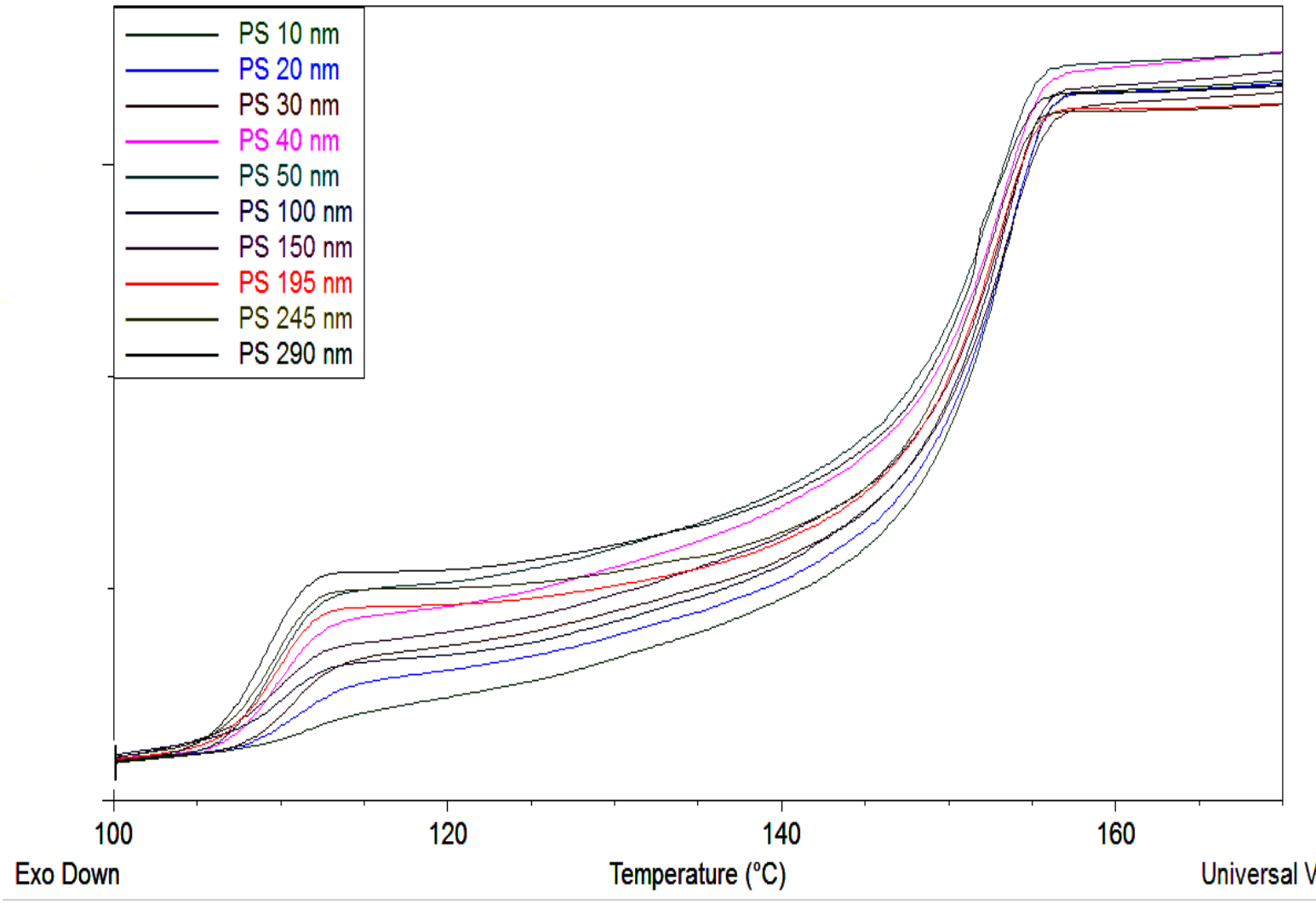

Figure 3.6. Heating thermograms of multilayerd films PC/PS with different thicknesses of PS layers – Table 1 and 2 in Experimental part of the thesis (DSC Q1000, films 25 and 125µm, weight around 10 mg, heating rate 30°C/min.).

From the analysis of this DSC results we can conclude that there is a small dependence of T_g on the thickness of PS layer, what was confirmed by the graph below. A small increase of T_g occurs when PS thickness goes below 150 nm.

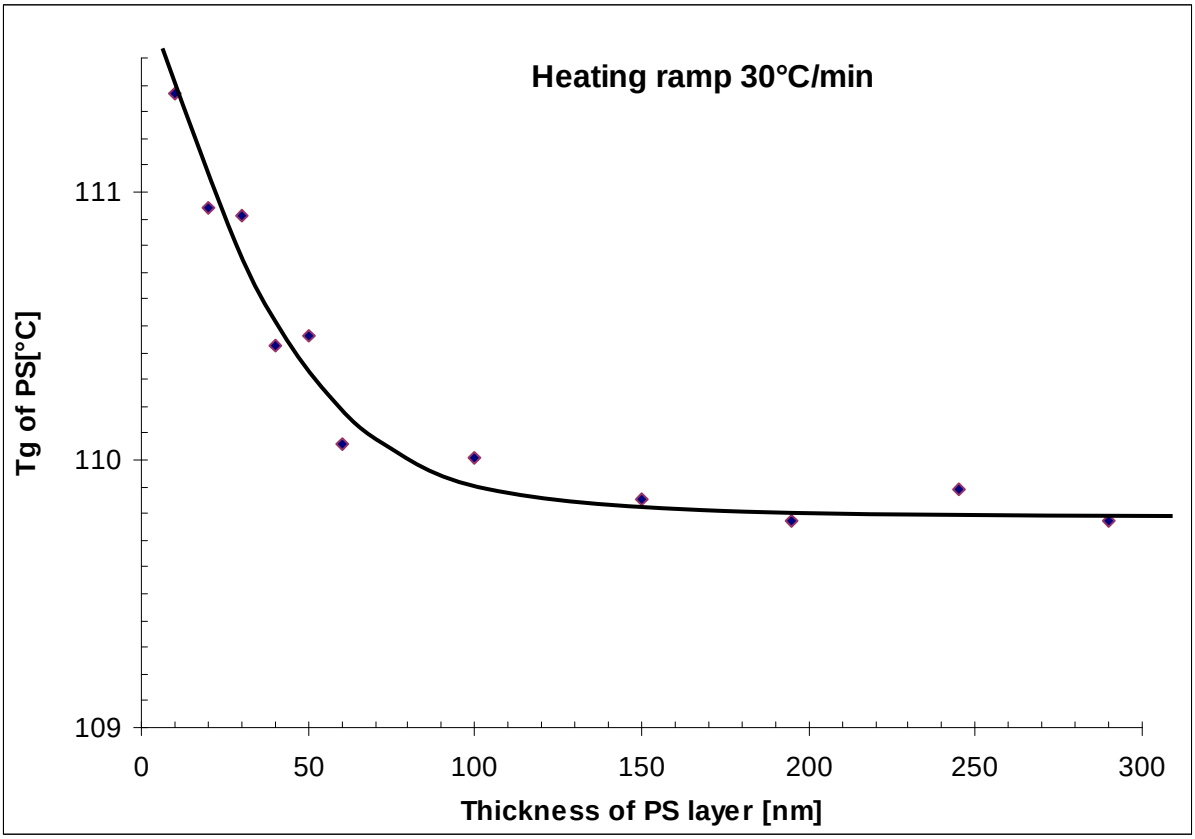

Figure 3.7. Dependence : T_g versus layers thicknesses: a continuous increase of T_g with decreasing PS layer thickness resulting in a difference of about 2°C between PS 10 nm and PS 290 nm.

In order to prove that T_g of PS in multilayers depends on the thickness of PS layer and does not depend on the weight composition of the film or on the thickness of PC layers three summary Figures are presented (Figures 3.8, 3.9, 3.10):

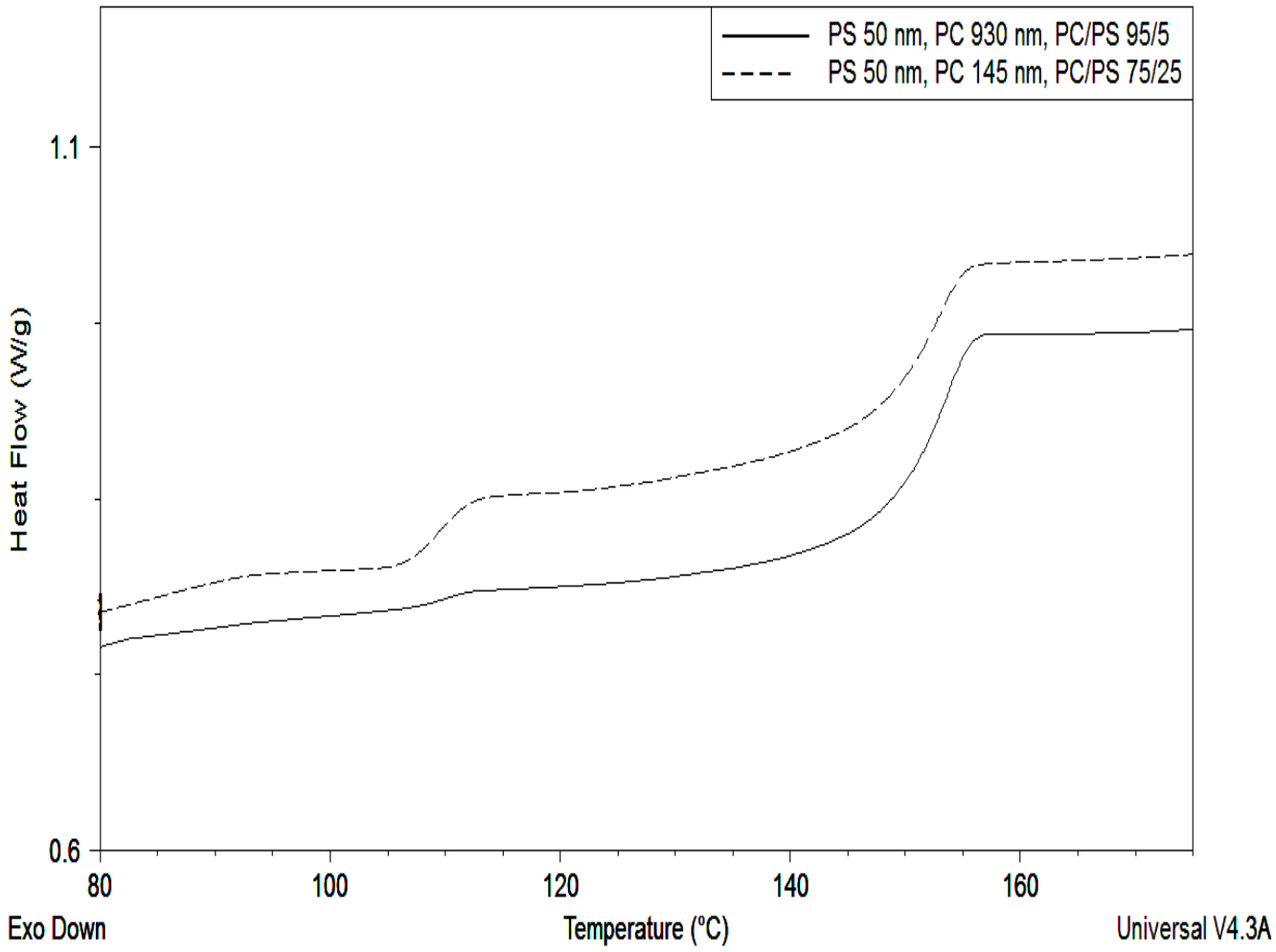

Figure 3.8. Heating thermograms for multilayerd films PC/PS with the same thickness of PS layer, different weight compositions and thickness of PC layer.

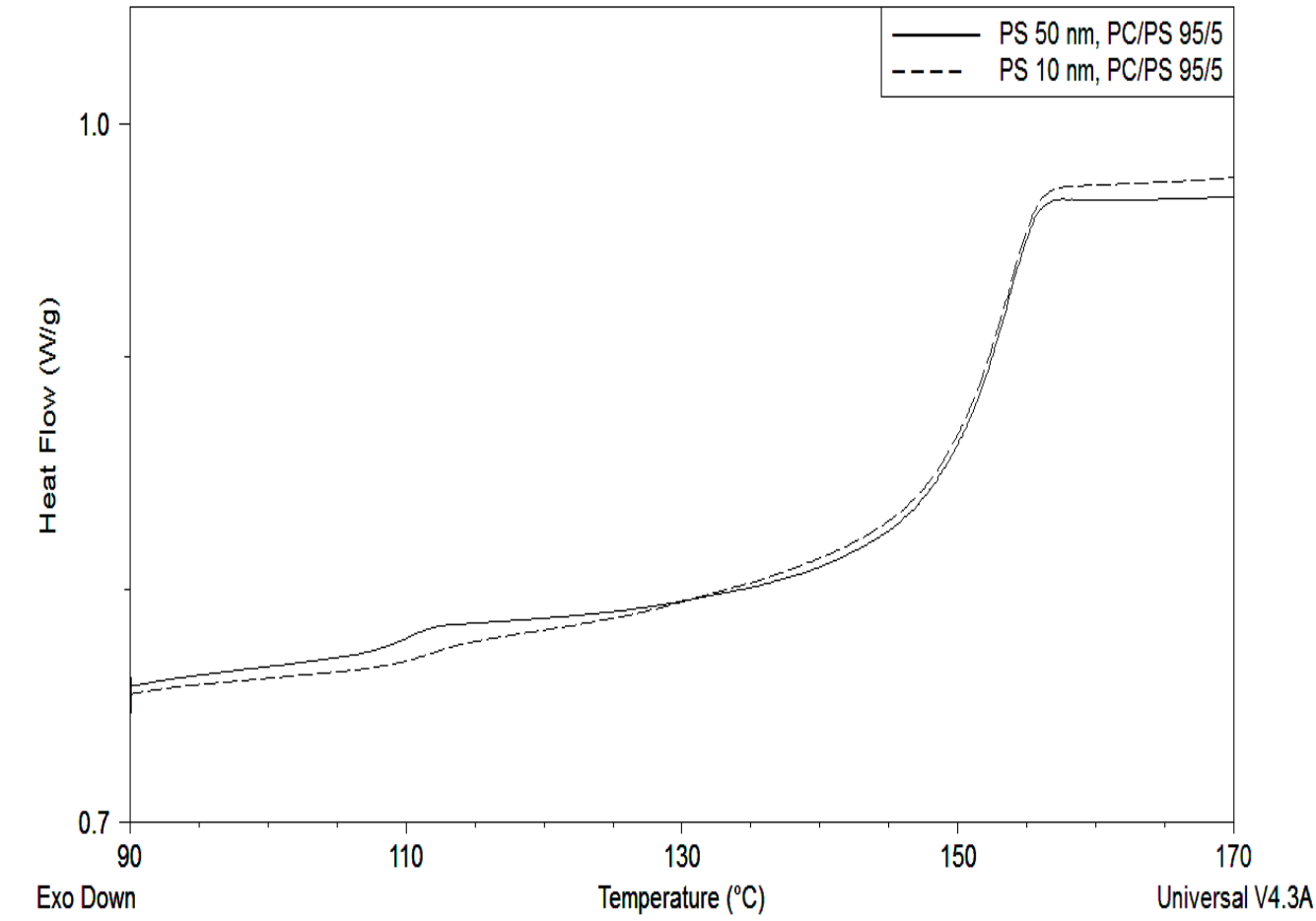

Figure 3.9. Heating thermograms for multilayerd films PC/PS with different thicknesses of PS layer, the same weight composition of the film (PC/PS, 95/5).

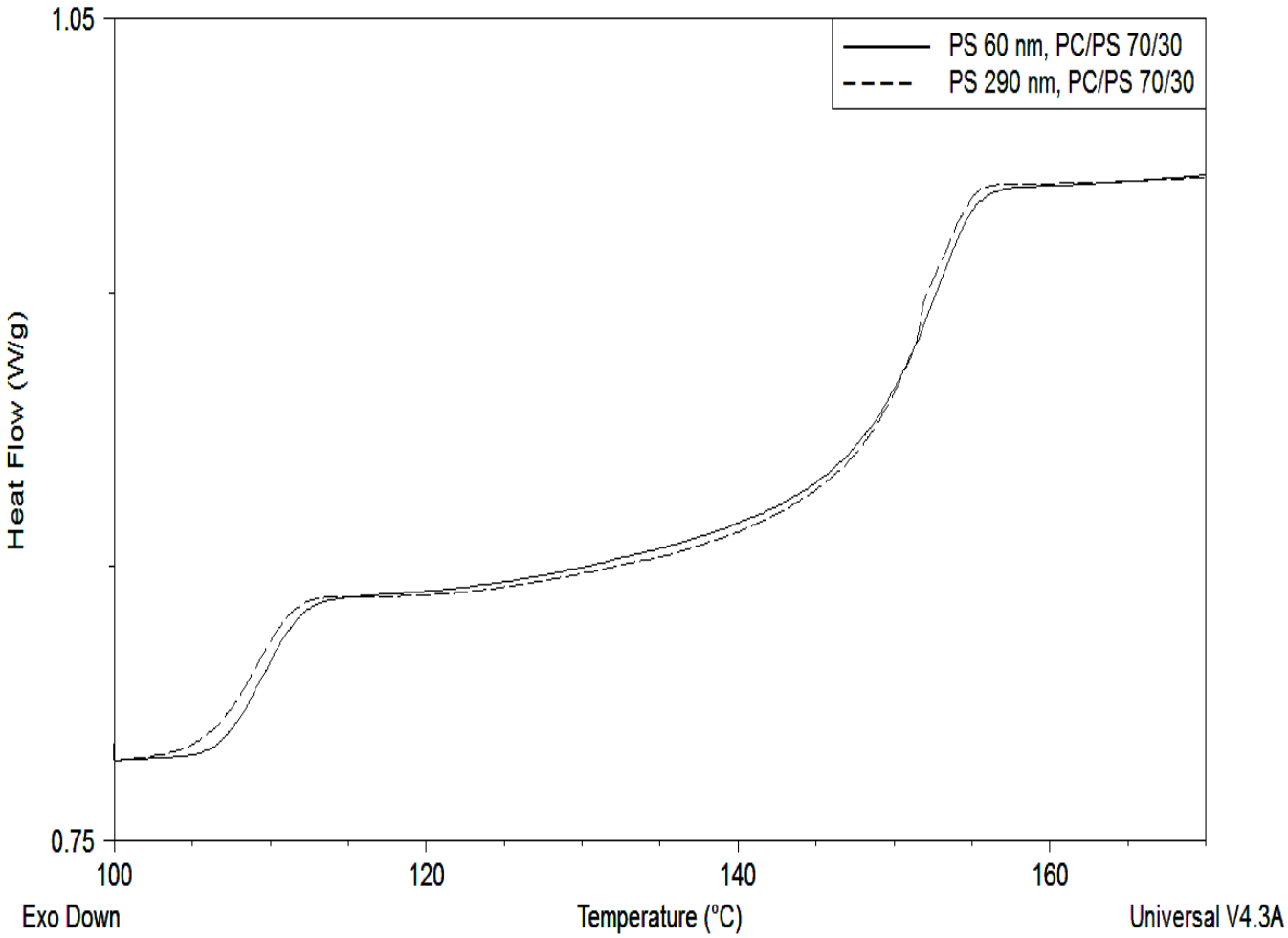

Figure 3.10. Heating thermograms for multilayerd films PC/PS with different thicknesses of PS layer, the same weight composition of the film (PC/PS, 70/30).

From Figure 3.8 we can conclude that when the thickness of PS layer in the multilayered films PC/PS is the same and during that time the weight composition of the film and the thickness of PC layer are different, the T_g of PS has the same value – 110,20 °C.

But when we look on Figures 3.9 and 3.10 where we have different thicknesses of PS layers and the same weight composition of the film we can see that there is a shift in

glass transition temperature of PS (PS 10nm – T_g = 111,37ºC, PS 50nm - T_g = 110,20 ºC, PS 60 nm – T_g = 110,06ºC, PS 290 nm – T_g = 109,09ºC).

Shifts of glass transition temperature are observed in multilayer films: for PS component towards higher temperature while PC still being glassy and for PC towards lower temperature while PS being in rubbery phase. The glass transition temperature shifts suggest rather significant interactions between PS and PC components. When PS layer thickness is decreasing, the molecular mobility seems to be lowered. This phenomenon begins for a thickness of about 150nm. For PC layers, smaller variations could be also noticed (less than 1 or 2 degrees), but T_g is decreasing, which means a small increase of molecular mobility.

3.2. Dynamics of the chains in the vicinity of PS/PC interface.

The aim of these studies was to find a way of sensing and to elucidate the influence of one polymer on the other at the interface.

Two different phases or two dissimilar polymers while being in contact interact with each other and form an interface. The interaction occurs at the surfaces of substances involved, that is at their interfaces. The interaction between polymers is usually described by interfacial tension or energy. Interfacial tension arises at an interface from the imbalance of forces between molecules at an interface, molecules at the interface experience an imbalance of forces. This leads to accumulation of free energy at the interface. The main forces involved in interfacial tension are adhesive forces between one phase or polymer and another phase or polymer. The interface is

not infinitely thin; the depth of interaction depends on a physico-chemical similarity of a pair of polymers, also the thickness of the interfacial layer.
Polymer blends are systems with highly developed interfaces. However, when two immiscible polymers are blended the interfaces are not anymore flat. That is because usually polymer blend morphology resembles a dispersion with micrometer sized inclusions of a minor component. In such blends surface tension exerts a pressure on a spherical drop that is higher if the drop is smaller according to the formula:

$$p = - \gamma_A / 2r \qquad (3.3)$$

where r is the radius of the drop. For small micro- and nanometer drops the pressure can reach significant values. In addition a difference in thermal expansibilities of polymers may produce extra component of pressure. Flat interfaces are then better defined objects for studying interfaces between two polymers.

Thickness of the interface layer depends very much on polymers being in contact. There are reports indicating that the interface layer between polymers can be as thick as 10 nm. A bilayer film will have a single interface layer; the volume of interface layer is, however, a small fraction of the entire volume of a bilayer film. Multilayer films that can be produced by forced assembly through layer-multiplying coextrusion contain multifold larger amount of interfaces because for 2^n layers there are $2^n - 1$ interfacial layers.

Solid state nuclear magnetic resonance (SSNMR) was chosen as the main tool for investigation of interactions at interfaces. Dielectric relaxation spectroscopy was chosen as the second method for these purposes.

3.2.1. SS NMR study

Important source of information about the structure and dynamics of polymers are dipolar recoupling experiments which are well suited for measuring motional averaging at multiple sites simultaneously in biomolecules and synthetic polymers. In two-dimensional (2D) approach, separated local field sequences can reintroduce dipolar anisotropic interactions and correlate them to isotropic chemical shifts. The Lee–Goldburg cross-polarization (LG CP) and polarization inversion spin exchange at the magic angle (PISEMA) pulse sequences were recently used to correlate the motionally average anisotropic dipolar interactions with high-resolution chemical shift dimensions during MAS in 2D approach.

We expected to gain the information about how far is the interaction between PS and PC reaching, how it changes with temperature when the mobility of PS or PC macromolecules is activated and what is the influence of the other component. Finally we wanted to learn how the interactions at interfaces influence the overall properties of multilayered film.

3.2.1.1. ^{13}C CP/MAS NMR spectra for PC and PS.

To reach such a goal firstly we performed ^{13}C CP/MAS NMR of pure PC and PS and then of multilayered film PC/PS, 70/30, 125μm.

Figure 3.11 displays ^{13}C CP/MAS NMR spectra of PC and PS films recorded at room temperature with the spinning rate 8 kHz (Figure 3.11a and 3.11b respectively). The structure assignment is given also in those Figures. The numbering system for PC and PS polymers is shown as inset in the top of spectra. From inspection of data it is apparent that signals for PC sample representing C1, C2 and C5 carbons are overlapped and observed as broadened peak at average chemical shift at *ca* 150 ppm. Resonances of C3 and C4 carbons are well separated and found at δ = 120.4 ppm and δ=128.3 ppm. Aliphatic part of PC is represented by two sets of NMR signals, quaternary carbon C6 at δ =42.4 and methyl group carbons D1 at δ =30.9 ppm.

^{13}C CP/MAS spectrum of PS film shown in Figure 3.11b is represented by three sets of signals, quaternary carbons B1 at δ =145.4 ppm, overlapped aromatic B2, B3 and B4 at δ = 126-128 ppm and broadened aliphatic A1 and A2 signals at 40-46 ppm. From preliminary study of pure polymer films it was evident that some NMR signals from both samples are in very similar regions. This observation is confirmed by NMR investigation of coextruded multilayered PC/PS film in Figure 3.12.

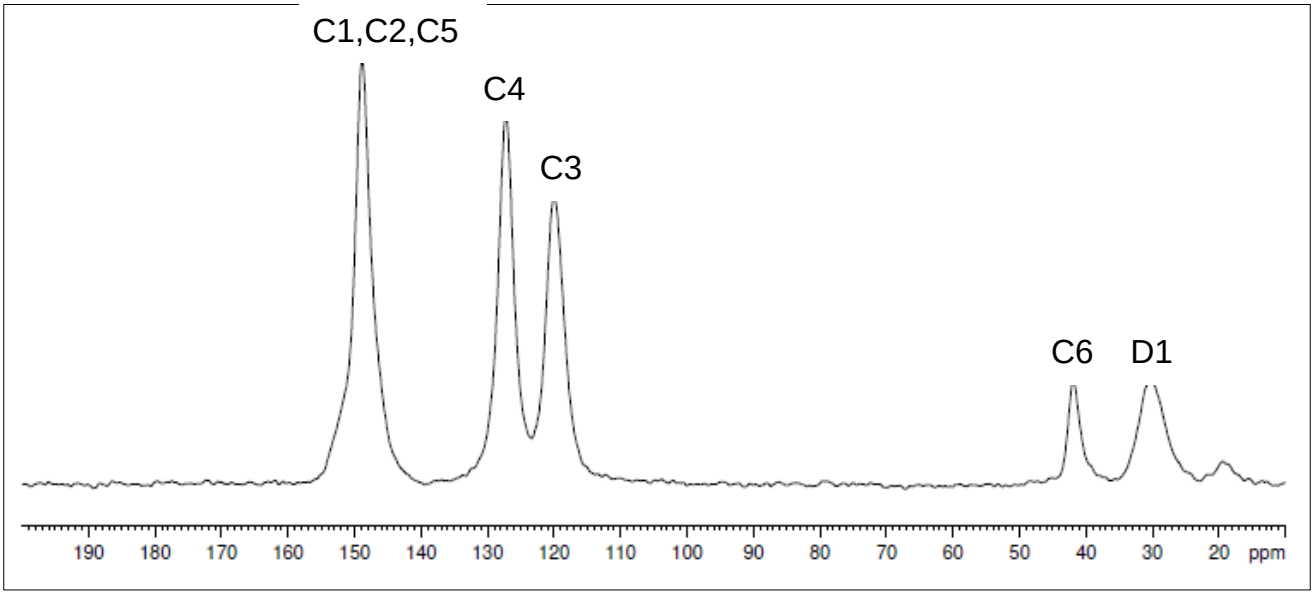

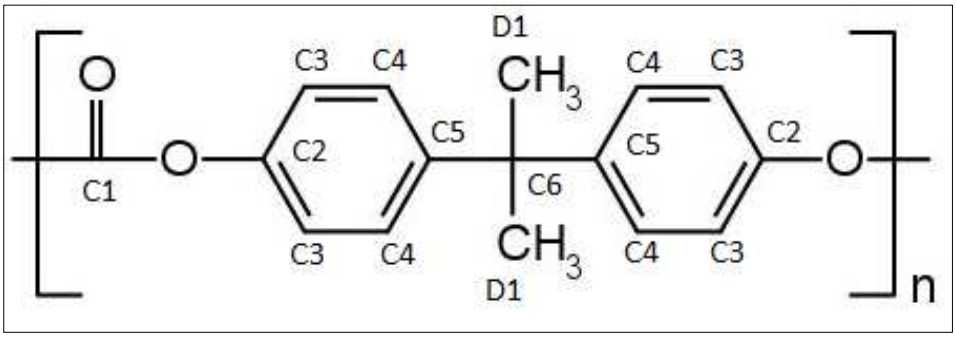

Code	Shift (ppm)
C1	152.1
C2	148.4
C3	120.4
C4	128.3
C5	149.3
C6	42.4
D1	30.9

Figure 3.11a. ^{13}C CP/MAS NMR spectra of PC.

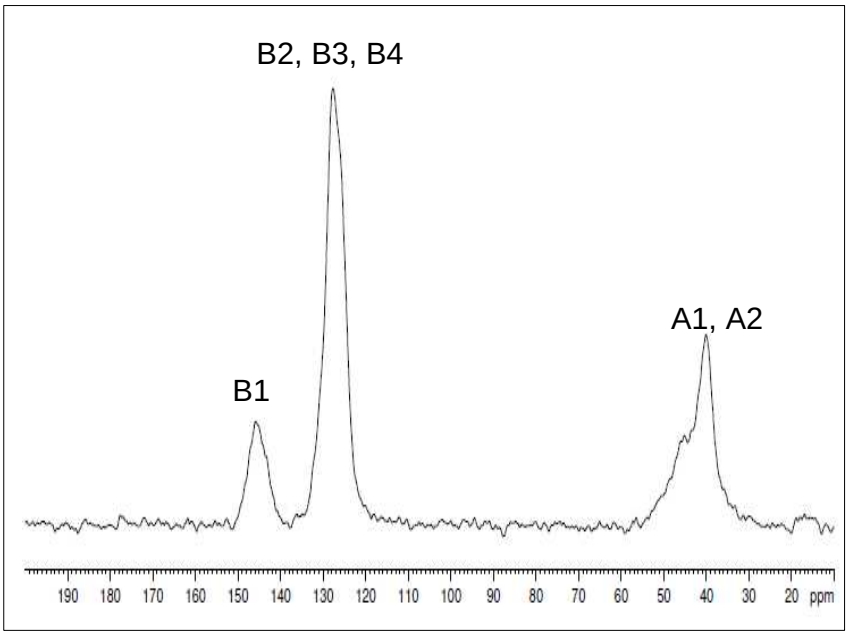

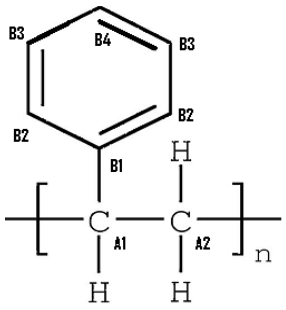

Code	Shift (ppm)
A1	41-46
A2	40.5
B1	145.4
B2	128.0
B3	128.0
B4	125.7

Figure 3.11b. ^{13}C CP/MAS NMR spectra of PS.

3.2.1.2. ^{13}C CP/MAS NMR spectra for multilayered films PC/PS.

Figure 3.12 shows ^{13}C CP/MAS NMR spectrum of multilayer film PC/PS, 70/30, 125 μm recorded under exactly the same conditions as those presented in Figures 3.11. As predicted some resonances representative for PC and PS polymer films are overlapped (Figure 3.13). For instance, signal centered at δ=128 ppm represents C4 carbon of PC and B2, B3,B4 carbons of PS. Signal at δ=120.4 ppm represents exclusively carbon C3 of PC. Thus, by simple integration of these two signals we can conclude the proportion of PC and PS components in the films (Figure 3.14) keeping in mind that region of 128 ppm represents one carbon of PC and three carbons of PS while the region around 120.4 ppm is only for PC.

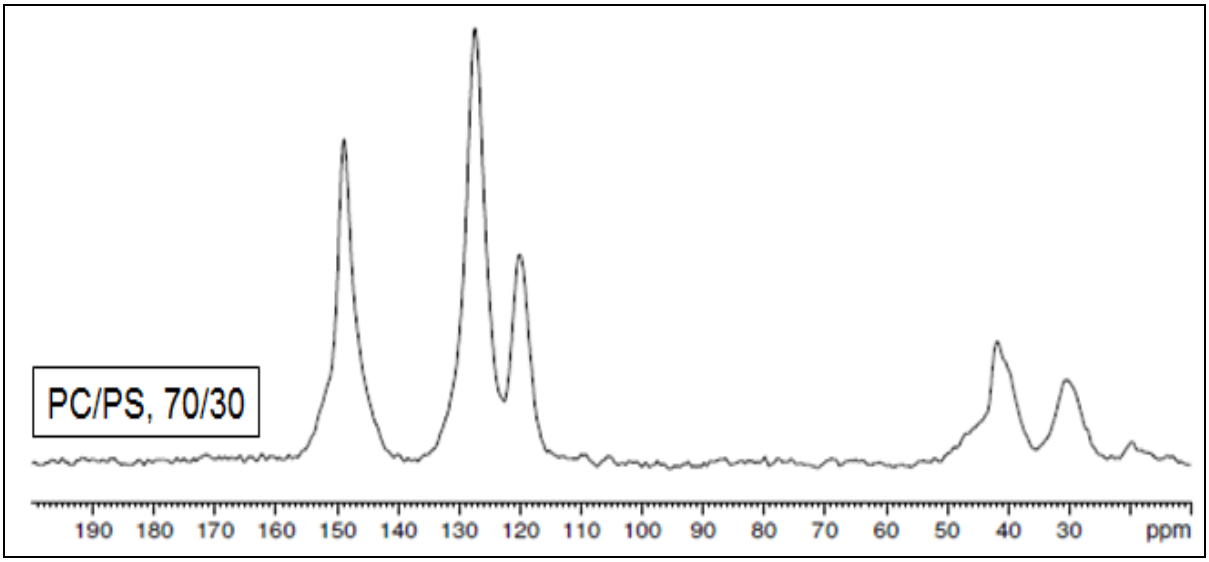

Figure 3.12. ^{13}C CP/MAS NMR spectra of PC/PS, 70/30, 125 μm thick film.

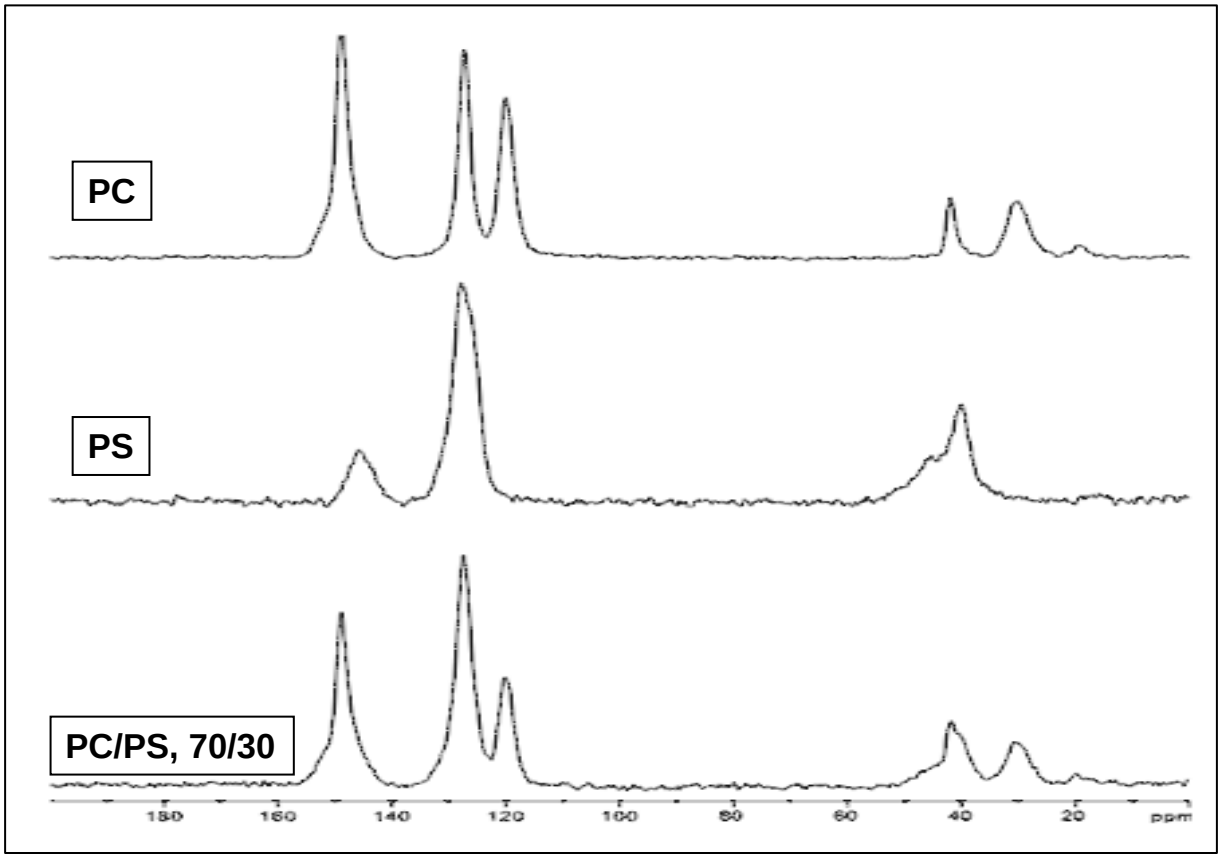

Figure 3.13. Comparison of ^{13}C CP/MAS NMR spectra of PC, PS and PC/PS, 70/30, 125 μm thick film.

^{13}C CP/MAS NMR spectrum of multilayer film PC/PS, 95/5 , 125 μm was recorded under exactly the same conditions as those for pure PC and PS samples and for multilayered film PC/PS, 70/30.

From Figure 3.13 we can see, as it was said above, that it is possible to measure the proportion of PC and PS components in the multilayered films PC/PS by integrating the respective peaks and solving simple equation.

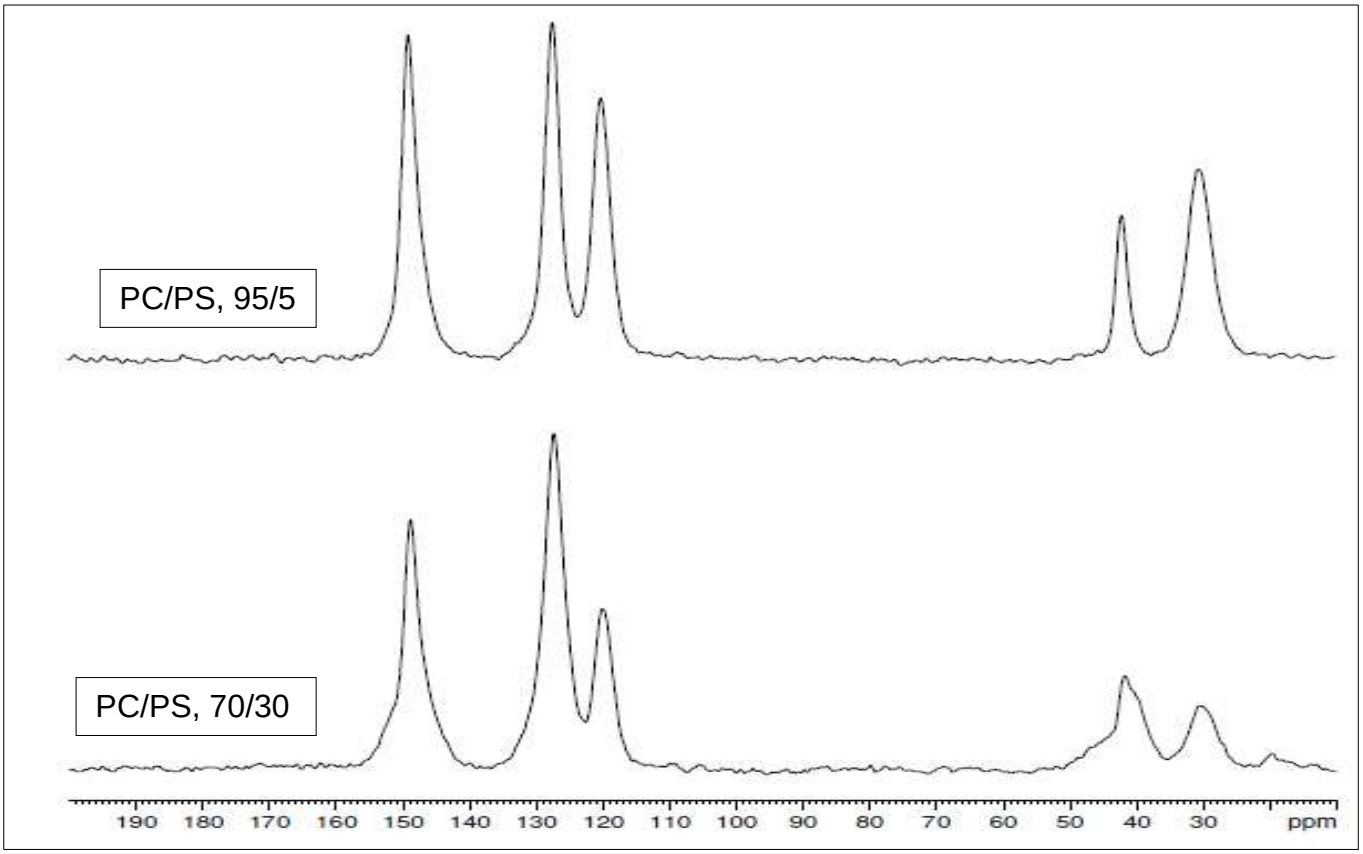

Figure 3.14. Comparison of ^{13}C CP/MAS NMR spectra of PC/PS, 70/30, 125 μm thick film and PC/PS, 95/5, 125 μm thick film.

3.2.1.3. LG-CP - phase-inverted LG recoupling under MAS measurements.

Further in this study, for analysis of the effect of molecular motion on the line shape of the dipolar spectra, sensitivity-enhanced LG-CP measurement was carried out, employing PILGRIM pulse sequence (phase-inverted LG recoupling under MAS) as shown in Figure 3.15a. Compared to standard LG CP (Figure 3.15b) the theoretical sensitivity enhancement factor for PILGRIM is equal 2 (in practice less).

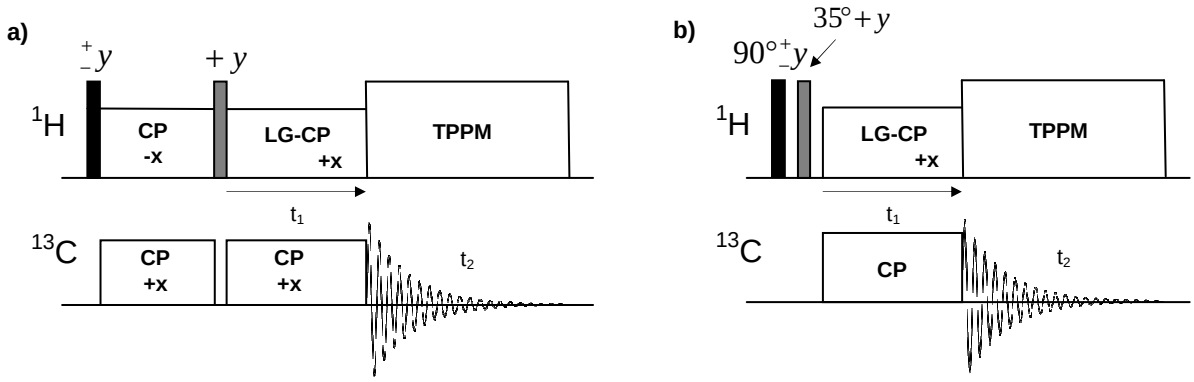

Figure 3.15. Pulse sequences : (a) 2D PILGRIM, (b) 2D LG-CP MAS.

Figures 3.16 a, b, c, shows contour plots of 2D spectrum for PC,PS and PC/PS 70/30 film recorded with spinning rate 13 kHz at ambient temperature. The ^{1}H effective field strength, ω_{1Heff}, was matched to the ^{13}C spin-lock field strength δ_{13C}, by $\omega_{1Heff} - \omega_{13C} = \omega_r$ (-1 condition). The LG CP contact time was incremented asynchronously with rotation to yield the heteronuclear dipolar dimension of the 2D experiment. The ^{13}C-spin isotropic chemical shift was detected in the second dimension of the experiment. Similar experiment, under exactly the same conditions as for sample PC was carried out for PS as well as for the PC/PS, 70/30, 125 μm film.

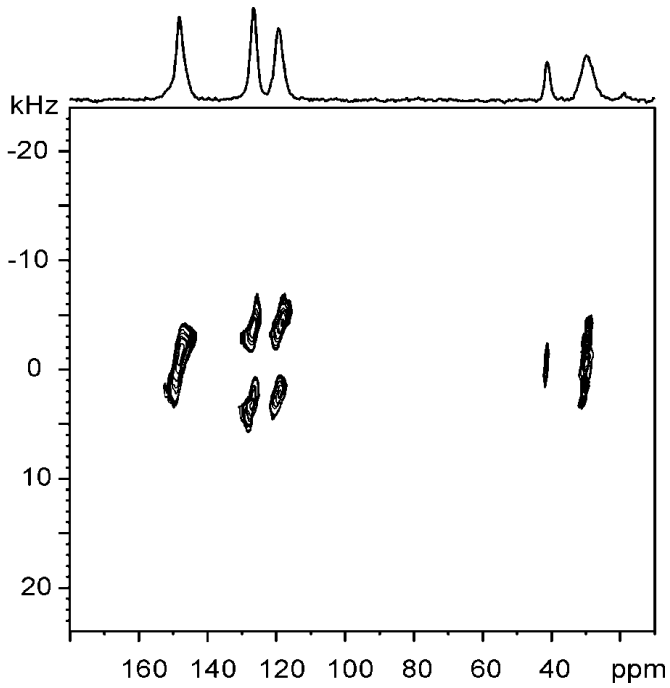

Figure 3.16a. Contour plot of 2D spectrum for PC film at room temperature.

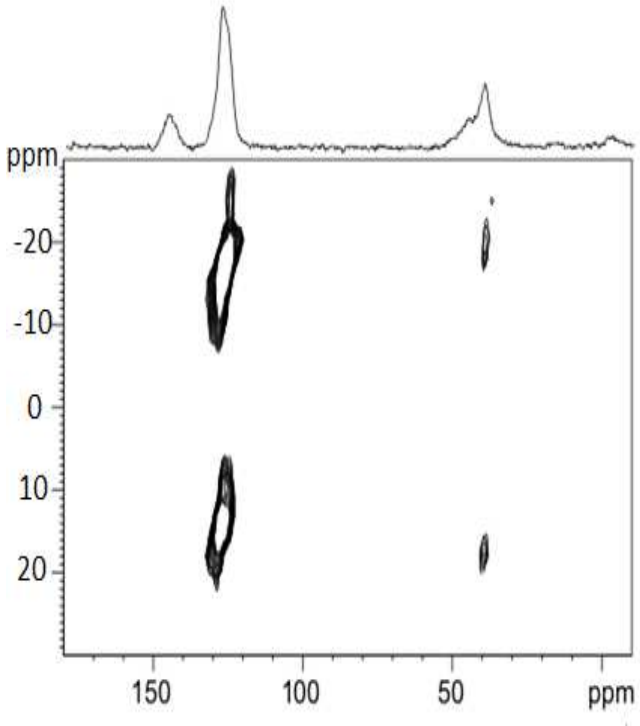

Figure 3.16b. Contour plot of 2D spectrum for PS film at room temperature.

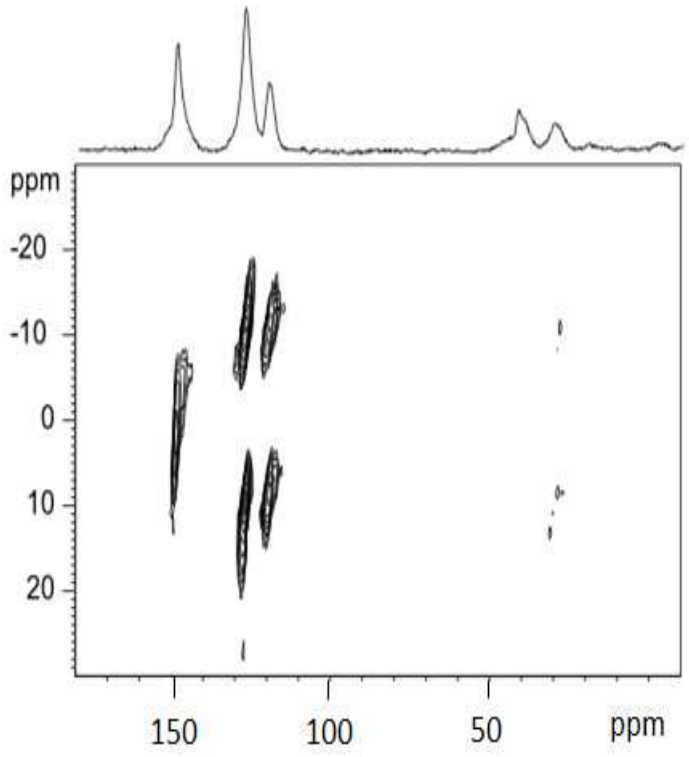

Figure 3.16c. Contour plot of 2D spectrum for PC/PS70/30 film at room temperature.

Figure 3.17 shows the 1D projections taken from PILGRIM correlations for PC film recorded at temperatures 296 K, 373 K and 393 K. Similar Variable Temperature (VT) measurements were carried out for PS film, however since the glass transition for PS is in the range of 378 K- 383 K, measurements for PS were performed at 296 K, 348 K , 373 K and 388K (middle column). The VT LG CP approach was also employed for 70/30, PC/PS 125μm thick multilayered film (right column).

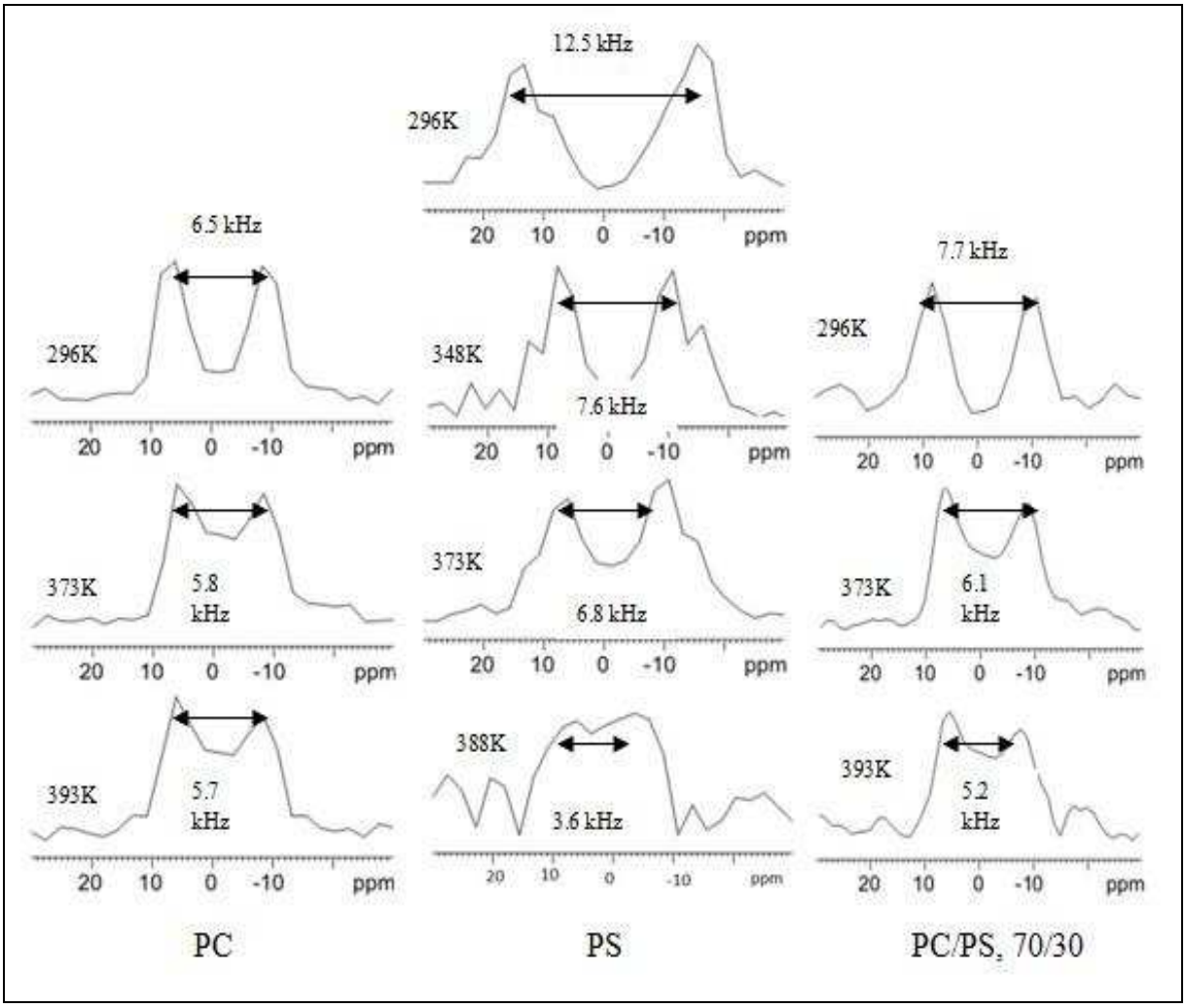

Figure 3.17. 1D projections taken from PILGRIM correlations.

From inspection of 1D spectra shown in Figure 3.17 the distinct molecular dynamics for pure polymers can be concluded. For PC film measured at 296 K the line shape of ^{1}H - ^{13}C doublet and splitting between singularities is exactly the same as those reported for powdered PC sample[127]. With the increase of temperature the dip between singularities becomes smaller. It is very likely related to the increase of wobbling amplitude with temperature.

The lineshape of PS film (middle column) at 296 K is significantly different compared to PC.

That LG CP results clearly prove that at 296 K phenyl ring orientation in PS film is static. The splitting between singularities is 12.5 kHz, typical value for rigid aromatic systems[128]. The few percents of mobile component (if exists in this sample) was not

detected by PILGRIM experiment. At slightly higher temperature (348 K) the presence of two subspectra with splitting equal to 7.6 kHz and 11.8 kHz is apparent. The mobile component, undergoing fast molecular motion is dominating. At the temperature 388 K the phenyl rings are very mobile. Splitting between singularities for Pake doublet is very small.

Finally the influence of PS on dynamics of phenyl rings of PC was searched for PC/PS film with ratio 70/30 in the temperature range from 296 K to 393 K (right column). It is clear from this study that at 296 K the splitting for this film is slightly larger (7.7 kHz) compared to PC. At 373 K the splitting is 6.1 kHz while at 393 K splitting is 5.2 kHz.

The influence of PS on dynamics of phenyl rings of PC for PC/PS film depends very much on the temperature or rather on the level of departure from its glassy state. It is clear from this study that the splitting between singularities in 1D spectra of PILGRIM decreases with the increase of the temperature. The value of splitting gets significantly smaller than in the case of pure PC film. It means that above the glass transition temperature of PS the PC component of a multilayer film, although still being in glassy state, becomes more flexible.

In order to obtain more information about the molecular dynamics of the systems also relaxation times $^{1}H_{T1\varsigma}$ were measured.

$^{1}H_{T1\varsigma}$ times were measured for PC, PC/PS,70/30 and 95/5, 125µm and PS in the range of temperatures 296K- 373K. From those measurements we prepared an Arrhenius plot, presented in Figure 3.18:

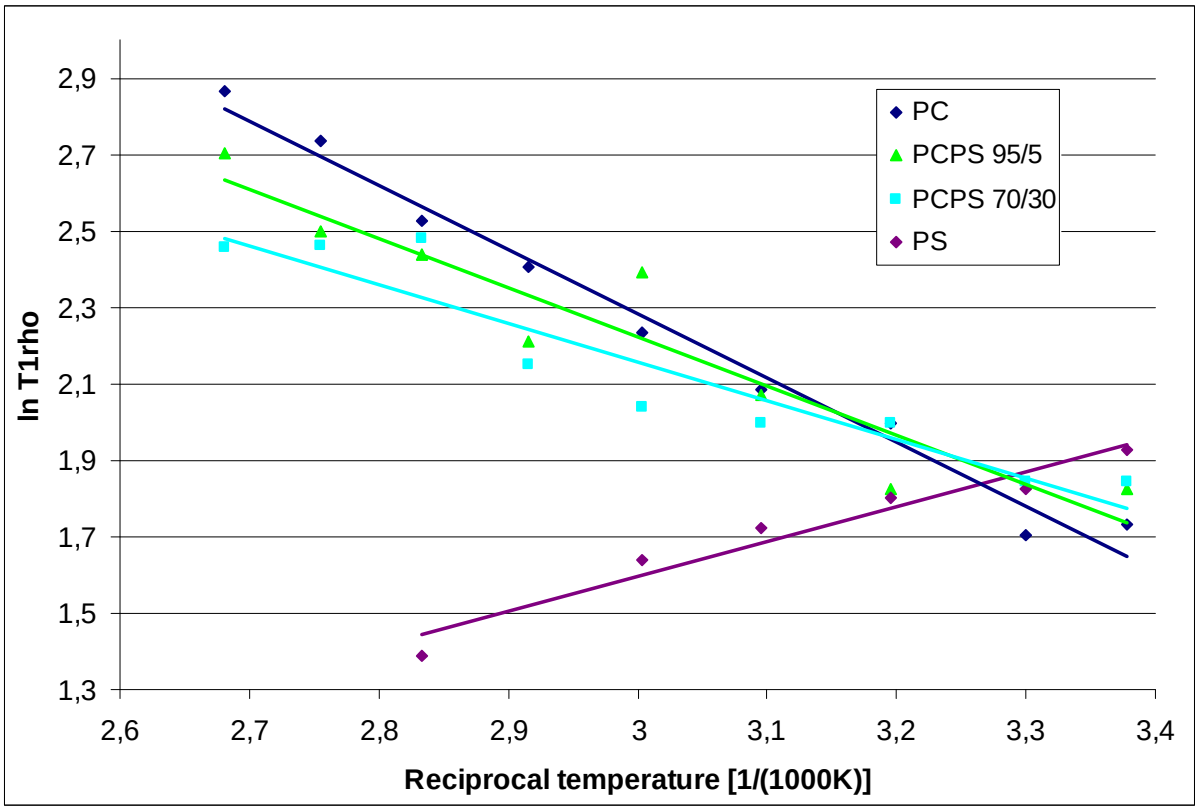

Figure 3.18. Arhenius plot : $^{1}H_{T1\varsigma}$ relaxation times measured for PC, PC/PS and PS in the range of temperatures 296K- 373K.

From this plot we can see that polystyrene is behaving totally different from other films (PC, PC/PS 70/30 and 95/5). The reason of these is that polystyrene is in different domain on the spin-lattice relaxation time vs. inverse temperature graph:

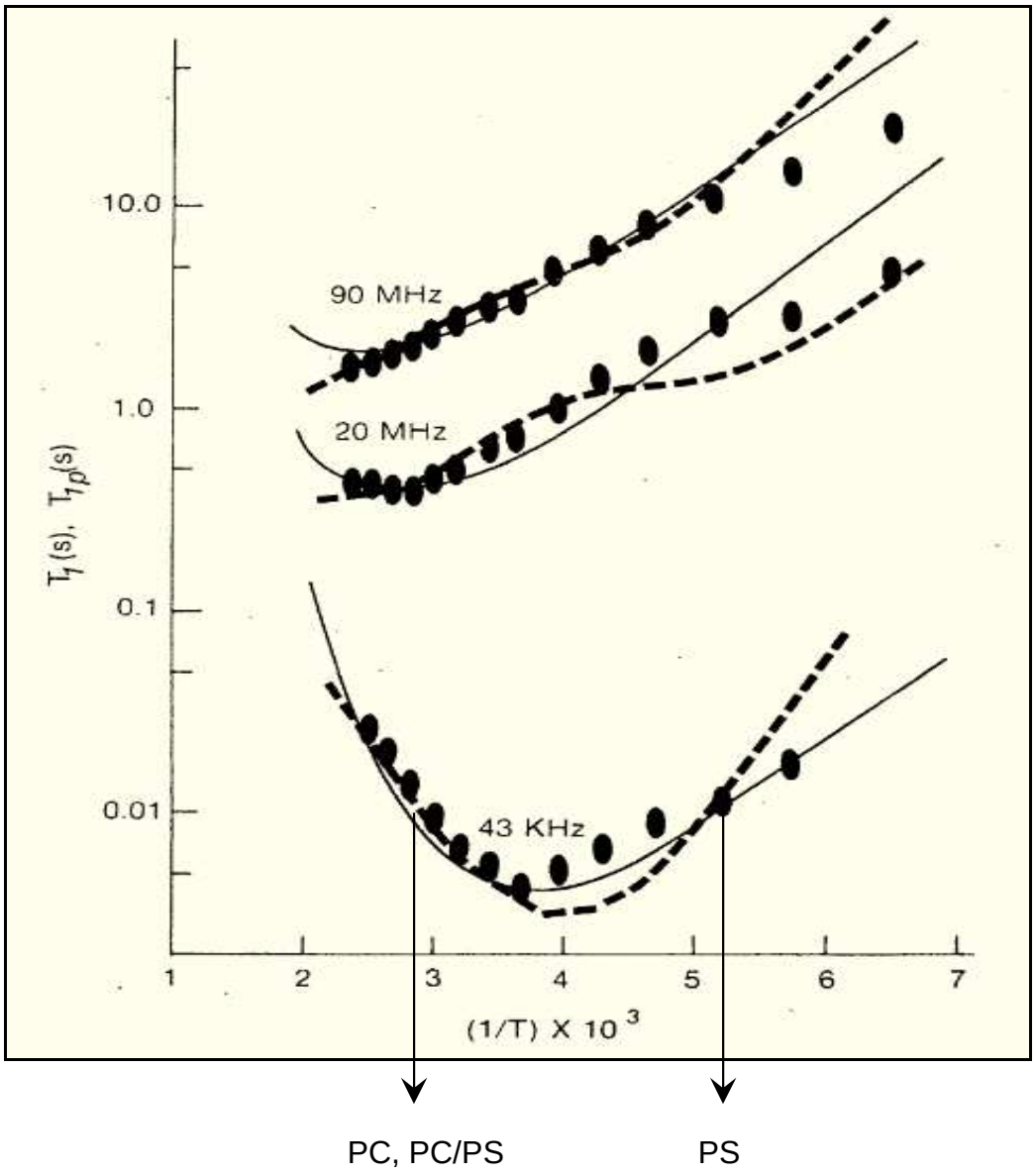

Figure 3.19. Spin-lattice relaxation time and the spin-lattice relaxation time in the rotating frame vs. inverse temperature[[129]].

That is why the correct Arrhenius analysis can be performed just for results of PC and films PC/PS 70/30 and 95/5 and not for PS alone.

.

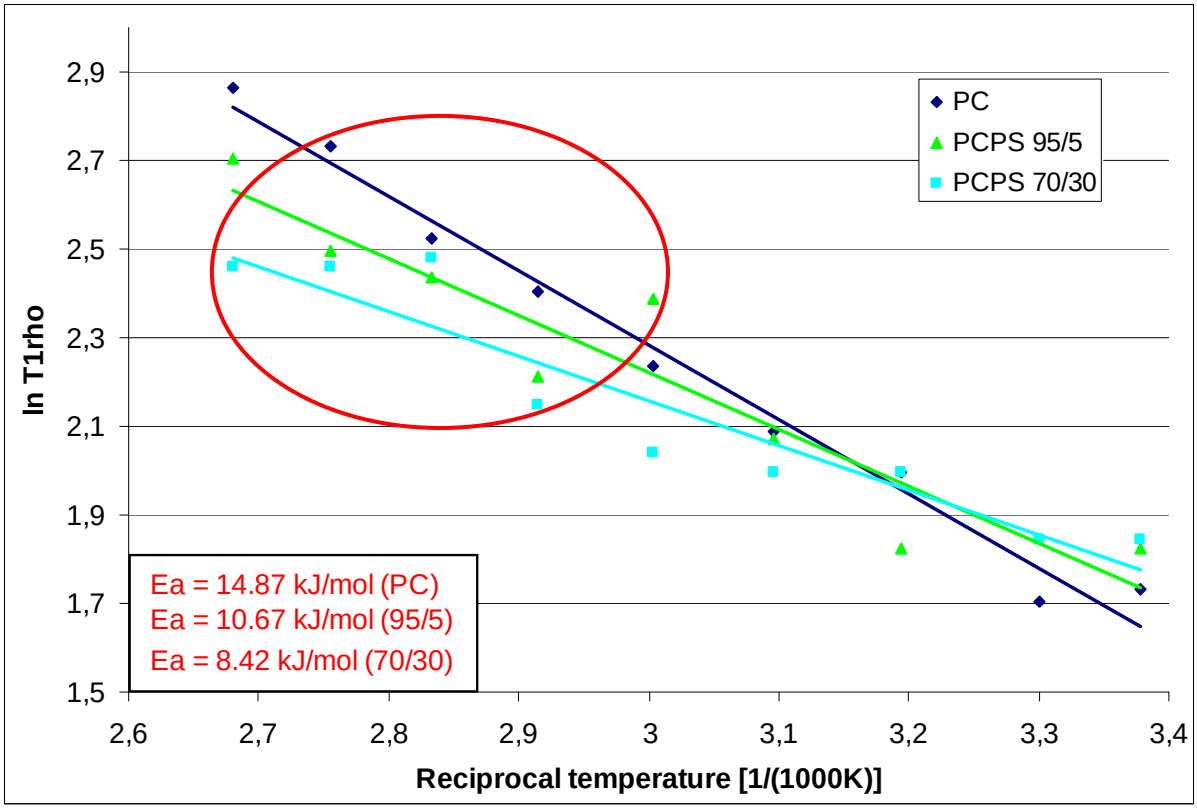

Figure 3.20. ^{1}H $T_{1\rho}$ relaxation times measured for PC and PC/PS composites in the range of temperatures 296K- 373K.

The activation energy of ^{1}H spin-lattice relaxation is the lowest for 70/30 multilayered film while the highest for pure PC. With lower activation energy the relaxation time is shorter hence ; the system is characterized by higher mobility.
From this graph we can conclude that the largest mobility has the film PC/PS, 70/30. As expected, the mobility, increases with temperature.

To summarize the SSNMR study we can say that our LG CP NMR spectra clearly proved that at room temperature phenyl ring orientation in PS film is rather random. The splitting between singularities is 12.5 kHz, which is a typical value for rigid aromatic systems. A mobile component was not detected by PILGRIM experiment. At 348 K the presence of two subspectra with different splitting is apparent. The mobile component, undergoing fast molecular motion is dominating. This effect is even

better seen at a higher temperature. At the temperature around and above the glass transition the phenyl rings of PS are very mobile.

The influence of PS on dynamics of phenyl rings of PC for PC/PS film depends very much on the temperature or rather on the level of departure from its glassy state. It is clear from our study that the splitting between singularities in 1D spectra of PILGRIM decreases with the increase of the temperature. The value of splitting gets significantly smaller than in the case of pure PC film. It means that above the glass transition temperature of PS the PC component of a multilayer film, although still being in glassy state, becomes more flexible.

3.2.2. Dielectrical properties.

3.2.2.1. Dielectric relaxation spectroscopy for reference materials PC and PS.

The first step to explore dielectrical properties of the multilayerd films PC/PS and to know if this 257 layered system is behaving like a normal 2-phase system, was to execute dielectric relaxation spectroscopy for reference materials PC and PS:

a)

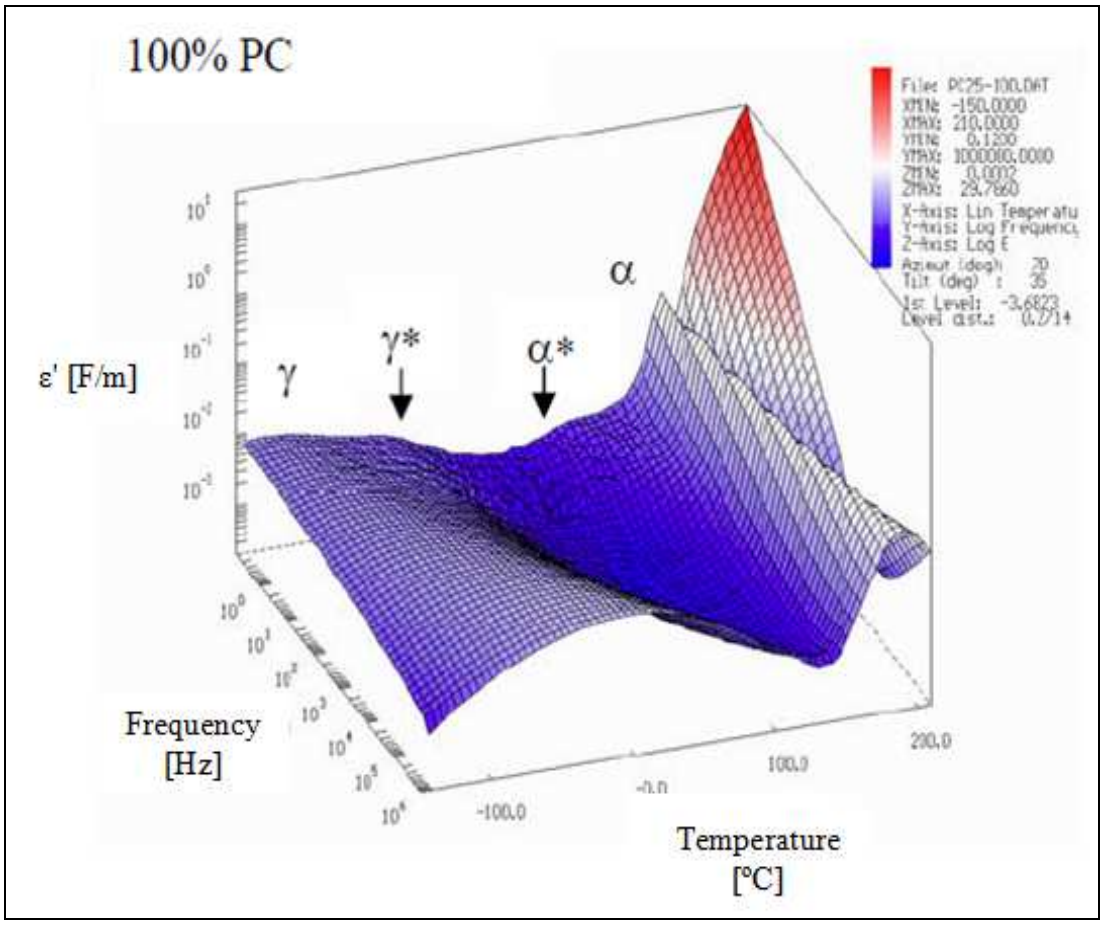

b)

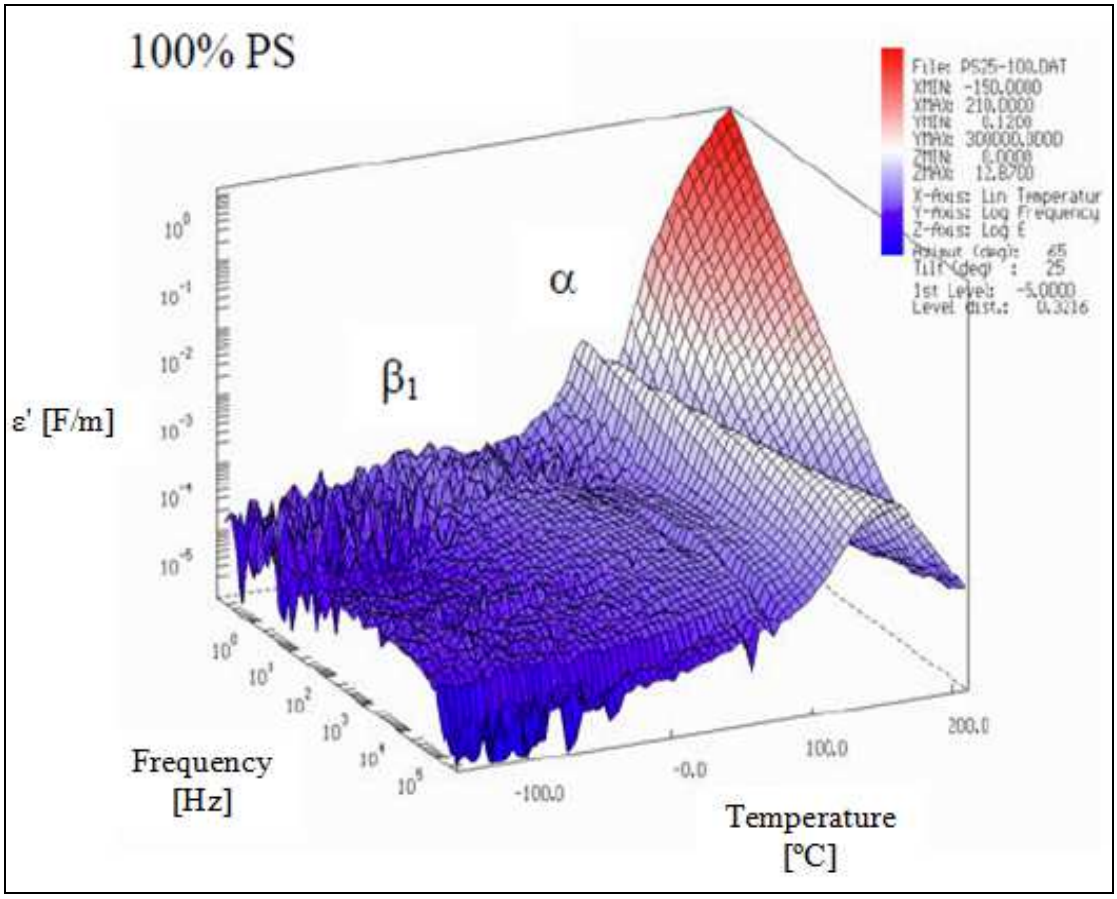

Figure 3.21. Dielectric relaxation spectroscopy for reference materials: a) PC and b) PS: permittivity versus frequency and temperature.

From inspection of the spectra for reference materials (Figure 3.21) we can see that single component films show the known relaxation processes:

- Polycarbonate: α-relaxation, γ-process
- Polystyrene: α-relaxation

In addition, PC reveals a slow component in the vicinity of the γ-process as well as a peak (α*) that might be related to local α-modes due to hindered physical aging. Another interesting feature is the β_1 relaxation for PS, a relaxation mode that was recently assigned to a dynamic helix inversion process caused by conformationally ordered syndiotactic sequences [130].

3.2.2.2. Dielectric relaxation spectroscopy for multilayered films PC/PS.

Subsequently dielectric relaxation spectroscopy for multilayered films with relative compositions 95/5, 90/10, 85/15, 80/20, 25μm thick, was done under exactly the same conditions. Those films were chosen in order to work with layers in the nano range.

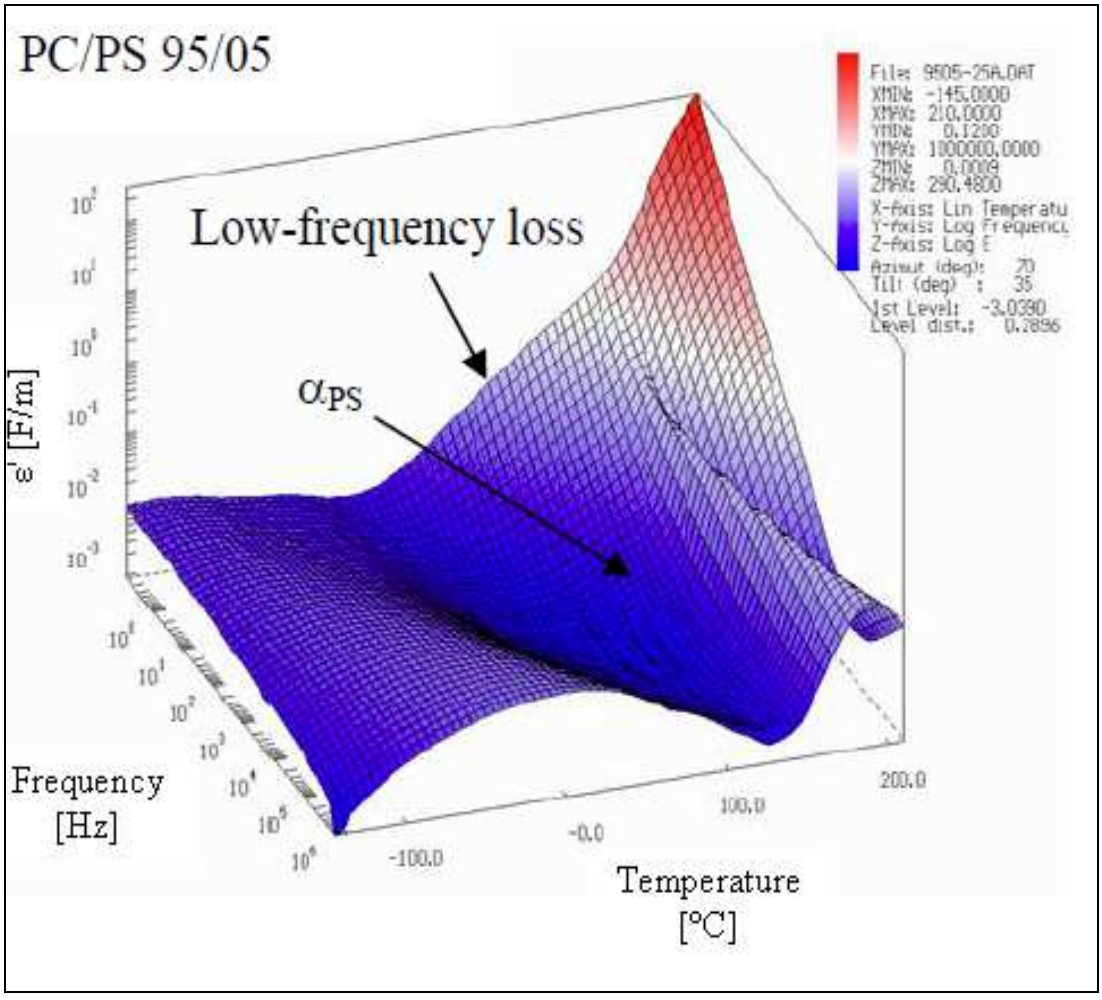

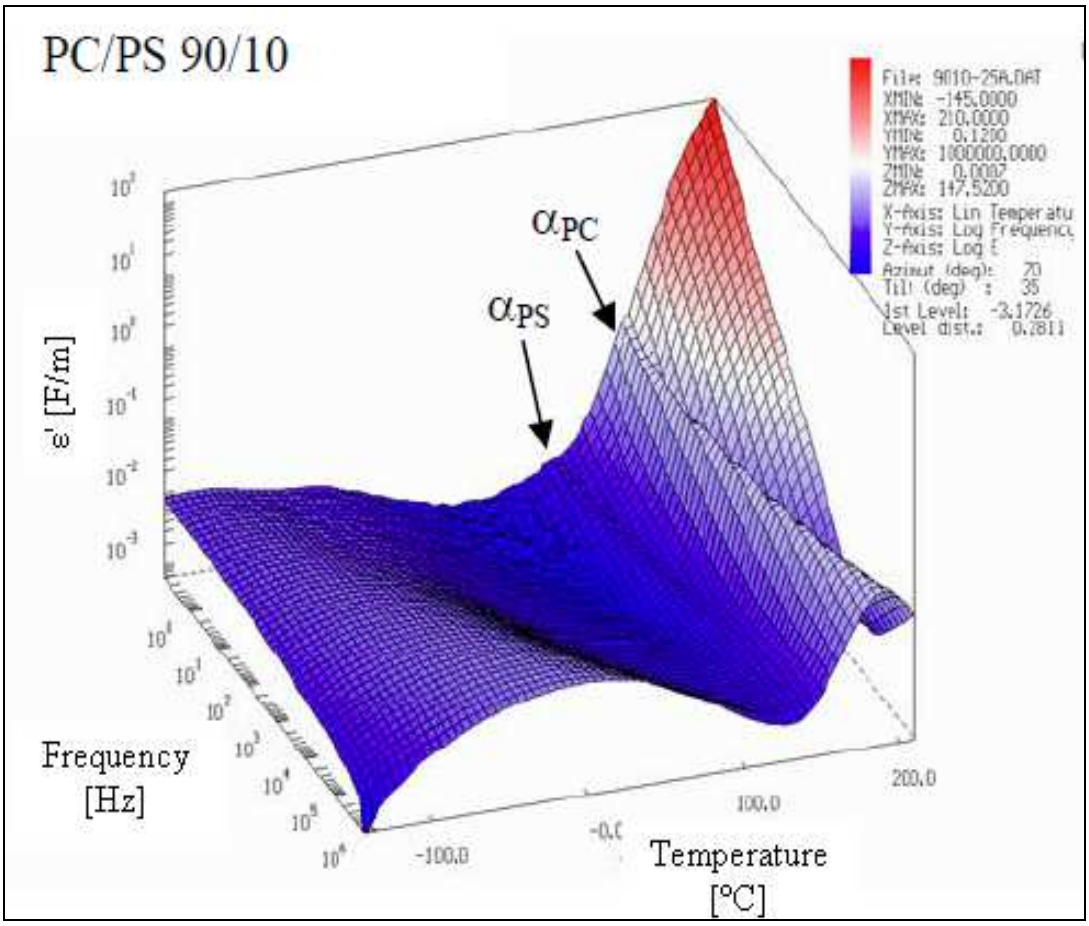
PC/PS 90/10
ε' [F/m]
α_{PC}
α_{PS}
Frequency
[Hz]
Temperature
[°C]
-100.0
100.0
200.0

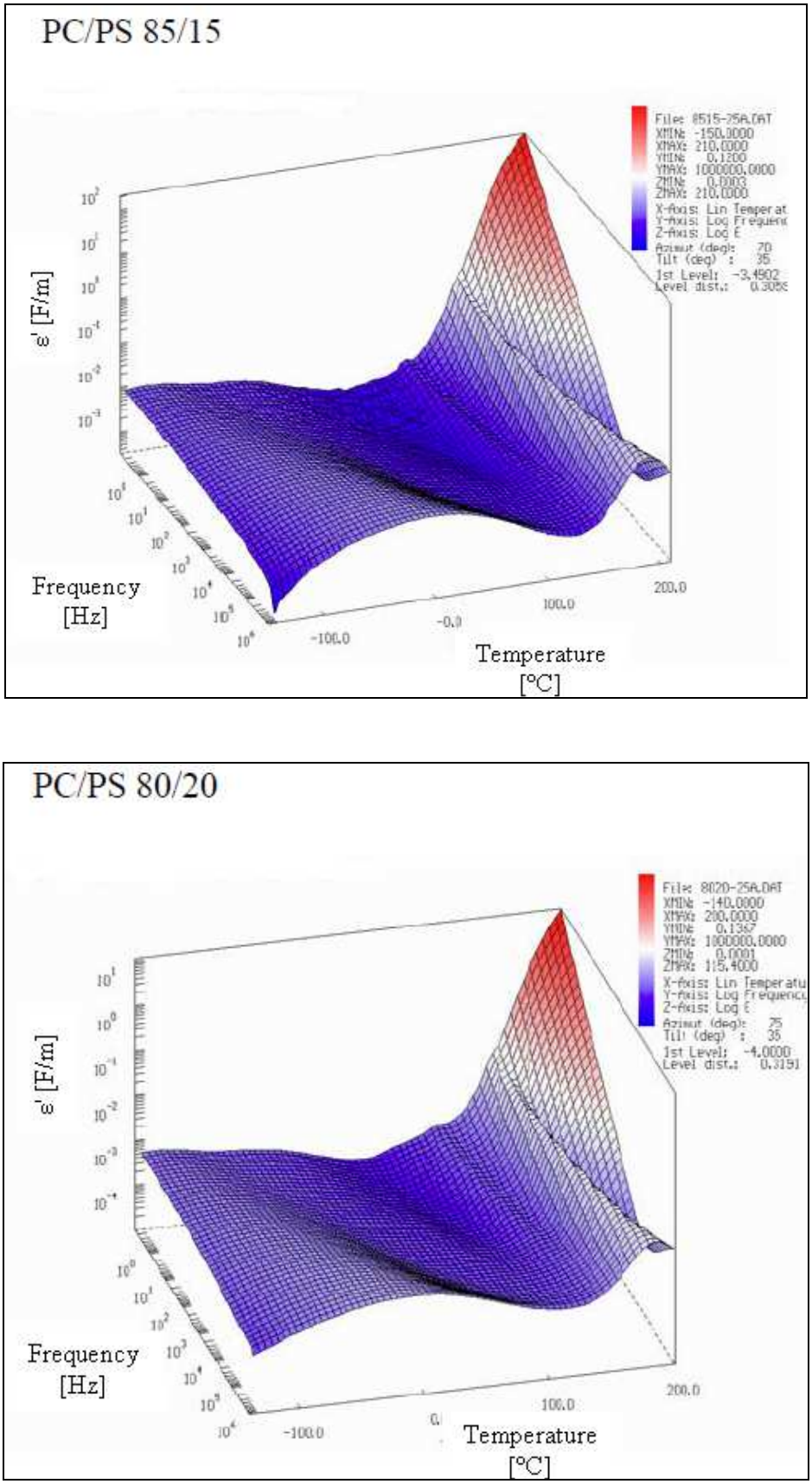

Figure 3.22. Dielectric relaxation spectroscopy for multilayered films PC/PS with relative compositions(from the top) 95/5, 90/10, 85/15, 80/20, 25 μm thick.

From those spectra it is obvious that glass transition processes superimposed as expected for all the films, but not for film PC/PS, 95/5.
Film with 5% PS content showed unexpected low-frequency loss below T_g of PC, what is difficult to explain.

To screen the multilayer spectra for features that are beyond an ideal superposition of the pure single polymer samples, some modelling of the expected “ideal” multilayer response was done.

The dielectric response of the multilayer samples was modelled using the following assumptions:

1. The individual contributions sum-up via a series model.
2. The actual multilayer system can be modeled by a bilayer-arrangement.
3. No size effects are so far taken into account, neither the Debye screenings length (typically in the µm range) nor the existence of an interdiffusion layer (~ 5 nm).

Discrepancies between the simulated spectra and the measured multilayer spectra should then be the result of phenomena such as:

- Intermixing zones between the PC and PS layers,
- Orientation and other structural effects originating from size effects and/or the specific way of film processing,
- Finite size effects on the charge transport for the case that the periodicity of the layer structure interferes with the Debye lengths. This would be manifested in a modified electrical conductivity/Maxwell Wagner relaxation,
- Alterations in the “glassy” dynamics below T_g in each polymer fraction due to modified physical aging behavior.

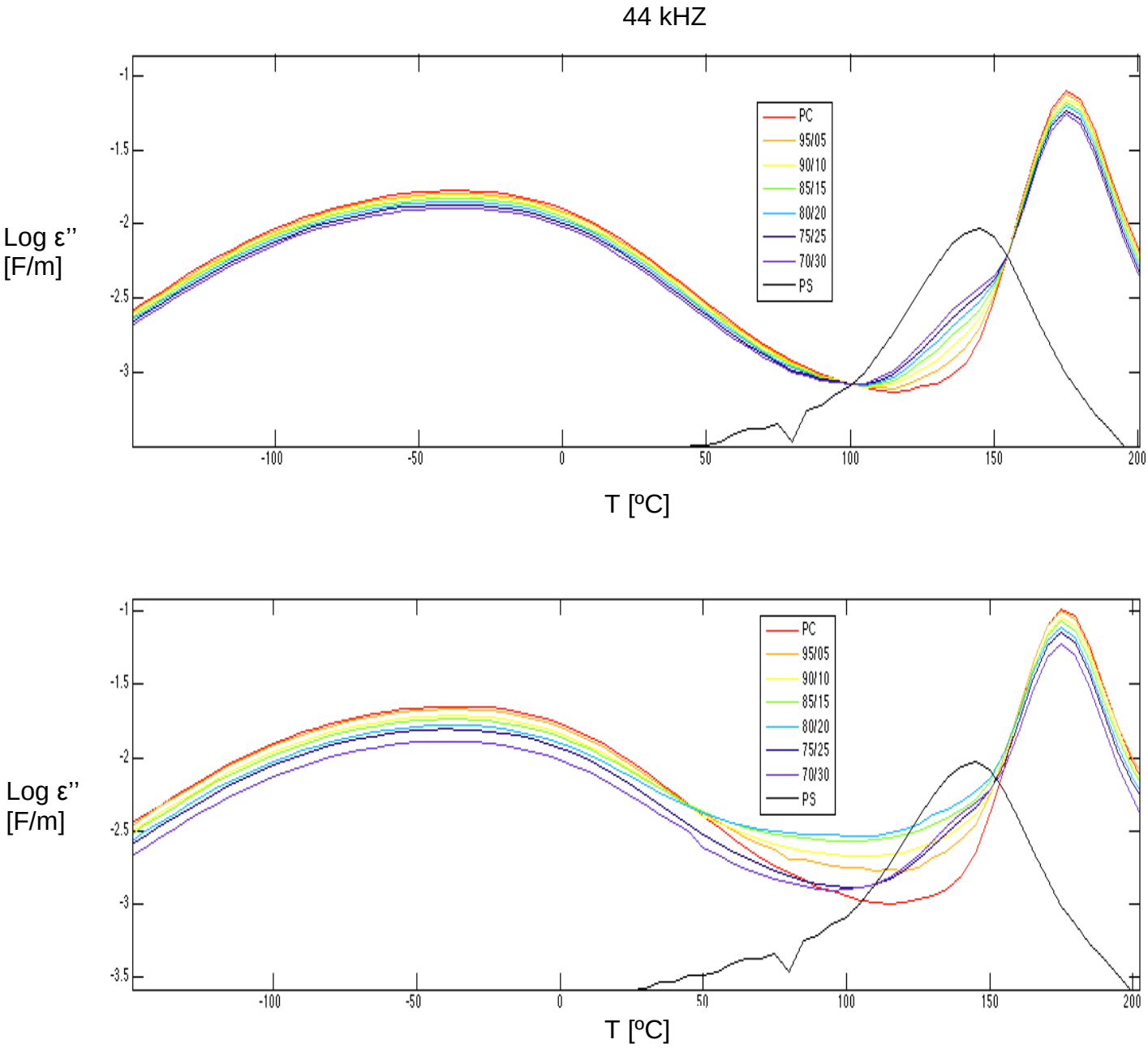

Figure 3.23. Isochronal plot of the dielectric loss ε"(T) at 44 kHz as a function of the layer composition:
Top: calculated response,
Bottom: measured response.

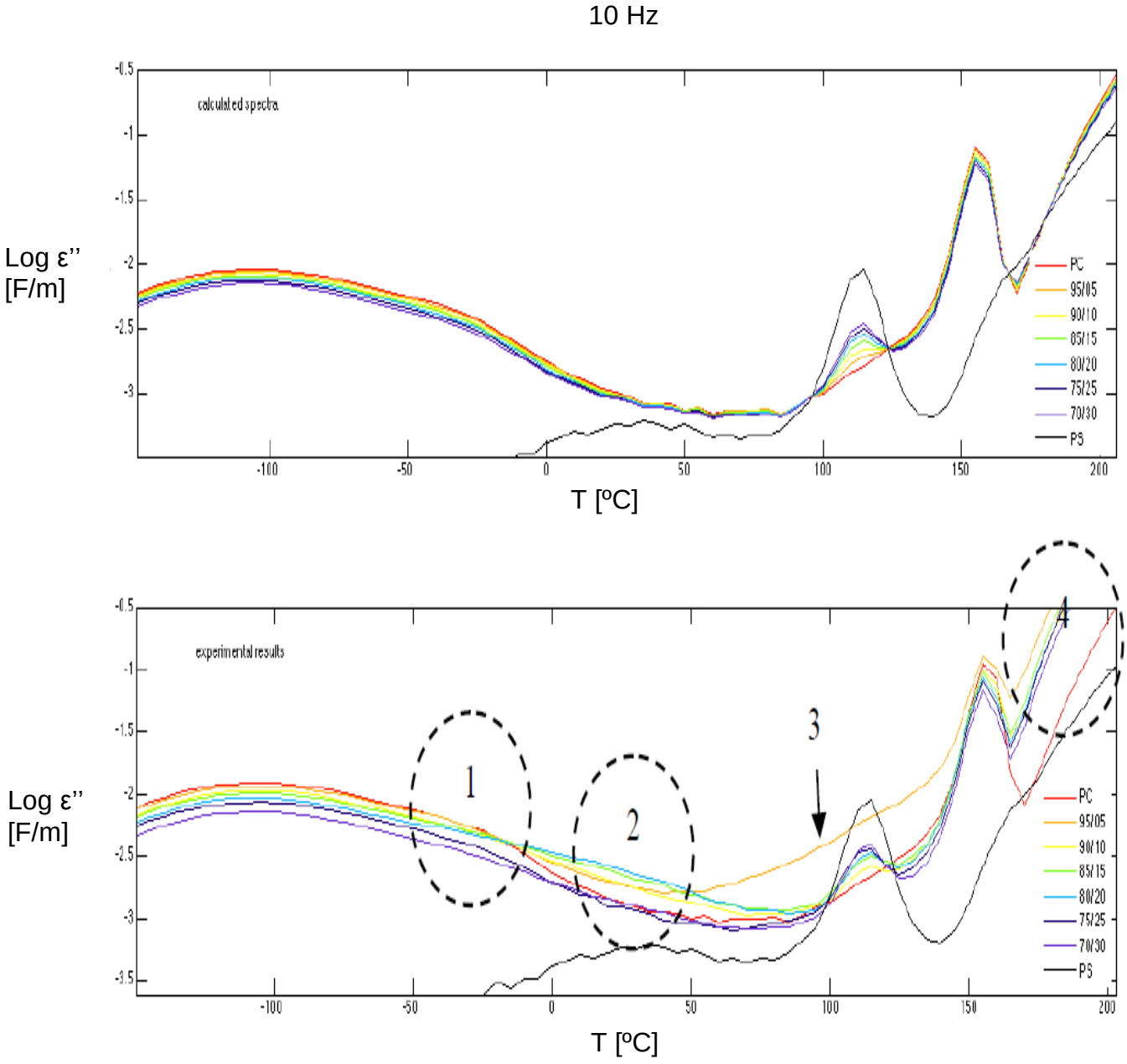

Figure 3.24. Isochronal plot of the dielectric loss ε"(T) at 10 Hz as a function of the layer composition:
Top: calculated response,
Bottom: measured response.

A comparison of the simulated with the measured curves shows that the main processes (αPS, αPC, γPC) basically scale in the correct way. Careful inspection of the curves, however, reveals several interesting features (Figure 3.24, bottom):

1. The α-process of PC has a shoulder (1) that is usually not observed in reference material and which gradually fades towards higher contents of PS.
2. There is an additional low-frequency loss (2), again assigned to the PC fraction.
3. Polystyrene shows a strange low-frequency loss (3) in the glass transition region, which eventually is the signature of the intermixed PC/PS phase.
4. Finally, the conductivity shows a composition dependence not predicted by our simplified model.

After those observations we can conclude that the dielectric relaxation spectroscopy measurements clearly provide evidence for deviations from a simple 2-phase structure in multilayered films PC/PS, that is worth to be analyzed more in the future.

3.3. Viscoelastic properties of multilayered films

The aim of this part of the study is to determine the variation of viscoelastic properties of the rubbery and confined PS when its layer thickness decreases. The idea was to work between T_g of PC (~150ºC) and T_g of PS (~ 105 ºC) in order to have one polymer in a rubbery state and another still rigid, in the glassy state. The temperature of 140°C was chosen.

The viscoelastic properties of bulk materials PS and PC were first characterized in order to predict the viscoelastic properties of multilayered films. These predictions are compared to macroscopic characterization of multilayered films.

3.3.1. Experimental characterization

a) Polystyrene

The viscoelastic behavior of the bulk PS in the melting state was characterized in shear between plates from 0.12mm-thick films, which were stacked on each other and welded in the rheometer at 160°C just before the tests. Tests were made at different temperatures (Table 3.6) to obtain a master curve of this material at 140°C (Figure 3.25). The shift factor of each temperature follows a WLF law (Figure 3.26), and WLF coefficients are C1 = 5.26 and C2 = 64.05 K.

T (°C)	Strain (%)	Frequency (rad/s)
125	0.1	100 to 0.1
140	0.6	100 to 0.1
160	0.6	100 to 0.1
180	1	100 to 0.1
240	1	100 to 0.1
260	1	100 to 0.1

Table 3.6. Testing conditions of dynamic frequency sweep tests for PS.

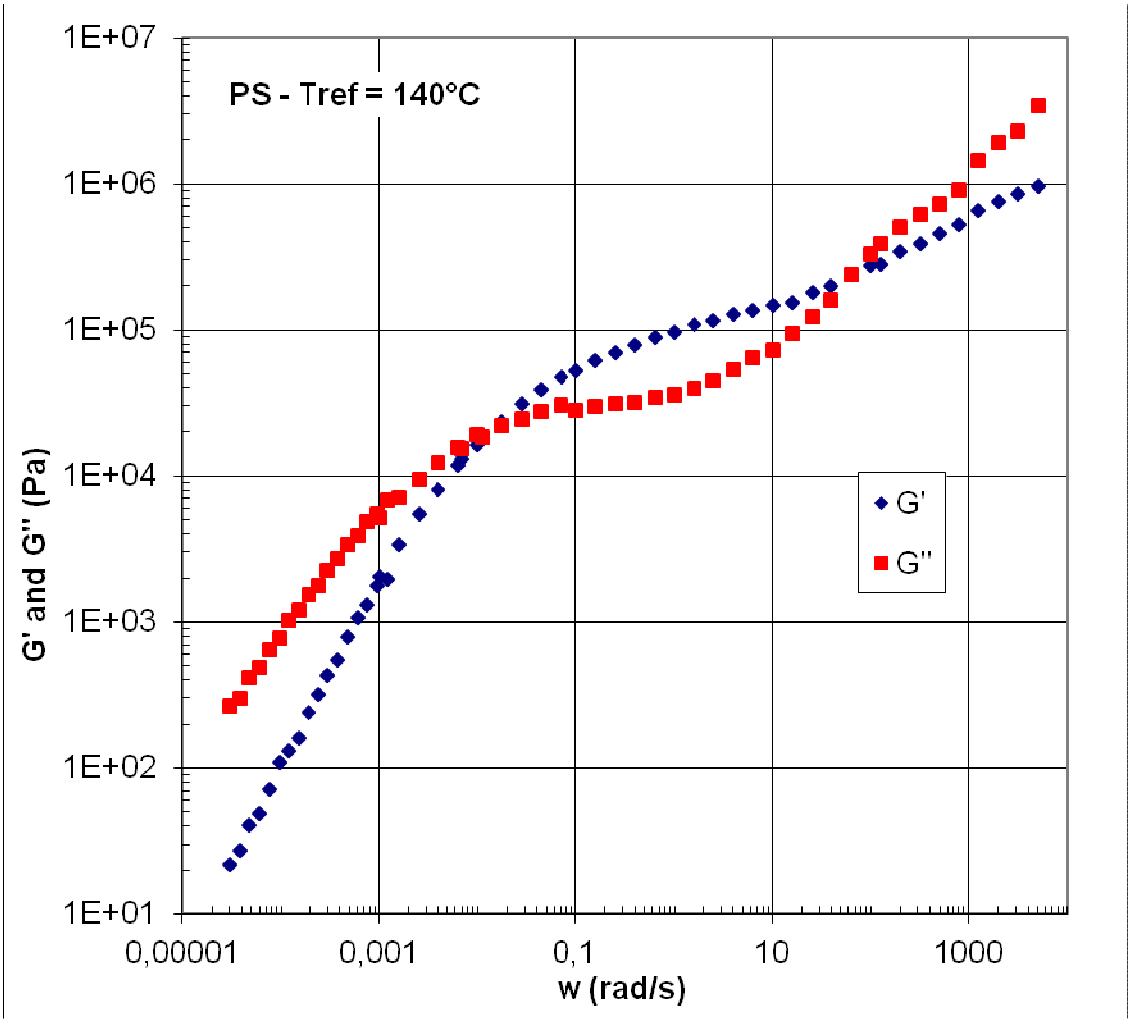

Figure 3.25. G' and G'' master curves of PS at 140°C.

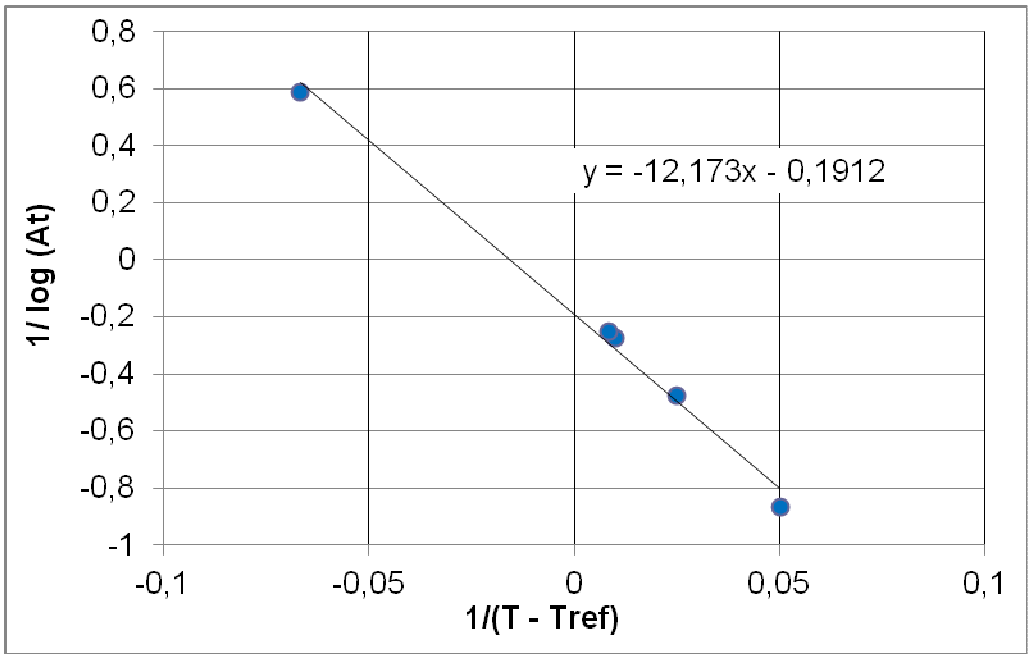

Figure 3.26. C1 and C2 identification of WLF law for PS at T_{ref} = 140°C.

b) Polycarbonate

At 140°C PC is in the solid state and torsion tests were done on rectangular and 1mm-thick samples which were obtained from dried and pressed granules. Tests were made at different temperatures (Table 3.7) to obtain a master curve of this material at 140°C (Figure 3.27). The shift factor of each temperature follows a WLF law (Figure 3.28), and WLF coefficients are C1 = 16.94 and C2 = 44.57 K.

T (°C)	Strain (%)	Frequency (rad/s)
135	0.002	100 to 0.1
140	0.002	100 to 0.1
145	0.01	100 to 0.1
150	0.04	100 to 0.1
155	0.1	100 to 0.1
160	0.3	100 to 0.3

Table 3.7. Testing conditions of dynamic frequency sweep tests for PC.

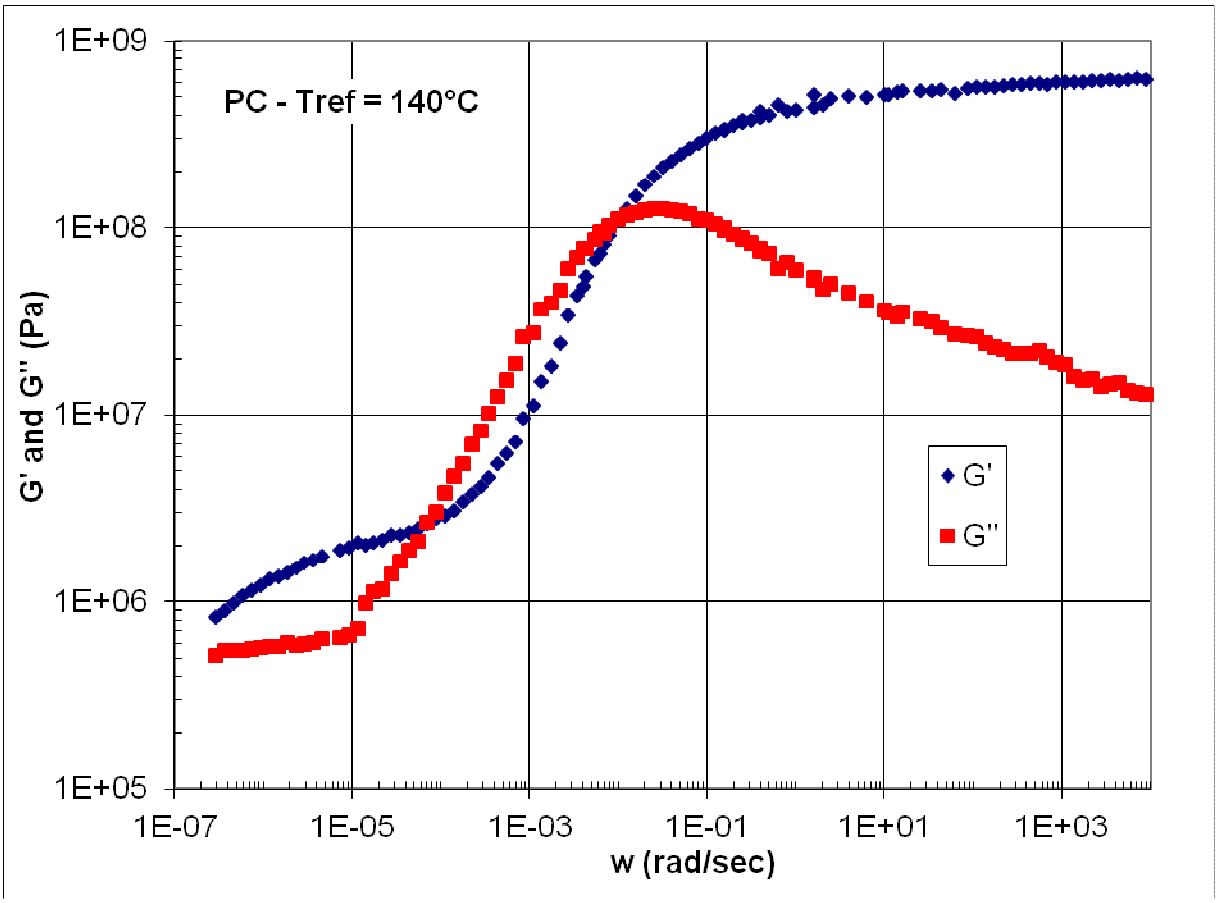

Figure 3.27. G' and G'' master curves of PC at 140°C.

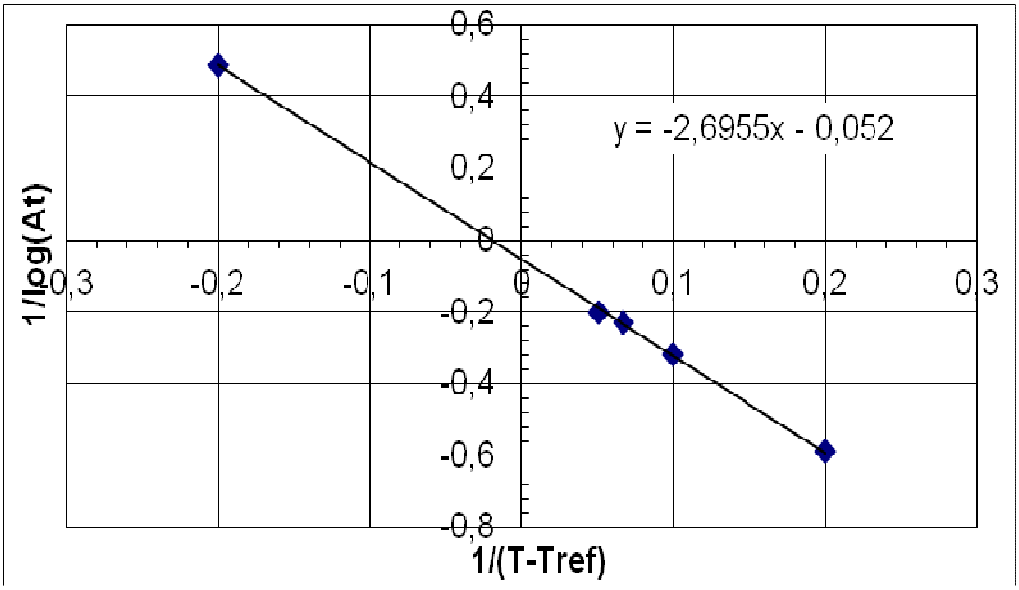

Figure 3.28. C1 and C2 identification of WLF law for PC at T_{ref} = 140°C.

c) Characterization of multilayered films.

All multilayered films were characterized at the studied temperature: 140°C. An example is given in Figure 3.29.

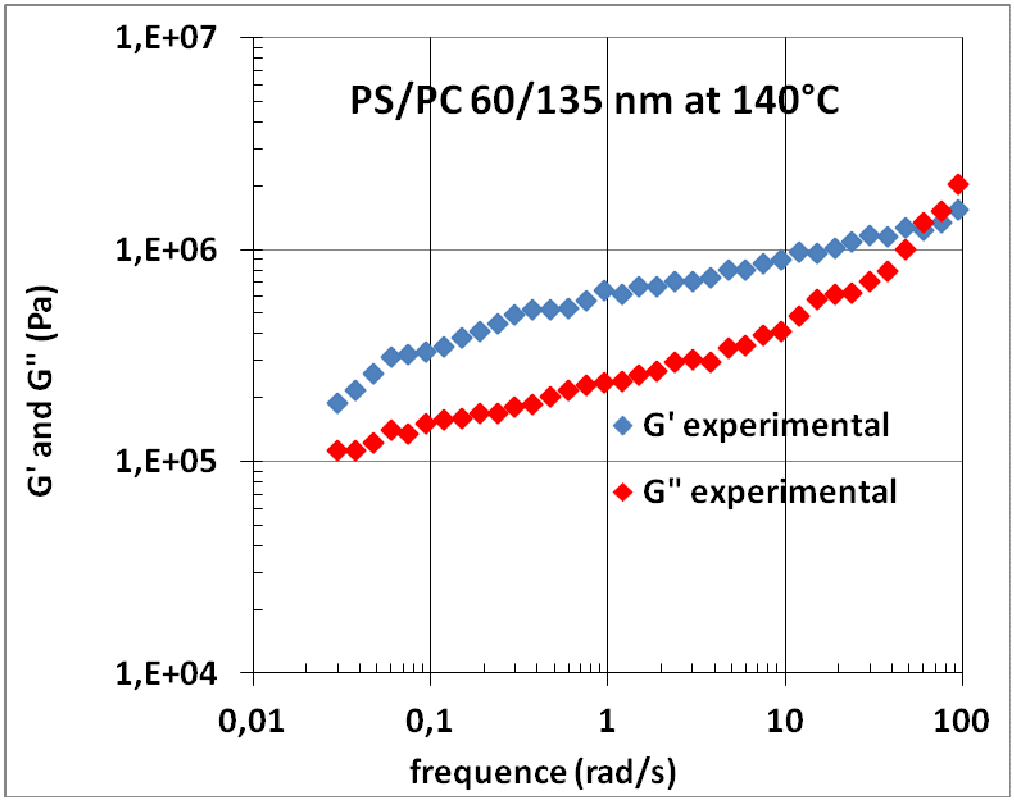

Figure 3.29. Dynamic frequency sweep test on PS/PC 60/135 nm film at 140°C.

3.3.2. Modelling the viscoelastic behavior of polymers

a) Maxwell model

The simplest and basic model to describe the viscoelastic behaviour of material is the Maxwell model. It is a serial association of a spring and a dashpot (Figure 3.30). Knowing the two parameters (viscosity η and shear modulus G), the differential equation controlling the system is given by equation 3.4. The ratio of viscosity to

shear modulus is homogeneous to a time and can be seen as the relaxation time of the system (equation 3.5).

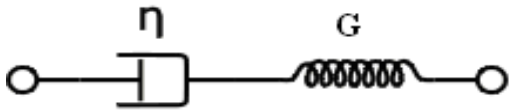

Figure 3.30. Simple Maxwell model.

$$\frac{\dot{\tau}}{G} + \frac{\tau}{\eta} = \dot{\gamma} \qquad (3.4)$$

$$\theta = \frac{\eta}{G} \qquad (3.5)$$

Considering a sinusoidal oscillating shear strain with an amplitude γ_0 and a frequency ω, the viscoelastic responses G' and G'' can be calculated analytically:

$$G' = \frac{G\,\omega^2\theta^2}{1 + \omega^2\theta^2} \qquad (3.6)$$

$$G'' = \frac{G\,\omega\,\theta}{1 + \omega^2\theta^2} \qquad (3.7)$$

This simple Maxwell model is qualitatively reasonable, but it does not fit typical polymer data very well, because polymers are polydisperse and only one relaxation time is not sufficient to represent physically the whole relaxation phenomenon. A logical improvement on this model is to set several relaxation times, which amounts to put several simple Maxwell in parallel.

b) Generalized Maxwell model

It is a parallel association of several simple Maxwell models (Figure 3.31). Each branch has a different relaxation time. Constitutive equation can be established as a system of n equations (eq. 3.8) if there is n branches.

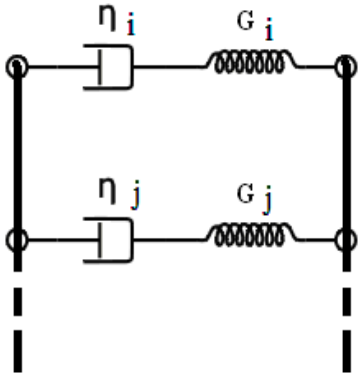

Figure 3.31. Generalized Maxwell model.

$$\frac{\dot{\tau i}}{Gi} + \frac{\tau i}{\eta i} = \dot{\gamma} \qquad (3.8)$$

$$\theta i = \frac{\eta i}{Gi} \qquad (3.9)$$

Again, considering a sinusoidal oscillating shear strain with an amplitude γ_0 and a frequency ω, the viscoelastic responses G' and G'' can be calculated analytically (3.10 and 3.11):

$$G' = \sum_{i=1}^{n} \frac{Gi\ \omega^2 \theta i^2}{1 + \omega^2 \theta i^2} \qquad (3.10)$$

$$G'' = \sum_{i=1}^{n} \frac{Gi\ \omega\ \theta i}{1 + \omega^2 \theta i^2} \qquad (3.11)$$

To model the viscoelastic behavior of a material by a Generalized Maxwell model, the parameters couples (Gi, θi) have to be identified from the measurement of G' or (and) G''. In general, the identification algorithm is non-linear. The published Fortran program was used and adapted to do this identification [131].

3.3.2.1. Modelling viscoelastic behavior of the studied polystyrene

The viscoelastic behavior of PS was modelled by a generalized Maxwell model with 12 branches (Figure 3.32). The 12 identified couples of parameters (Gi, θi) are presented in Figure 33. The modelling of G' does not fit the data for frequencies larger than 100 rad/s, the parameter identification can be improved by putting more branches and by increasing the experimental frequency range, but it was not worth to do that because the studied frequency range of multi-layered films remained under 100 rad/s.

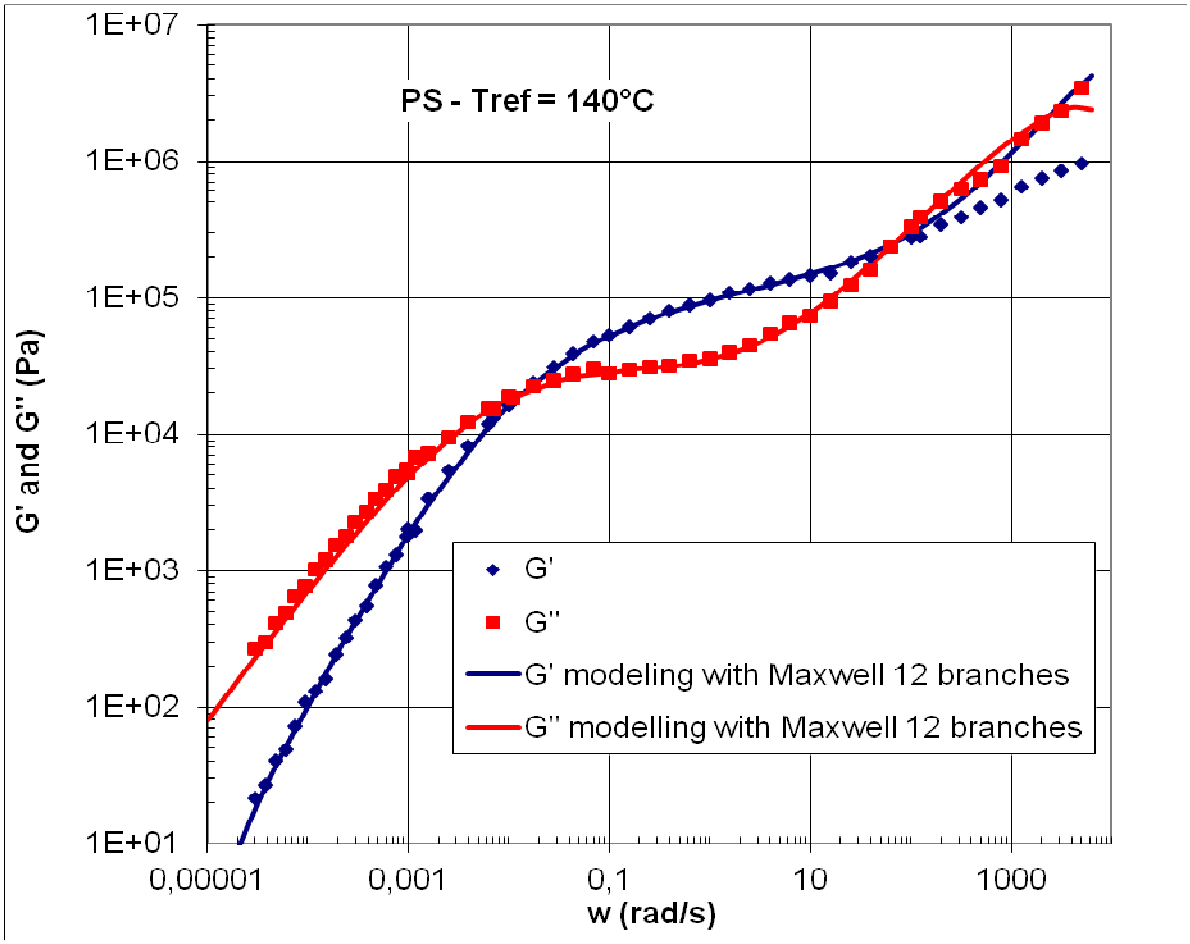

Figure 3.32. Viscoelastic behavior modeling of the studied PS at 140°C.

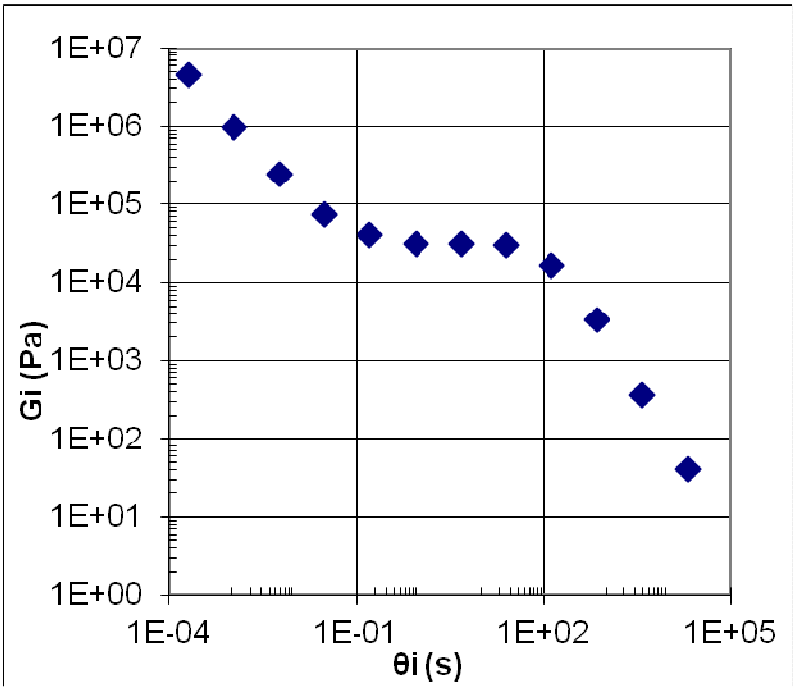

Figure 3.33. (Gi,θi) couples of generalized Maxwell model for the studied PS at 140°C.

3.3.2.2. Modelling the viscoelastic behavior of the studied polycarbonate

The viscoelastic behavior of PC was also modelled by a generalized Maxwell model with 12 branches (Figure 3.34). The 12 identified couples of parameters (Gi, θi) are given in Figure 3.35. The modelling is poor at very low frequencies (lower than 10^{-5} rad/s), but these frequencies are out of the range of study.

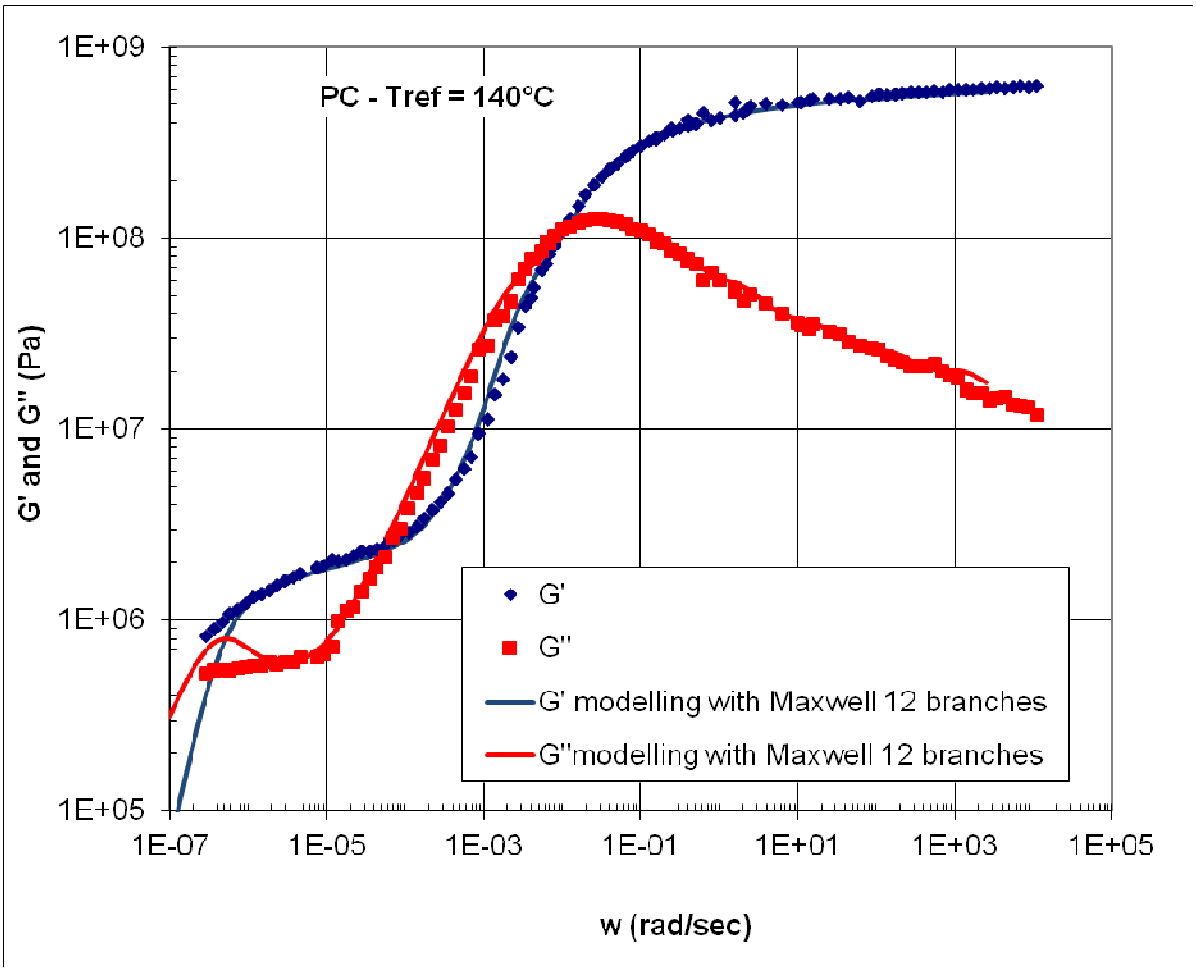

Figure 3.34. Viscoelastic behavior modeling of the studied PC at 140°C.

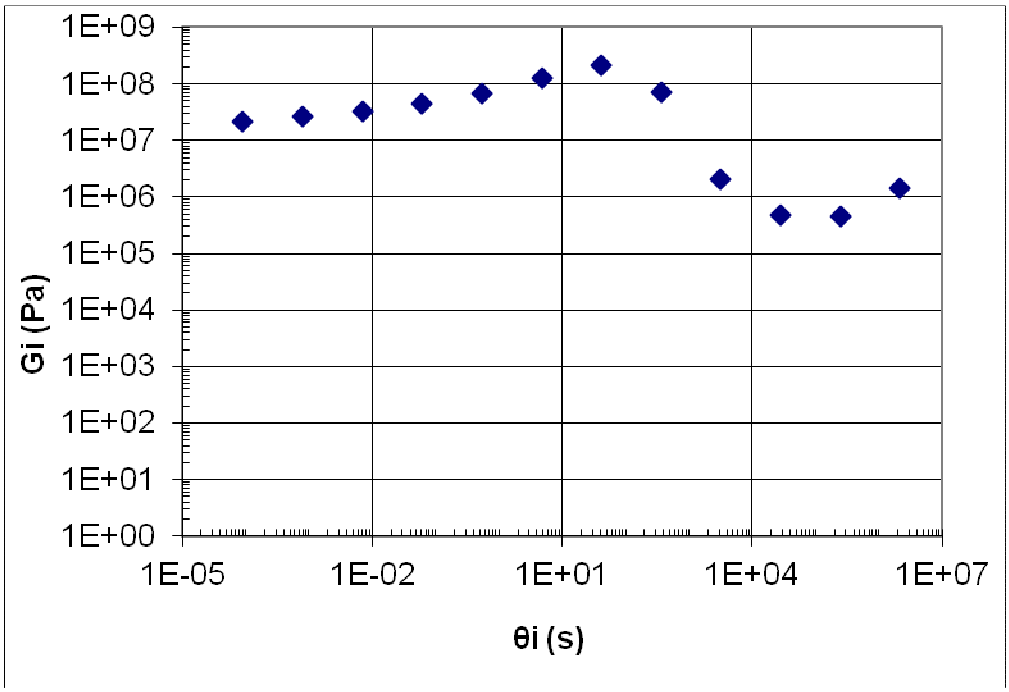

Figure 3.35. (Gi,θi) couples of multi-mode Maxwell model for PC at 140°C.

3.3.3. Modelling the linear viscoelastic behavior of multilayer films

From viscoelastic characterisations of PS and PC we wanted to predict numerically the viscoelastic behavior of multilayer films containing an alternated stack of PC and PS layers arranged in a sandwich like structure.

Firstly, simple Maxwell model was used to model the behaviour of each layer in order to understand the physical problem. Then a more realistic modelling was performed by using the identified generalized Maxwell model for PS and PC.

3.3.3.1. Viscoelastic model of multilayered films constituted of two simple Maxwell material.

Let us consider a multilayer film constituted of n layers of a simple Maxwell material A and n+1 layers of a simple Maxwell material B. The thickness of each layer of material A and B are respectively e_A and e_B, ,then the total thickness of the film is $e_0 = n.e_A + (n+1).e_B$ (Figure 3.36).

The displacement of each layer is noted u_i, the shear strain in each layer γ_i, the total displacement u_0 and the total shear strain γ (Figure 3.37). We have the following relationships:

$$\gamma_A = \frac{u_A}{e_A} \quad and \quad \gamma_B = \frac{u_B}{e_B} \tag{3.12}$$

$$\overset{\circ}{\gamma}_A = \frac{\overset{\circ}{u}_A}{e_A} \quad and \quad \overset{\circ}{\gamma}_B = \frac{\overset{\circ}{u}_B}{e_B} \tag{3.13}$$

$$\overset{\circ}{u}_0 = \sum_{i=1}^{n} \overset{\circ}{u}_A + \sum_{i=1}^{n+1} \overset{\circ}{u}_B \tag{3.14}$$

$$e_0 \overset{\circ}{\gamma} = \sum_{i=1}^{n} e_A \overset{\circ}{\gamma}_A + \sum_{i=1}^{n+1} e_B \overset{\circ}{\gamma}_B \tag{3.15}$$

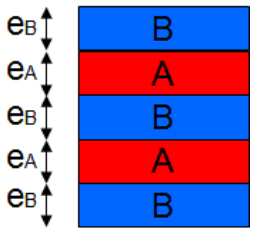

Figure 3.36. Scheme of a multilayered film.

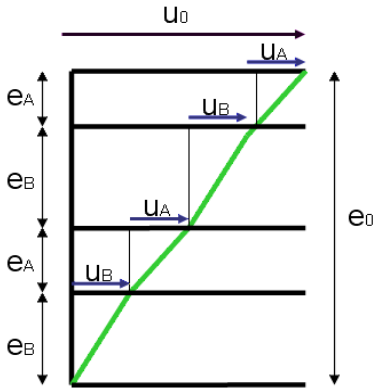

Figure 3.37. Scheme of displacement profile in a multilayered film.

Each layer is modelled by simple Maxwell model and each layer obeys equation 3.16. Because we have a serial assemblage and according to perfect interface between two layers, the stress in each layer is the same (τi = τ). Then constitutive equation 3.17 can be written from equations 3.15 and 3.16:

$$\frac{\dot{\tau}}{Gi} + \frac{\tau}{\eta i} = \dot{\gamma}_i \tag{3.16}$$

$$\dot{\gamma} = \frac{e_A}{e_0}\sum_{i=1}^{n}\left(\frac{\dot{\tau}}{G_A} + \frac{\tau}{\eta_A}\right) + \frac{e_B}{e_0}\sum_{i=1}^{n+1}\left(\frac{\dot{\tau}}{G_B} + \frac{\tau}{\eta_B}\right) \tag{3.17}$$

Considering the total thickness of material A (noted E_A), which is equal to $E_A = n.e_a$ and the total thickness of material B, $E_B = (n+1).e_b$, equation 16 can be simplified into:

$$\frac{\dot{\tau}}{e_0}\left(\frac{E_A}{G_A} + \frac{E_B}{G_B}\right) + \frac{\tau}{e_0}\left(\frac{E_A}{\eta_A} + \frac{E_B}{\eta_B}\right) = \dot{\gamma} \tag{3.18}$$

Then, the multi-layered film of two simple Maxwell material behaves like a simple Maxwell material with equivalent viscosity and modulus equal to:

$$\frac{1}{G_{eq}} = \frac{1}{e_0}\left(\frac{E_A}{G_A} + \frac{E_B}{G_B}\right) \qquad \frac{1}{\eta_{eq}} = \frac{1}{e_0}\left(\frac{E_A}{\eta_A} + \frac{E_B}{\eta_B}\right) \tag{3.19}$$

3.3.3.2. Modelling the behavior of multilayered films constituted of two generalized Maxwell material.

A more realistic modelling is performed for multi-layered films by taking generalized Maxwell modelling identified from previous experiments for PS and PC. As a perfect interface is supposed between layers, the stress is the same at each interface and a serial association of generalized Maxwell models can be simplified to the modelling of a two-layers films according to equation 3.15 (Figure 3.38):

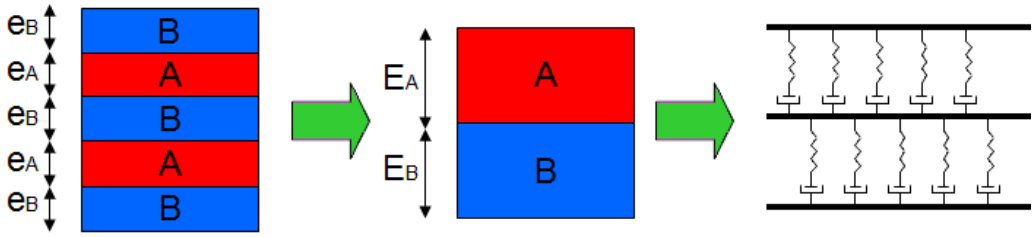

Figure 3.38. Simplification and schematization of multilayer containing 2 materials.

It is not possible in this case to find an analytical solution describing the sinusoidal viscoelastic response of a multilayered film constituted of two generalized Maxwell material. Only a numerical solution has to be computed.

Then, the idea was to simulate a rheological test. Firstly, we determine the effect of a small increment of strain $\Delta\gamma$ on the stress τ. The centred finite difference method will be used, to assure a better stability of the system.

a) Effect of a small strain increment.

In one branch of the layer A, we have a simple Maxwell behavior:

$$\frac{d\gamma_A}{dt} = \frac{\tau_{Ai}}{\eta_{Ai}} + \frac{d\tau_{Ai}}{dt}\frac{1}{G_{Ai}} \qquad (3.20)$$

The centred finite discretization gives:

$$\Delta\gamma_A = \frac{\tau_{Ai}(t)}{\eta_{Ai}}\Delta t + \Delta\tau_{Ai}\left(\frac{1}{G_{Ai}} + \frac{\Delta t}{2\eta_{Ai}}\right) \qquad (3.21)$$

For the Generalized Maxwell layer A and B, the stress increment can be determined for a strain increment $\Delta\gamma$ after a time increment Δt:

$$\Delta\tau_A = \sum_{i=1}^{k}\left(\frac{\Delta\gamma_A - \frac{\tau_{Ai}(t)\Delta t}{\eta_{Ai}}}{\frac{1}{G_{Ai}} + \frac{\Delta t}{2\eta_{Ai}}}\right) \qquad (3.22)$$

where *k* is the number of branches for the Generalized Maxwell material A.

$$\Delta\tau_B = \sum_{j=1}^{l}\left(\frac{\Delta\gamma_B - \frac{\tau_{Bj}(t)\Delta t}{\eta_{Bj}}}{\frac{1}{G_{Bj}} + \frac{\Delta t}{2\eta_{Bj}}}\right) \qquad (3.23)$$

where *l* is the number of branches for the Generalized Maxwell material B.

The hypothesis of perfect interface is made, so there is equality between $\Delta\tau_A$ and $\Delta\tau_{B:}$. The strain increment after a time increment in each layer can be determined as:

$$\Delta\gamma_A = \frac{\Delta\tau + A1}{A2} \qquad \Delta\gamma_B = \frac{\Delta\tau + B1}{B2} \tag{3.24}$$

where A1, A2, B1, B2 are known at time t:

$$A1 = \sum_{i=1}^{k} \left(\frac{\tau_{Ai}(t)\Delta t}{\frac{1}{G_{Ai}} + \frac{\Delta t}{2\eta_{Ai}}} \right) \tag{3.25}$$

$$A2 = \sum_{i=1}^{k} \left(\frac{1}{\frac{1}{G_{Ai}} + \frac{\Delta t}{2\eta_{Ai}}} \right) \tag{3.26}$$

$$B1 = \sum_{j=1}^{l} \left(\frac{\tau_{Bj}(t)\Delta t}{\frac{1}{G_{Bj}} + \frac{\Delta t}{2\eta_{Bj}}} \right) \tag{3.27}$$

$$B2 = \sum_{j=1}^{l} \left(\frac{1}{\frac{1}{G_{Bj}} + \frac{\Delta t}{2\eta_{Bj}}} \right) \tag{3.28}$$

Using equation 3.15, the stress increment $\Delta\tau$ can be obtained, where e_0 is the total thickness, E_A is the total thickness of layers of material A and E_B the total thickness of layers of material B:

$$\Delta\tau = \frac{e_0\Delta\gamma - \frac{E_A A1}{A2} - \frac{E_B B1}{B2}}{\frac{E_A}{A2} + \frac{E_B}{B2}} \qquad (3.29)$$

b) Application to a sinusoidal strain.

An explicit numerical scheme was performed. A sinusoidal shear strain γ is applied. At time t, for a time increment Δt, it is possible to determine:

- the strain increment $\Delta\gamma$:

$$\Delta\gamma = \gamma_0\omega\sin(\omega t).\Delta t \qquad (3.30)$$

- the stress increment $\Delta\tau$ according to (3.29) and then the stress $\tau(t+\Delta t)$ at time $(t+\Delta t)$,
- the strain increments $\Delta\gamma_A$ and $\Delta\gamma_B$ in the layer A and B (eq. 3.24) and then the strains $\gamma_A(t+\Delta t)$ and $\gamma_B(t+\Delta t)$ in the layer A and B at time $t+\Delta t$,
- the stresses $\tau_A(t+\Delta t)$ and $\tau_B(t+\Delta t)$ at time $t+\Delta t$ in all the branches of the two material A and B.

Therefore, all strains and stresses are known at time $(t+\Delta t)$, and a new increment can be performed.

The determination of G' and G'' needs to calculate the phase angle between strain and stress. In the simulation of shearing tests, the stabilization of phase angle appears after three times the longest the longest relaxation times in the material. If θ_{max} is this maximum value of relaxation time, stresses and strains must be

calculated during 3 x θ_{max}. If ω is the frequency, number of period p should be larger than:

$$p > \frac{3\omega\theta_{\max}}{2\pi} \tag{3.31}$$

Then, the strain delay is calculated after p periods (Figure 3.39).

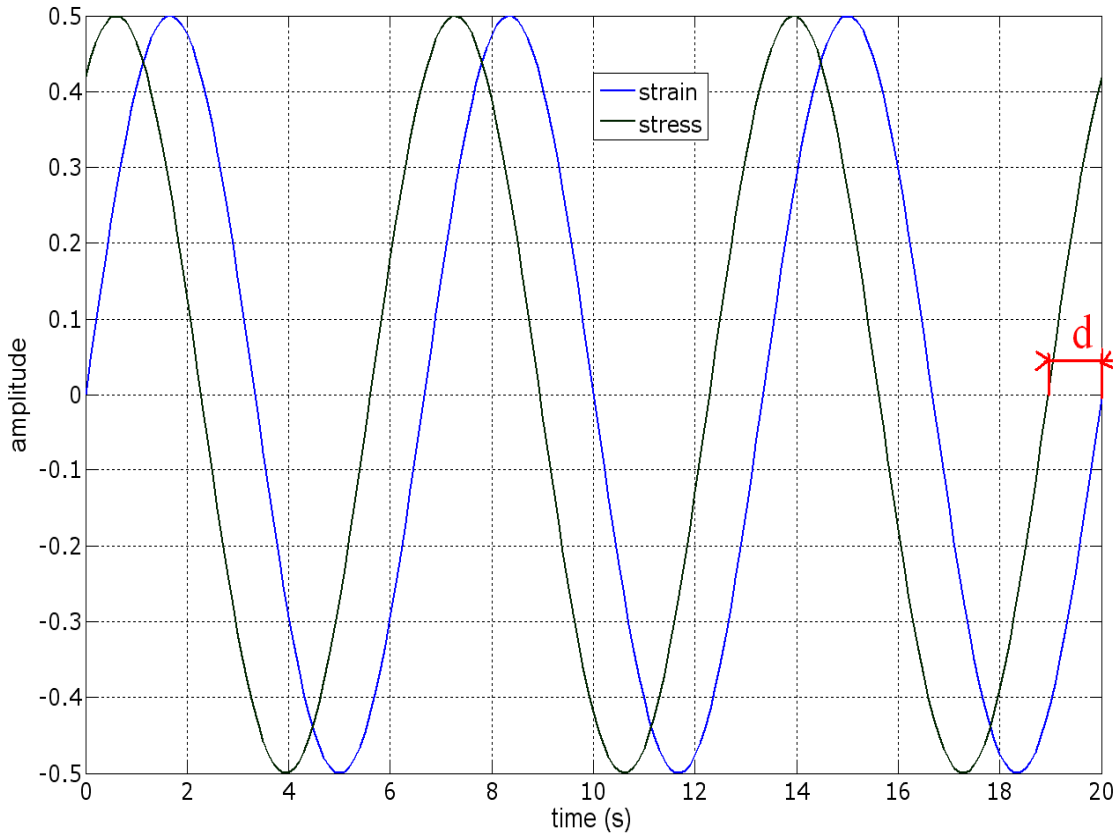

Figure 3.39. Strain delay determination.

c) Validation of the code.

The code was written on Matlab. Two different tests were done to validate the code thanks to known analytical solutions.

First validation consists to run the program with two layers of the same material. The studied PS and its parameters identification of Generalized Maxwell model (Figure 3.33) were chosen. The numerical solution is compared to the analytical solutions (Equations 3.10 and 3.11) in Figure 3.40, the agreement is perfect.

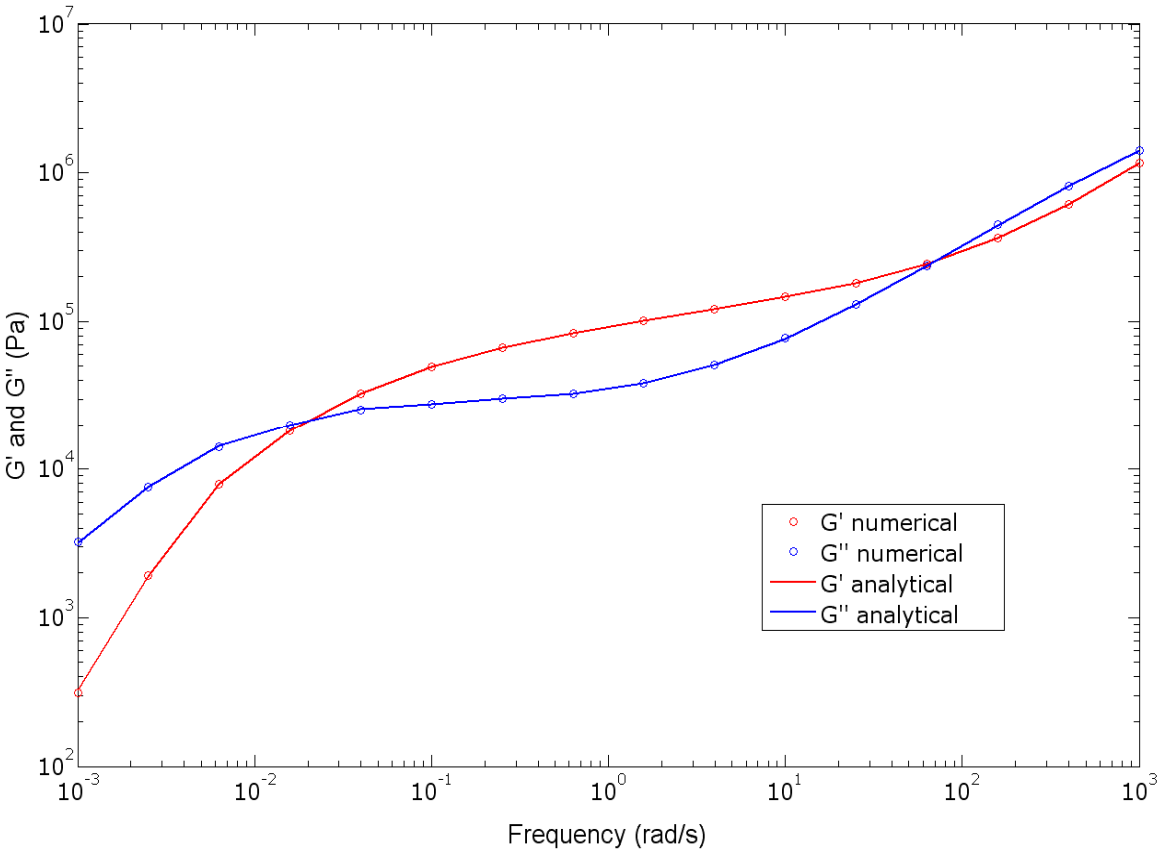

Figure 3.40. Validation of the code by using the same material for the two layers: PS data.

The second code validation was done by comparing the numerical response of a film constituted of two simple Maxwell materials with the analytical solution (Equations 3.6, 3.7 and 3.19). Each layer was modelled by a generalized Maxwell model with 5 identical branches, which are equivalent to a simple Maxwell material (Figure 3.41). We got a perfect superposition of two solutions.

For a given frequency, a time increment equal to a period divided by 30 was enough to give a good agreement between numerical and analytical solutions. Then all

numerical calculations were done with a time increment equal to the thirtieth of a strain period.

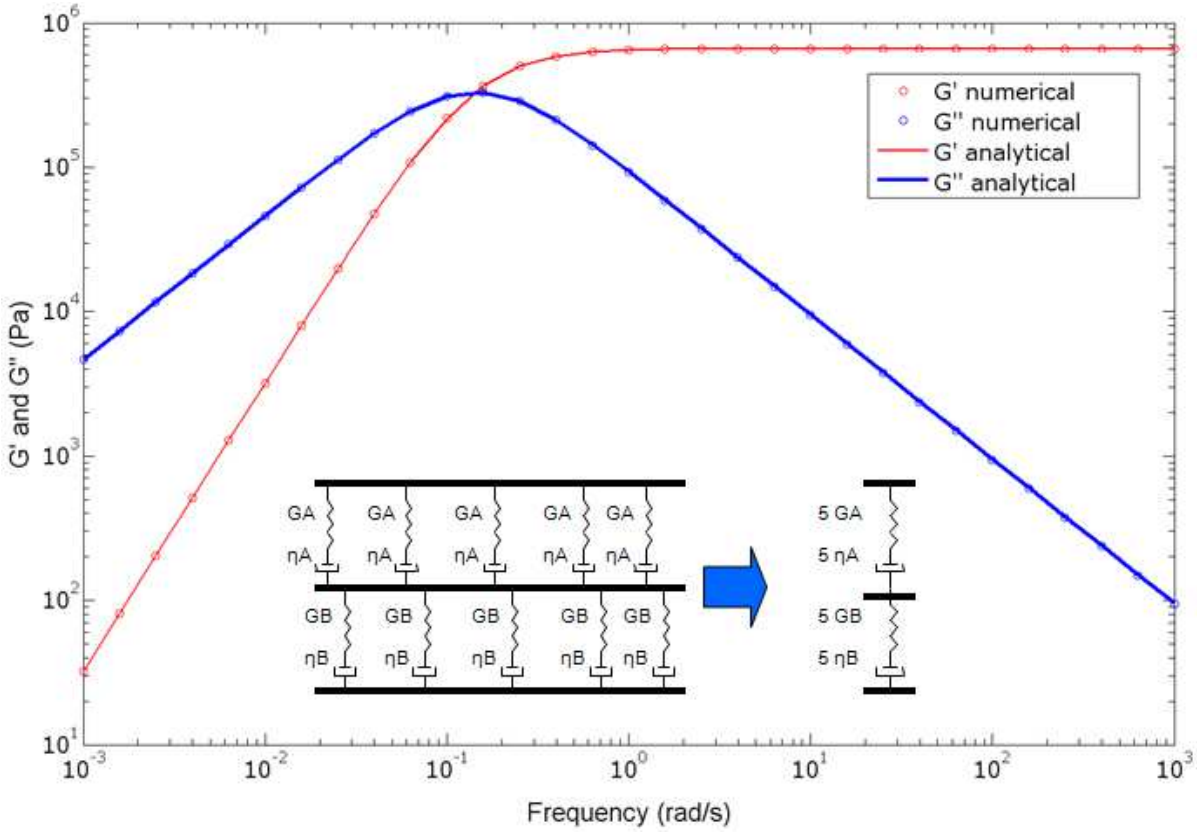

Figure 3.41. Analytical versus numerical solution for a multilayer, each layer modeled by a generalized Maxwell model:
G_A=100000 Pa, G_B=40000 Pa, η_A=1000000 Pa.s and η_B=800000 Pa.s.

Now, we can consider the code is validated. We can use it to predict the linear viscoelastic behavior of multilayered films without any effect of confinement..

3.3.3.3. Viscoelastic modelling of the studied multilayered films.

Firstly, we want to know if it is possible to predict the macroscopic viscoelastic behavior of a film constituted of non-confined layers considering the knowledge of the viscoelastic behavior of each layer.

a) Microscopic layer multilayered films.

Before predicting the behavior of nanomultilayer films, microscopic multilayered films are considered. A plaque with 5 layers (three layers of PS and two layers of PC) was built (Figure 3.42). The initial thickness of PS film is 0.15 mm, the one of PC 0.14 mm. To get a good adhesion between layers, a normal load of 15N is applied during five minutes at 160°C before a test. The total film thickness of plaque is decreasing a little bit, therefore it was supposed that this decrease of thickness occurred only for PS layers. Then, the corrected thickness PS values were used in the numerical simulation.

The numerical simulation gives a good prediction of the viscoelastic behaviour of the macroscopic film (Figure 3.43). Therefore; we can consider that both numerical simulation and experimental procedure are validated.

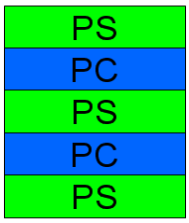

Figure 3.42. Handmade multilayer sample assembled with PS and PC films.

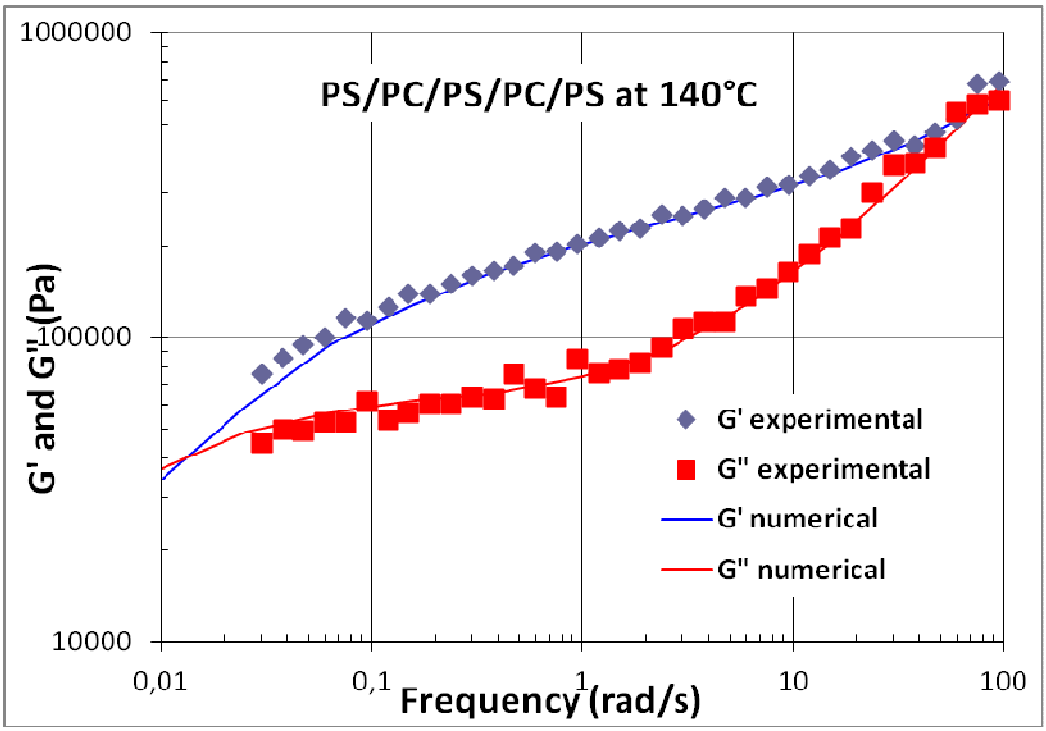

Figure 3.43. Experimental and numerical behavior of handmade multilayer film.

b) Confined multilayered films.

The same experimental procedure was applied for multilayer films than the one for handmade films (previous paragraph). The thickness of tested sample was about 1mm, then the films had to be stacked and welded before being tested (Figure 3.44).

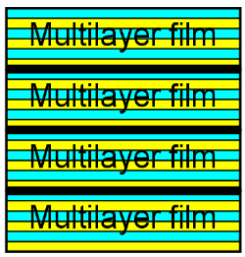

Figure 3.44. Stack of films.

Like for the handmade composite film, the numerical prediction of the viscoelastic macroscopic behavior for PS/PC 290/680 nm film is very close to the experimental response (Figure 3.45).

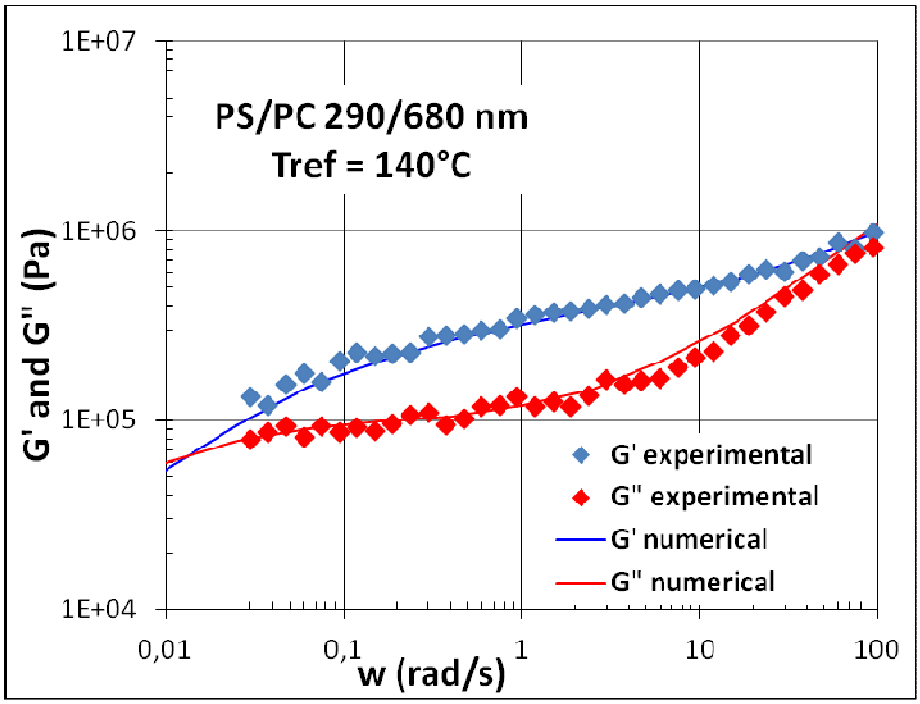

Figure 3.45. Comparison between experimental viscoelastic responses and numerical predictions for PS/PC 290/680 nm film.

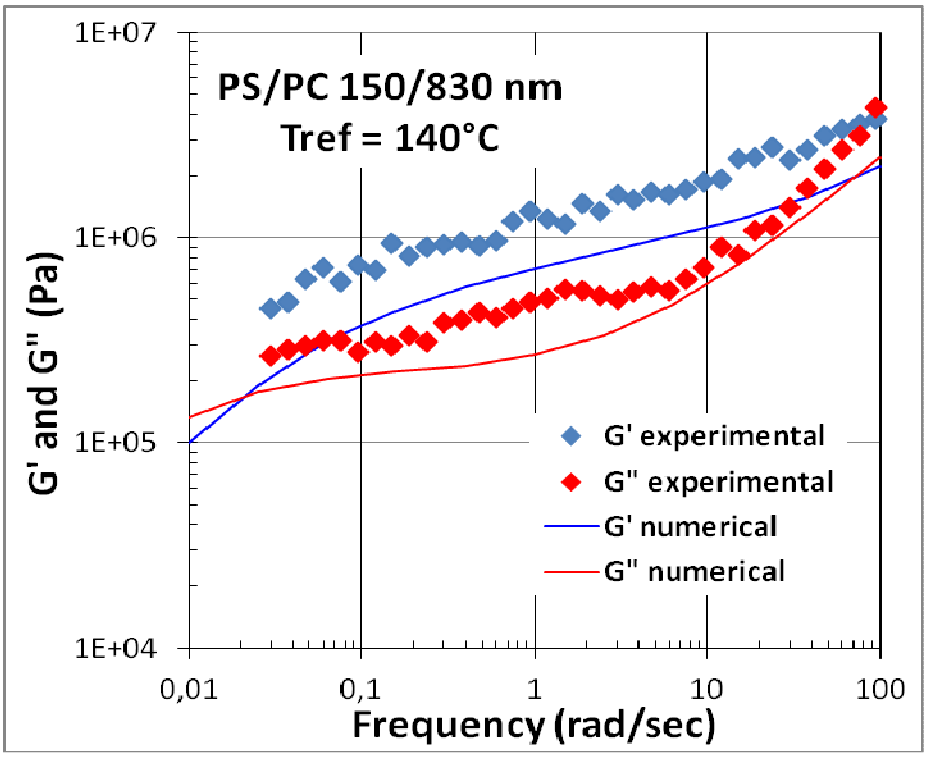

Figure 3.46. Comparison between experimental viscoelastic responses and numerical predictions for PS/PC 150/830 nm film.

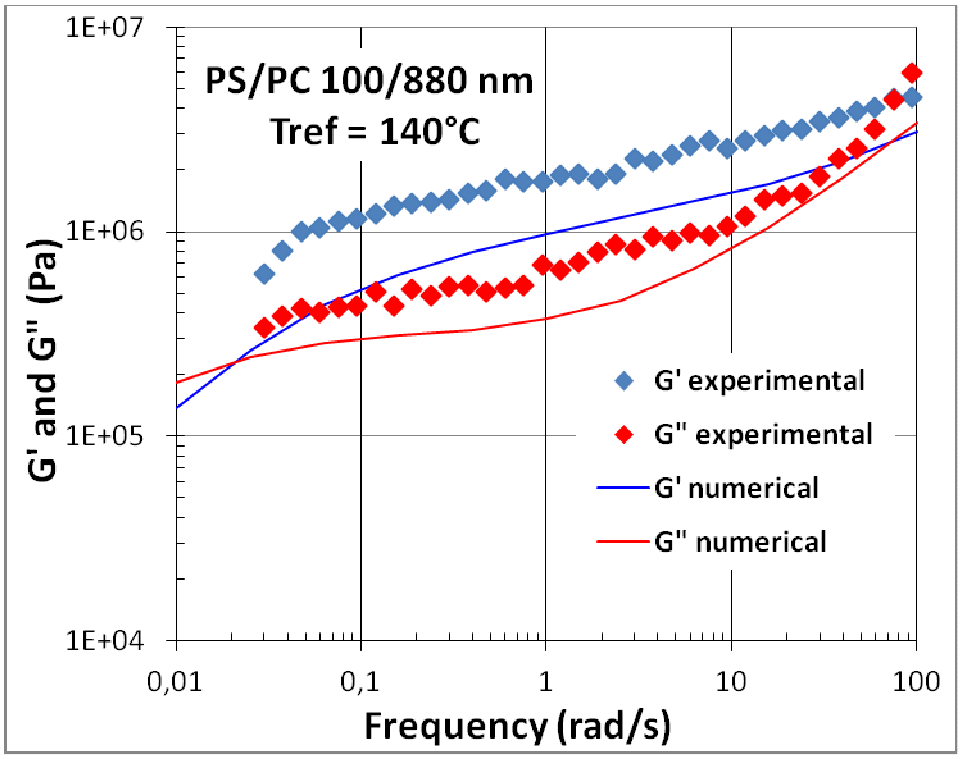

Figure 3.47. Comparison between experimental viscoelastic responses and numerical predictions for PS/PC 100/880 nm film.

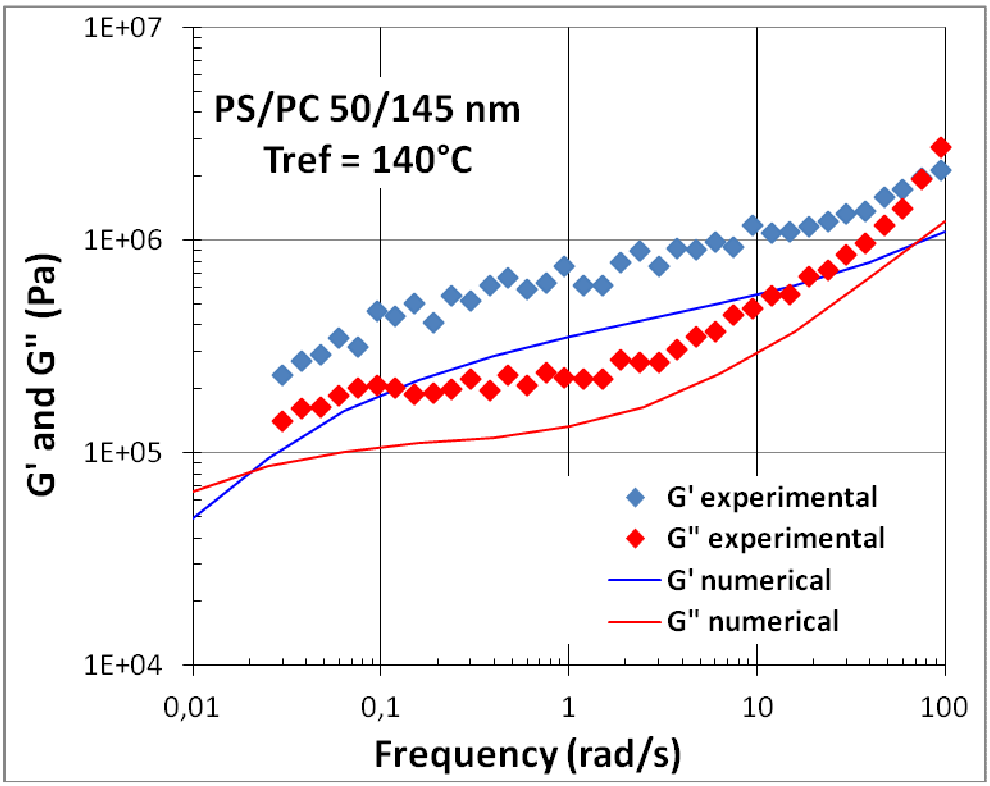

Figure 3.48. Comparison between experimental viscoelastic responses and numerical predictions for PS/PC 50/145 nm film.

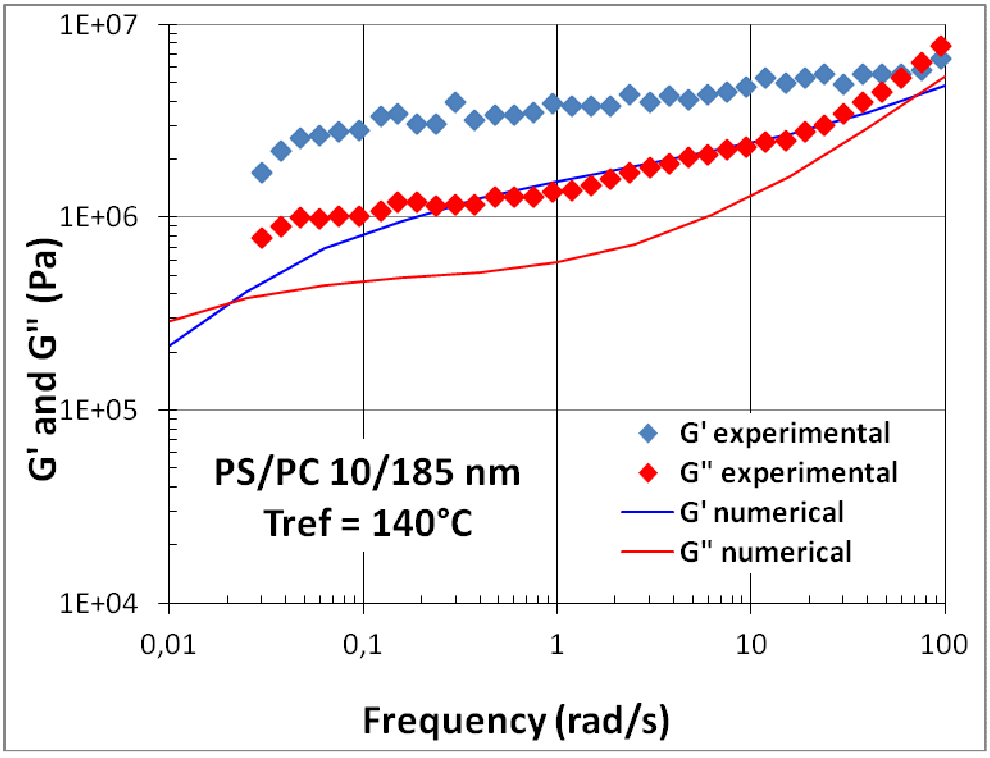

Figure 3.49. Comparison between experimental viscoelastic responses and numerical predictions for PS/PC 10/185 nm film.

When PS layer thickness is decreasing to values less than 200 nm, the experimental behavior does not follow anymore the numerical prediction (Figure 3.46, 3.47, 3.48, 3.49). More the thickness of confined PS layers are low, more the stiffness of the composite is high. This gap can be clearly attributed to PS confinement.. The confinement of PS layer seems to begin at about 200 nm.

3.3.4. Variation of PS mechanical properties with layer confinement.

3.3.4.1.Viscoelastic responses of confined PS.

The objective of this part of the study is to determine the viscoelastic behavior of confined PS (values of G' and G") in the multilayer film PC/PS. For that, we have done the hypothesis that the behavior of the glassy PC layers of is the same as the behavior of the bulk PC. This hypothesis does not seem very strong because the PC layers have a larger thickness than PS ones and are larger than 150 nm.

Using complex calculation and general equations 3.32, and 3.33 the link between stress and strain can be written as in equation 3.35:

$$\gamma^* = \frac{\tau^*}{G^*} \tag{3.32}$$

$$\dot{u}_0^* = e_0 \dot{\gamma}^* = \dot{u}_{PC}^* + \dot{u}_{PS}^* \tag{3.33}$$

$$e_0 \dot{\gamma}^* = e_0 \frac{\tau^*}{G^*} = E_{PC} \dot{\gamma}_{PC}^* + E_{PS} \dot{\gamma}_{PS}^* = E_{PC} \frac{\tau_{PC}^*}{G_{PC}^*} + E_{PS} \frac{\tau_{PS}^*}{G_{PS}^*} \tag{3.34}$$

Knowing that stress is the same at interfaces, we can find in equation 3.35:

$$\frac{1}{G*} = \frac{E_{PC}}{e_0}\frac{1}{G^*_{PC}} + \frac{E_{PS}}{e_0}\frac{1}{G^*_{PS}} \tag{3.35}$$

Separating real and imaginary parts, we obtain:

$$\frac{G'}{\left\|G^*_0\right\|^2} = \frac{E_{PC}}{e_0}\frac{G'_{PC}}{\left\|G^*_{PC}\right\|^2} + \frac{E_{PS}}{e_0}\frac{G'_{PS}}{\left\|G^*_{PS}\right\|^2} \qquad \frac{G''}{\left\|G^*_0\right\|^2} = \frac{E_{PC}}{e_0}\frac{G''_{PC}}{\left\|G^*_{PC}\right\|^2} + \frac{E_{PS}}{e_0}\frac{G''_{PS}}{\left\|G^*_{PS}\right\|^2} \tag{3.36}$$

The composite behavior is known from shear tests and PC behavior is considered to be the same in the composite and in the bulk. We are looking for the behavior of PS . Let us define the terms A and B (equation 3.37) to simplify equations 3.36:

$$A = \frac{G'_{PS}}{\left\|G^*_{PS}\right\|^2} \qquad B = \frac{G'_{PC}}{\left\|G^*_{PC}\right\|^2} \tag{3.37}$$

Then, the linear viscoelastic behavior of PS (G' and G") can be determined (equation 3.38) and was calculated for the different multilayered films (Figure 3.50):

$$G'_{PS} = \frac{A}{A^2 + B^2} \qquad G''_{PS} = \frac{B}{A^2 + B^2} \tag{3.38}$$

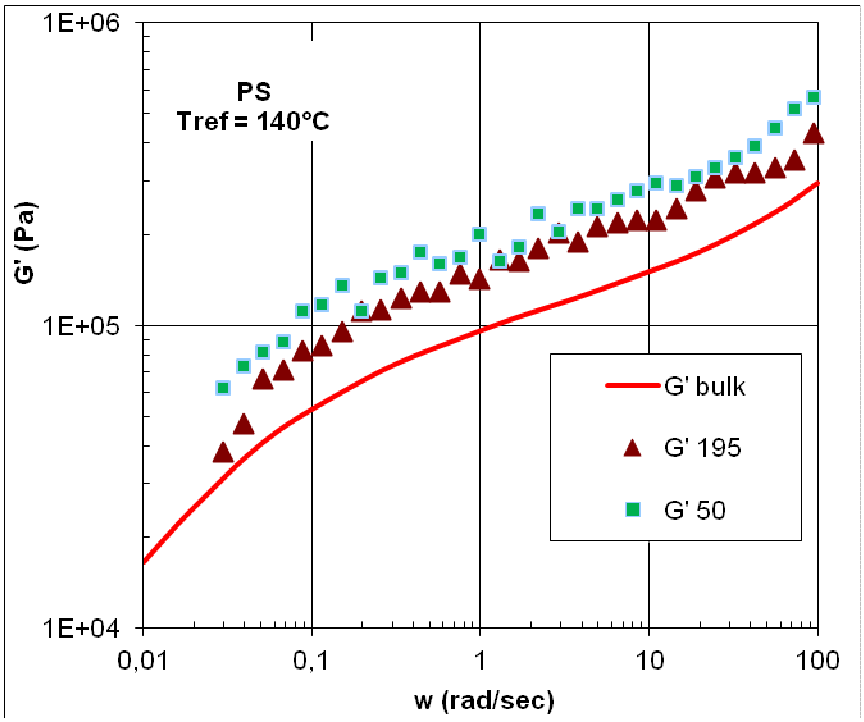

Figure 3.50. G' variation of PS in confined layers.

To compare the viscoelastic behavior of PS in the bulk with the viscoelastic behavior of the confined PS, we define the ratio r of the storage modulus of PS in confined layers to the one in the bulk:

$$r = \frac{G'_{confined}}{G'_{bulk}} \qquad (3.39)$$

The storage modulus was smoothed and determined at inflexion point according to Osaki et all. [132] method and ratio r was determined for all films at 140°C (Figure 3.51).

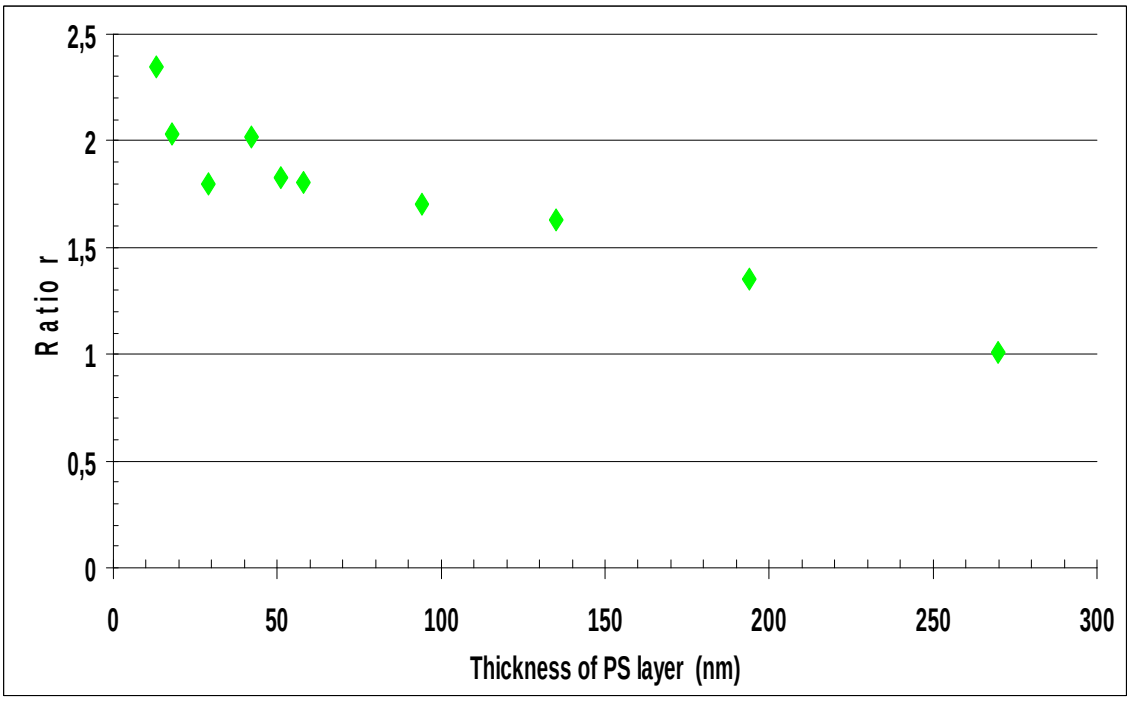

Figure 3.51. Ratio r in a function of the PS layer thickness.

Under a PS layer thickness of 200 nm, an increase of rigidity appears. Is it already a confinement effect? Is it possible to find a physical explanation?

3.3.4.2. Modelling the PS behavior in confined layer.

The increase of G' and G'' with confinement suggests a decrease of molecular mobility, which enhances elasticity. The studied PS is in the rubbery state at 140°C, then it is well known that its entropic elasticity is directly linked to the molar mass between entanglements M_e:

$$G_{PS} = \frac{\rho RT}{Me} \qquad (3.40)$$

where ρ is the volume mass and T the temperature.

If we suppose that PC reduces the mobility of PS chains at interface, this decrease of mobility could be seen as an increase of entanglements at the PC/PS interface. One may also suppose a more rigid interphase between PC and PS layer.

a) A decrease of molecular mobility as an increase of entanglements at interface.

Let us consider a PS layer (thickness e) confined between two PC layers (Figure 3.52). We suppose that this PS layer has the bulk PS density of entanglements d_e in its core plus a certain surface density of entanglements d_s at the interface. This surface density of entanglements d_s should not depend on the thickness of PS layer. The total entanglement density in the PS layer d can be written as:

$$d = d_e + \frac{d_s}{e} \qquad (3.41)$$

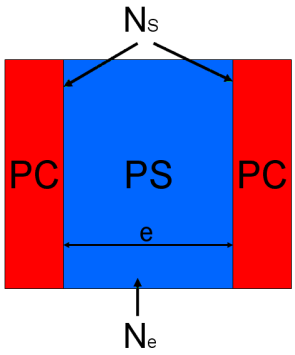

Figure 3.52. Scheme of an entangled confined PS layer.

The relationship between the density of entanglements d_e, the molar mass between entanglements M_e and Avogadro number N_A is:

$$d_e = \frac{\rho N_A}{M_e} \tag{3.42}$$

Knowing that molar mass between entanglements is equal for PS to about M_e = 19 kg/mol [133], its density of entanglements d_e is about 0.03 1/nm^3, that is about 30 entanglements in cube of 10 nm side. Let us consider a mean molar mass between entanglements M_{layer} in the PS layer. Equations 3.41 and 3.42 give:

$$\frac{1}{M_{layer}} = \frac{1}{M_e} + \frac{d_s}{\rho e N_A} \tag{3.43}$$

If we suppose that the rubbery elasticity theory applies (Equation 3.40), it is possible to define the ratio r between the rubbery modulus of the PS layer G_{layer} and the bulk one G_{PS}:

$$r = \frac{G_{layer}}{G_{PS}} = 1 + \frac{1}{e}\frac{d_s}{d_e} \tag{3.44}$$

This ratio, which depends only on the adjustable parameter d_s, should be a linear function of reciprocal thickness 1/e. The best fit with experimental data (Figure 3.51) was obtained for a surface density of entanglements equal to d_s = 0.6 1/nm^2, which is not out of physical meaning (Figure 3.53). But, we cannot consider that this modelling is good because the variation of r with the reciprocal thickness of PS layer does not seem linear as the model predicts it.

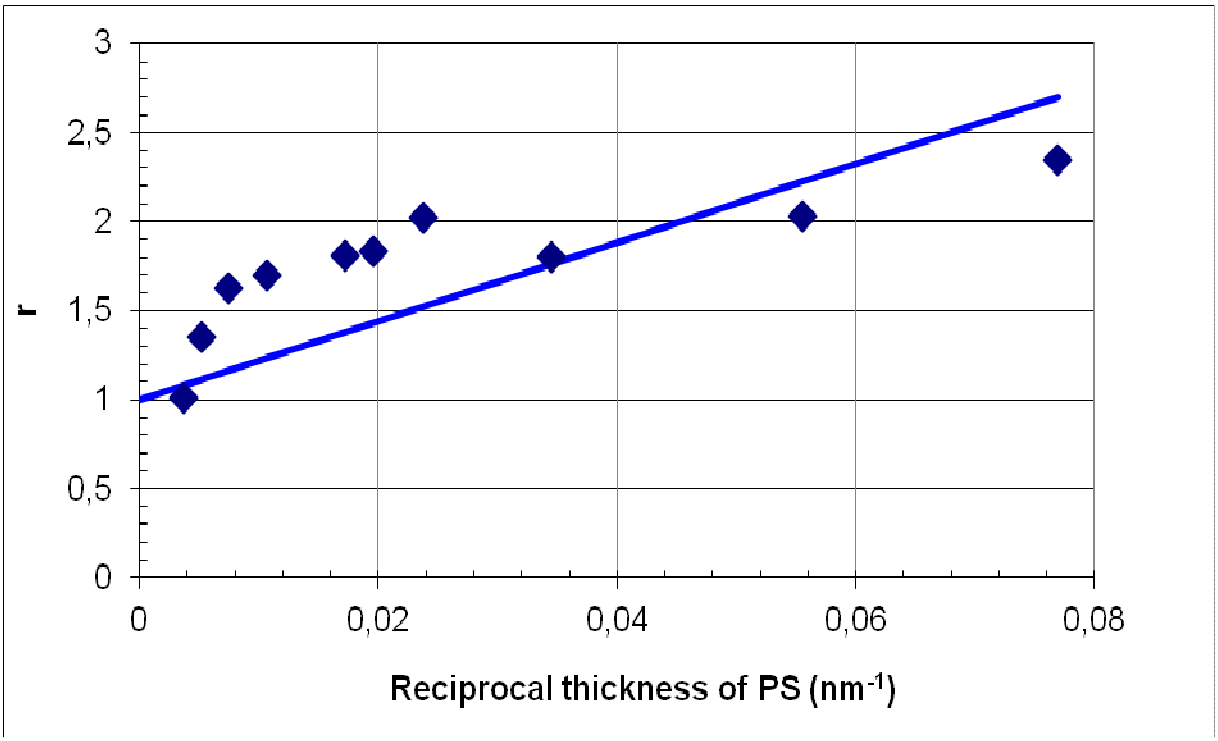

Figure 3.53. Elastic modulus increase modeled by an increase of entanglements at interface.

b) Influence of a more rigid interphase between PC and PS layers.

Let us now consider that the decrease of molecular mobility is induced by an interphase layer between PC and PS layers (Figure 3.54). This modelling can be seen as a three layers model if the thickness of this interphase is less than the half of the PS layer. If not, only an interphase should exist. In all cases, this interphase layer should have the same rigidity and the same thickness whatever the thickness of PS layer. This model has two adjustable parameters:

- the modulus of the interphase or its density of entanglements,
- the interphase thickness.

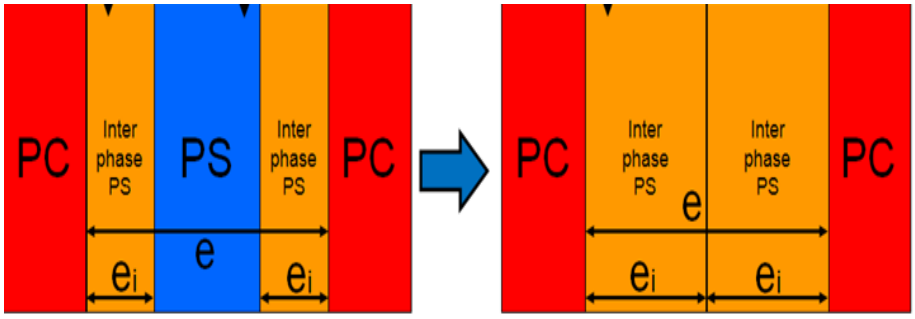

Figure 3.54. Three layers model.

Case where e > 2 e_i

If we consider the interphase and the core layer elastic with the respective shear moduli G_i and $G_{PS.}$, the equivalent modulus G of the whole PS layer is:

$$\frac{e}{G} = \frac{2e_i}{G_i} + \frac{e - 2e_i}{G_{PS}} \qquad (3.45)$$

Then the ratio of shear bulk modulus G_{PS} to the equivalent shear modulus of the whole PS layer is:

$$\frac{1}{r} = \frac{G_{PS}}{G} = 1 + \frac{2e_i}{e}\left(\frac{G_{PS}}{G_i} - 1\right) \qquad (3.46)$$

Case where e < 2 e_i

In that case, the PS layer is only constituted by the interphase and then it has the properties of the interphase.

The comparison between the 3 layers model and experimental data is done in Figure 3.55. The best fit was obtained for a interphase thickness e_i = 30 nm and a shear modulus of the interphase G_i / G_{PS} = 2.

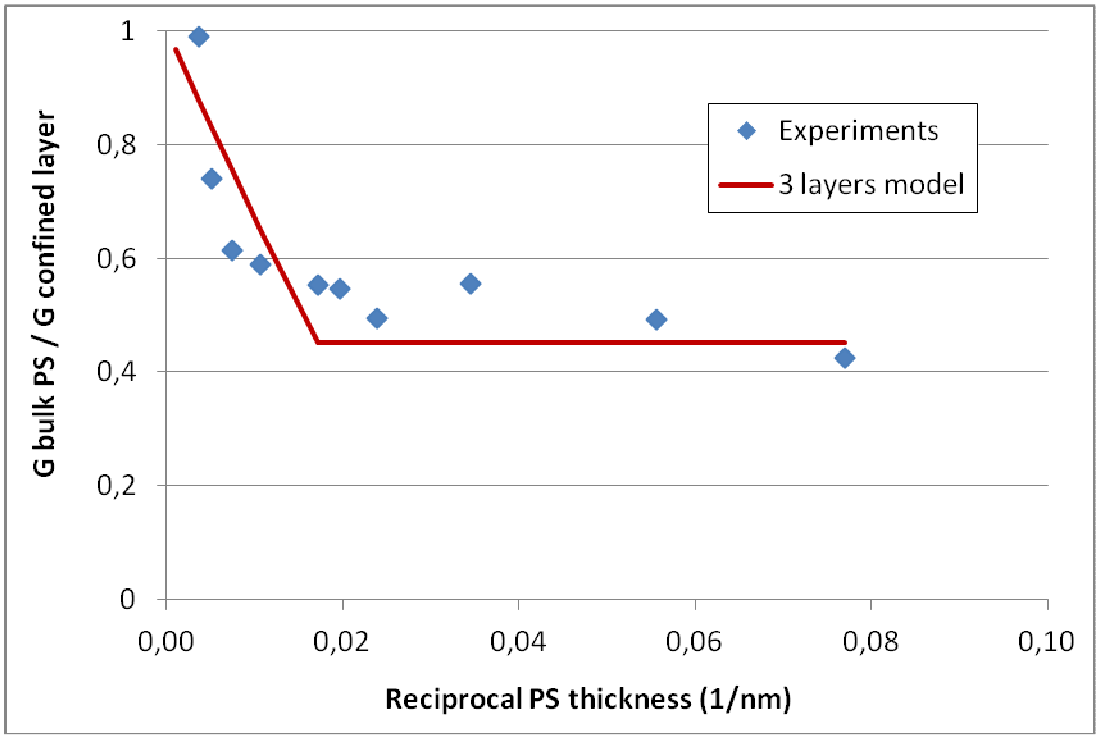

Figure 3.55. Comparison between 3 layers model and experimental data.

The modelling does not fit the data very well because it is difficult to consider that the trends are reproduced:

- the initial experimental slope is not reproduced for large thicknesses,
- the low decrease of the ratio when the thickness is decreasing is not modelled.

Moreover, the best model fit gives a thickness of interphase of about 30 nm, which seems to be very important.

c) Concluding remarks on the stiffening of PS layers

Therefore the two simple models, which have been presented, are not really able to explain the stiffening of PS layers when they go down to 200 nm.

Nevertheless, it is very surprising to see a confinement effect for PS thickness as large as 200 nm while this phenomenon is generally observed under 50 nm [134]. A phenomenon which could play an important role is molecular orientation because polymer flow in such ultrathin layer should induce very high molecular orientation. Yet we try to relax PS orientation at 140°C during a time larger than its terminal relaxation time at 140°C, which can be assessed to 3 hours on Figure 3.33. No significant effect can be observed on viscoelastic properties (Figure 3.56).

Could PC play itself a role in the stiffening of the composite film? In other words, is our hypothesis of non-variation of PC layer properties in the multi-layered film valid?

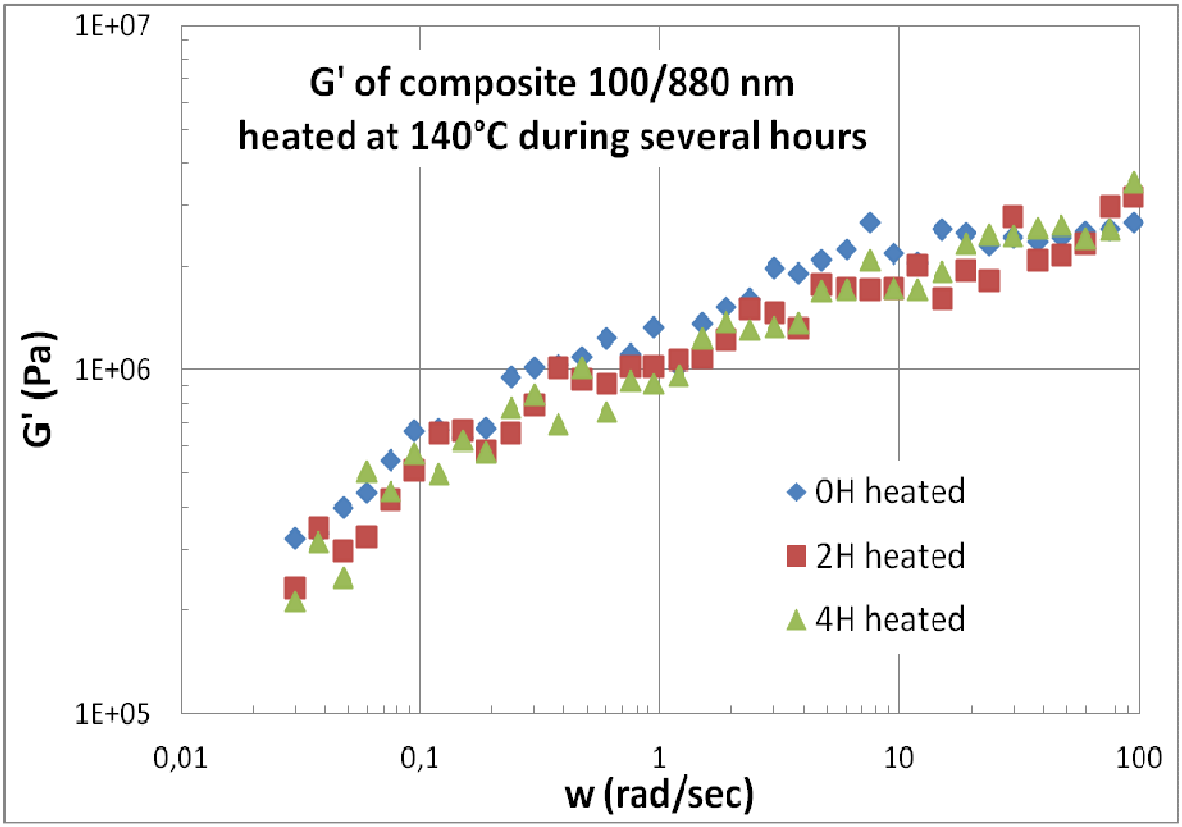

Figure 3.56. Influence of a thermal annealing on the viscoelastic properties of the multilayered films.

4. Conclusions

The aim of the thesis was to elucidate the effect of confinement of amorphous phase of a polymer above its glass transition temperature being in contact with another polymer in a rigid state. Confinement is unavoidably connected with surfaces enforcing confinement. It is very difficult to separate the effect of confinement from the effect of interfaces because both effects arise parallel and coincide. Multilayered films were chosen as the base material for the studies because they contain multifold number of confined layer and response from confinement and interfaces is multifold increased. Hoping that some of experimental techniques are more sensitive to interfaces while others to confinement we selected the following:

- microcalorimetry, that is able to sense variation in glass transition temperature,
- atomic force microscopy in tapping mode, sensitive in principle to changes in mechanical properties at a nanoscale,
- nuclear magnetic resonance in solid state, able to probe molecular dynamics of specific groups of atoms in macromolecules,
- dielectric spectroscopy for observing discrepancies from simple two-phase model
- rheology in order to measure viscosity and shear modulus of a single layer.

The behavior of 257 layered films containing PC and PS assemblies was investigated in order to resolve the properties of confined PS amorphous layers. The temperature was an important variable enabling to change the properties of PS layers from rigid-glassy to soft-rubbery state.

First, the thermal properties were studied using DSC measurements. From the analysis of those DSC results one can conclude that there is a small dependence of T_g on the thickness of PS layer. T_g of PS in multilayers depends on the thickness of PS layer and does not depend on the weight composition of the film or on the thickness of PC layers. Shifts of glass transition temperature are observed in multilayer films: for PS component towards higher temperature while PC still being glassy and for PC towards lower temperature while PS being in rubbery phase. The glass transition temperature shifts suggest rather significant interactions between PS and PC components in terms of molecular mobility. When PS layer thickness is

decreasing, the molecular mobility seems to be lowered. For PC layers, smaller variations could be also noticed (less than 1 or 2 degrees), but T_g is decreasing, which means a small increase of molecular mobility. Those results suggest a significant influence of interfaces on thermal properties of PS layers rather than confinement alone. The naïve believe for confinement effect would suggest stiffening of PS, i.e. a shift of T_g towards higher temperature, which is in fact observed. However, simultaneously a decrease of T_g of PC is observed when PS is in rubbery state which is evidently the effect of interface because PC layers are thick and are not seriously confined.

Further, AFM technique was used to measure each layer thickness. The thicknesses of each PC and PS layers determined from cross sections of coextruded films with alternating layers were in reasonably good correlation with the estimated thicknesses determined from the processing parameters. However, the spatial resolution, that was achieved, was not sufficient to resolve interfaces as separate entities.

For analysis of molecular motion the line shape of the dipolar spectra was detected in sensitivity-enhanced LG-CP measurement, employing PILGRIM pulse sequence (phase-inverted LG recoupling under MAS). Our LG CP results clearly prove that at 296 K phenyl ring orientation in PS film is static (room temperature, glassy state of PS). The splitting between singularities in 1D spectra is 12.5 kHz, typical value for rigid aromatic systems. At slightly higher temperature (348 K) the presence of two subspectra with splitting equal to 7.6 kHz and 11.8 kHz is apparent. The mobile component, undergoing fast molecular motion is dominating in PS. At the temperature 388 K the phenyl rings of PS are very mobile which is obvious because PS is above T_g. Splitting between singularities in 1D spectra is very small.

Finally we have searched for the influence of PS on dynamics of phenyl rings of PC for PC/PS film with ratio 70/30 in the temperature range from 296 K to 393 K . It is clear from our study that at 296 K the splitting for this film is slightly larger (7.7 kHz) compared to PC. At 373 K the splitting is 6.1 kHz while at 393 K splitting is 5.2 kHz. The latter value is smaller than in the case of pure PC film. It means that above the glass transition temperature of PS the PC component became more flexible. It is at the first glance the effect of the interface because there is no significant confinement of thick PC layers.

Also dielectrical properties of multilayered films were examined. Dielectric relaxation spectroscopy measurements in our study clearly provide evidence for deviations from a simple 2-phase structure in multilayered films PC/PS that is worth to be analyzed more in the future.

The dielectric response of the multilayer samples was also modeled. Results from modelling were compared with experimental results. We obtained discrepancies between the simulated spectra and the measured spectra for multilayer films, again it is very interesting and worth further investigation. Nevertheless, no conclusion about decisive role of confinement of interface can be drawn.

The density measurements of multilayered films was quite precise but not sufficient to elucidate the packing differences in confined layers because of uncertainty in film composition. The density measurements have served only for estimation of volume mass of each layer fraction. Knowing the exact composition and viscoelastic behaviour of each component the theoretical viscoelastic behavior of composites has been predicted numerically. Then, rheological tests have been made, and confronted with numerical predictions, to detect the confinement effect. It appeared that the mechanical properties of PS are not the same for bulk and for confined layers: a stiffening of PS layers emerges as a discrepancy between prediction of viscoelastic modelling of multilayered films and measured shear modulus when PS layer thickness decreases. The upper limit of thickness of confinement beyond which PS in confined layers at rubbery state becomes stiffer than in bulk is about 150/200 nm. We can note that T_g of PS layers also begins to increase beyond this upper limit of thickness. It appeared that the shear modulus of the thinnest PS layers (10 nm) is nearly 2.5 times larger than that for bulk PS sample. Two attempts of simple physical modelling have been made considering:

- firstly, a decrease of PS mobility at interface modelled by an additional increase of surfacic density of entanglements at interface, which would induce a stiffening of PS layer according to the theory of rubber elasticity
- secondly a three layers model inside the PS layer, the middle one with the properties of bulk PS and two interphases layers having a constant thickness and a higher stiffness.

The modelling does not fit the data very well. For the first model, the variation of shear modulus should vary linearly with the reciprocal PS layer thickness that does not seem to be true for experimental data. For the second model, the best fit with experimental data gives a interphase thickness of 30nm which does not seem physically very realistic. However, it is difficult to attribute the deviations to confinement alone because:

- the initial experimental slope is not reproduced for large thicknesses when confinement effects are not expected,
- the ratio of shear moduli of confined layer to the bulk one is not increasing with a decrease of PS layer thickness as fast as predicted by modelling. The naïve expectation would be that confinement should increase the shear modulus even more.

None of the experiment could clearly deliver the information about the effect of confinement or interface on the behavior of PS layers alone. It seems that in the DSC and NMR studies most pronounced effect in properties change sensed by those techniques is by interface and not by confinement. In spite of that the rheological study clearly shows a stiffening of PS layer which begins surprisingly below a high value of about 200 nm, while confinement effects are rather waited for values of 50 nm.

The results obtained here point out that separation of the effects of confinement and interfaces is difficult. However, studying PS nanolayers confined by other than PC polymers can shed more light on those problems and lead to establishing the scale of infringement of layer properties by confinement. The other components of multi-layered films envisioned for further studies should include polymers that are rigid when PS is in the rubbery state and characterized by various surface tension and hydrophobicity. Those experiments would enable to understand better the confined amorphous phase, especially that embedded between lamellar crystals in crystalline polymers.

Summary:

Unique qualities of the new polymer materials and constant improvement of parameters of the already existing products cause an increased use of these materials. The possibility of using a material for a given application is derivative of its properties. Wide range of polymer properties results from a great variety of chemical structure and supermolecular structure complexity that are determined by the structure at a nanoscale. In the case of polymeric materials subjected to mechanical load, regardless of the type of deformation to which the material will be subjected, has to exhibit properties which will fulfill the desired requirements. Apart from the basic parameters, important while choosing a given material (mechanical properties), each material should meet a series of other requirements ascribed to a given application. Semicrystalline polymers are the class of materials with complicated multilayered lamellar structure at nanoscale. Despite extensive research the prediction of the macroscopic mechanical properties of nanostructured polymers is still a bottle neck.

The objective of the research performed in this thesis is to investigate the mechanical properties of confined layers of a polymer. As technological trends tend to master systems of nanometer size, it becomes imperative to gain a more complete understanding of how the properties of such nano-sized materials might differ from those of bulk systems.

To understand the behavior of nanostructured materials, our idea was to determine the properties of a nanostructured model material: a multilayer film in which one material could be confined in a large number of nanolayers, moreover interfaces and interphases should play a major role in these films. In this study 257 layered films, made by coextrusion process consisting of PC and PS were used.

First, AFM technique was used to measure the thickness of each layer. The thicknesses of each PC and PS layers determined from cross sections of coextruded films with alternating layers were in a reasonably good correlation with the estimated thicknesses determined from the processing parameters. However, the spatial resolution, that was achieved, was not sufficient to resolve interfaces as separate entities.

Further, the thermal properties were studied using DSC measurements. From the analysis of those DSC results one can conclude that there is a small dependence of T_g on the thickness of PS layer. T_g of PS in multilayers depends on the thickness of PS layer and does not depend on the weight composition of the film or on the thickness of PC layers. Shifts of glass transition temperature are observed in multilayer films: for PS component towards higher temperature while PC still being glassy and for PC towards lower temperature while PS being in rubbery phase. The glass transition temperature shifts suggest rather significant interactions between PS and PC components in terms of molecular mobility. When PS layer thickness is decreasing, the molecular mobility seems to be lowered. For PC layers, smaller variations could be also noticed (less than 1 or 2 degrees), but T_g is decreasing, which means a small increase of molecular mobility. Those results suggest a significant influence of interfaces on thermal properties of PS layers rather than confinement alone. The naive believe for confinement effect would suggest stiffening of PS, i.e. a shift of T_g towards higher temperature, which is in fact observed. However, simultaneously a decrease of T_g of PC is observed when PS is in rubbery state which is evidently the effect of interface because in most samples PC layers are thick and are not seriously confined.

For analysis of molecular motion the line shape of the dipolar spectra was detected in sensitivity-enhanced LG-CP measurement, employing PILGRIM pulse sequence (phase-inverted LG recoupling under MAS). Our LG CP results clearly prove that at 296 K phenyl ring orientation in PS film is static (room temperature, glassy state of PS). The splitting between singularities is 12.5 kHz, typical value for rigid aromatic systems. At slightly higher temperature (348 K) the presence of two subspectra with splitting equal to 7.6 kHz and 11.8 kHz is apparent. The mobile component, undergoing fast molecular motion is dominating in PS. At the temperature 388 K the phenyl rings of PS are very mobile which is obvious because PS is above T_g. Splitting between singularities in 1D spectra is very small.

Finally we have searched for the influence of PS on dynamics of phenyl rings of PC for PC/PS film with ratio 70/30 in the temperature range from 296 K to 393 K . It is clear from our study that at 296 K the splitting for this film is slightly larger (7.7 kHz) compared to PC. At 373 K the splitting is 6.1 kHz while at 393 K splitting is 5.2 kHz. The latter value is smaller than in the case of pure PC film. It means that above the

glass transition temperature of PS the PC component became more flexible. It is at the first glance the effect of the interface because there is no significant confinement of thick PC layers.

Also dielectrical properties of multilayered films were examined. Dielectric relaxation spectroscopy measurements in our study clearly provide evidence for deviations from a simple 2-phase structure in multilayered films PC/PS that is worth to be analyzed more in the future.

The dielectric response of the multilayer samples was also modeled. Results from modelling were compared with experimental results. We obtained discrepancies between the simulated spectra and the measured spectra for multilayer films, what is very interesting and worth further investigation. Nevertheless, no conclusion about decisive role either confinement or the interface can be drawn.

The density measurements of multilayered films was quite precise but not sufficient to elucidate the packing differences in confined layers because of uncertainty in film composition. The density measurements have served only for estimation of volume mass of each layer fraction.

Knowing the exact composition and viscoelastic behavior of each component the theoretical viscoelastic behavior of composites has been predicted numerically. Then, rheological tests have been made, and confronted with numerical predictions, to detect the confinement effect. It appeared that the mechanical properties of PS are not the same for bulk and for confined layers: a stiffening of PS layers emerges as a discrepancy between prediction of viscoelastic modelling of multilayered films and measured shear modulus when PS layer thickness decreases. The upper limit of thickness of confinement beyond which PS in confined layers at rubbery state becomes stiffer than in bulk is about 150/200 nm. We can note that T_g of PS layers also begins to increase beyond this upper limit of thickness. It appeared that the shear modulus of the thinnest PS layers (10 nm) is nearly 2.5 times larger than that for bulk PS sample. Two attempts of simple physical modelling have been made considering:

- firstly, a decrease of PS mobility at interface modelled by an additional increase of surface density of entanglements at interface, which would induce a stiffening of PS layer according to the theory of rubber elasticity

- secondly, a three layers model inside the PS layer, the middle one with the properties of bulk PS and two interphases layers having a constant thickness and a higher stiffness.

The modelling does not fit the data very well. For the first model, the variation of shear modulus should vary linearly with the reciprocal PS layer thickness that does not seem to be true for experimental data. For the second model, the best fit with experimental data gives a interphase thickness of 30nm which does not seem physically very realistic for PS and PC system.

None of the experiment could delivered the information about the effect of confinement or interface on the behaviour of PS layers alone. It seems that in the DSC and NMR studies most pronounced effect in properties change sensed by those techniques is by interface and not by confinement. In spite of that the rheological study clearly shows a stiffening of PS layer which begins surprisingly below a high value of about 200 nm, while confinement effects are rather waited for values of 50 nm.

Nevertheless, the results obtained here are very interesting and point out that studying PS nanolayers confined by other than PC polymers can lead to establishing the scale of infringement of layer properties by confinement.

References:

[1] M. Ma, K. Vijayan , A. Hiltner, E. Baer, Journal of Materials Science, 1990, 25, 2039.

[2] C. D. Mueller, S. Nazarenko, T. Ebeling, T. Schuman, A. Hiltner, E. Baer, Polym. Eng. Sci. 1997, 37, 355.

[3] A. Pandey, A.Toda, S. Rastogi, Macromolecules, 2011, 44, 8042.

[4] G. Strobl, The physics of polymers. Concepts for understanding their structures and Behavior, New York: Springer, 1997.

[5] P.J. Flory, Principles of polymer chemistry, New York: Cornell University Press, 1953.

[6] Z. Bartczak , M. Kozanecki, Polymer , 2005, 46, 8210.

[7] D.C. Basset, A. M. Hodge, Proc R Soc London A, 1981, 377, 25.

[8] I.G. Voigt-Martin, L.J. Mandelkern, Polym. Sci., Polym. Phys. Ed., 1981, 19, 1769. G.M.Stack, L.J. Mandelkern, I.G.,Voigt-Martin, Macromolecules, 1984, 17, 321.

[9] B. Wunderlich, Prog Polym Sci, 2003, 28, 383.

[10] J. Schelten, A. Zinken, D. G. H. Ballard, Colloid Polym. Sci., 1981, 259, 260.

[11] F. C. Frank, Faraday Discuss. Chem. Soc., 1979, 68, 7.

[12] J. D. Hoffman, Polymer, 1983, 24, 3.

[13] L. H. Sperling, Polym. Eng. Sci., 1984, 24, 1.

[14] H. Xu , P. Cebe, Macromolecules, 2004, 37, 2797.

[15] M. Alsleben , C. Schick, Thermochim Acta, 1994, 238, 203.

[16] J. Menczel , B. Wunderlich, J Polym Sci Polym Phys Ed.,1980, 18, 1433.

[17] J. Menczel , B. Wunderlich, J Polym Sci Polym Lett Ed., 1981, 19, 261.

[18] W. Meesiri , J.Menczel, U. Gaur , B. Wunderlich, J Polym Sci Polym Phys Ed., 1982, 20, 719.

[19] J. Menczel , J Therm Anal Calorim, 2011, 106, 7.

[20] Q. Ma , G. Georgiev, P. Cebe, Polymer, 2011, 52, 4562.

[21] P. Hong, W. Chuang, W. Yeh, T. Lin, Polymer, 2002, 43, 6879.

[22] M.C. Righetti, E. Tombari, M.L. Di Lorenzo, European Polymer Journal, 2008, 44, 2659.

[23] L. Chevalier, C. Linhone, G. Régnier, Rubber and Composites, 1999, 28, 393.

[24] R. Phillips, G. Herbert, J. News, M. Wolkowicz, Polym. Eng. Sci., 1994, 34, 1731.

[25] S. Ahzi, B.J. Lee , R.J. Asaro, ASME, 1995, 203, 35.

[26] S. Nikolov, I. Doghri, O. Pierarda, L. Zealouka, A. Goldbergb , J. Mech. Phys. Solids, 2002, 50, 2275.

[27] B. Crist, C.J. Fisher, P.R. Howard, Macromolecules, 1989, 22, 1709.

[28] R.H. Boyd, Polymer, 1985, 26, 1123.

[29] U.M. Vakil, C.S. Wang, M.H. Dotrong, M. Dotrong, C. Lee, R. Evers, Polymer, 1993, 34, 731.

[30] J.A.W. Van Dommelen, D.M. Parks, M.C. Boyce, W.A.M. Brekelmans, F.P.T. Baaijens, J.Mech. Phys. Solids, 2003, 51, 519.

[31] F. Bedoui, J. Diani, G. Régnier, Polymer, 2004, 45, 2433.

[32] S. Nikolov, I. Doghri, Polymer, 2000, 41, 1883.

[33] L. Mandelkern, R.G. Alamo, M.A. Kennedy, Macromolecules, 1990, 23, 4271.

[34] R. Seguela, F. Rietsch, J. Mater.Sci. Lett., 1990, 9, 46.

[35] R. Adhikari, M. Buschnakowski,S. Henning, S. Goerlitz,T.A. Huy, W. Lebek, R.Godehardt, G.H. Michler, R. Lach, K. Geiger, K. Knoll, Macromol Rapid Commun, 2004, 25, 653.

[36] Z.M. Li, C.G. Huang, W. Yang, Mater. Eng., 2004, 289, 1004.

[37] A. Manzur, J. I. Rivas, J Appl Polym Sci, 2007, 104, 3103.

[38] N.W. Brooks, R.A. Duckett, I.M. Ward, Polymer, 1992, 33, 9, 1872.

[39] G. Shan, W. Yang, M. Yang_, B. Xie, Z. Li, J. Feng, Polymer Testing, 2006, 25, 452.

[40] A. Drozdov, R. Gupta, International Journal of Engineering Science, 2003, 41.

[41] J.A.W. Van Dommelen, D.M. Parks, M.C. Boyce, W.A.M. Brekelmans, F.P.T. Baaijens, Polymer, 2003, 44, 6089.

[42] B.J. Lee, D.M. Parks, S. Ahzi, J Mech Phys Solids, 1993, 41, 1651.

[43] B.J. Lee, A.S. Argon, D.M. Parks, S. Ahzi, Z. Bartczak, Polymer, 1993, 34, 3555.

[44] J. Pinto, S. Castagnet, C. Nadot-Martin, F. Touchard, D. Mellier, Procedia Engineering, 2011, 10, 3140.

[45] R. F. Boyer, Encyclopedia of Polymer Science and Technology, New York, 1977, 2, 745.

[46] L. Xie, G.B. DeMaggio, D.W. Frieze, J. Devries, D.W. Gidley, H.A. Hristov, A.F. Yee, Phys. Rev. Lett., 1995, 74, 4947.

[47] Y.C. Jean, R. Zhang, H. Cao, J. Yuan, C. Huang, P Phys. Rev. B, 1997, 56, R8459.

[48] M. Efremov, E.A. Olson, M. Zhange, Z. Zhang, L.H. Allen, Phys. Rev. Lett., 2003, 91, 085703.

[49] M. Alcoutlabi, G.B. McKenna, J. Phys.: Condens. Matter, 2005, 17, R461.

[50] J.A. Forrest, K. Dalnoki-Veress, J.R. Stevens, J.R. Dutcher, Phys. Rev. Lett., 1996, 77 2002.

[51] J.A. Forrest, K. Dalnoki-Veress, J.R. Dutcher, Phys. Rev. E, 1997, 56, 5705.

[52] K. Dalnoki-Veress, J.A. Forrest, C. Murray, C. Gigault, J.R. Dutcher, Phys. Rev. E, 2001, 63, 031801.

[53] J. Mattsson, J.A. Forrest, L. Borjesson, Phys.Rev.E, 2000, 62, 5187.

[54] J.A. Forrest, K. Dalnoki-Veress, J.R. Dutcher, Phys.Rev.E, 1997, 56, 5705.

[55] K. Fukao, Y. Miyamoto, Europhys.Lett., 1999, 46, 649.

[56] H. Reichert, Oral presentation At third International Workshop on Dynamics In Confinement, Grenoble, FR, March, 2006.

[57] C.L. Jackson, G.B. McKenna, J. Non-Cryst. Solids, 1991, 131, 221–224; C.L. Jackson, G.B. McKenna, Chem. Mater., 1996, 8, 2128.

[58] J. Zhang, G. Liu, J. Jonas, J. Phys. Chem., 1992, 96, 3478.

[59] J.L. Keddie, R.A.L. Jones, R.A. Cory, Europhys. Lett., 1994, 27, 59.

[60] A. Serghei, Oral presentation at Third International Workshop on Dynamics in Confinement, Grenoble, FR, March, 2006

[61] G. Beaucage, R. Composto, R.S. Stein, J. Polym. Sci.,Polym. Phys. Ed., 1993, 31, 319.

[62] W.E. Wallace, J.H. Van Zanten, W.L. Wu, Phys. Rev. E., 1995, 52, R3329.

[63] Y.K. See, J.Cha, T. Chang, M.Ree, Langmuir, 2000, 16, 235.

[64] O. Prucker, S. Christian, H. Bock, J. Ruhe, C.W. Frank, W. Knoll, Macromol. Chem. Phys., 1998, 199, 1435.

[65] S. Ge, Y. Pu, W. Zhang, M. Rafailovitch, J. Sokolov, C.Buenviaje, R. Buckmaster, R.M. Overney, Phys. Rev. Lett., 2000, 85, 230.

[66] Y. Grohens, L. Hamon, G. Reiter, A. Soldera, Y. Holl, Eur.Phys.J.E, 2002, 8, 217.

[67] J.L. Keddie, R.A.L. Jones, R.A. Cory, Faraday Discuss., 1994, 98, 219.

[68] T.S. Jain, J.J. de Pablo, Macromolecules, 2002, 35, 2167.

[69] R.S. Tate, D.S. Fryer, S. Pasqualini, M.F. Montague, J.J. de Pablo, P.F. Nealey, J. Chem. Phys., 2001, 115, 9982.

[70] J.Q. Pham, P.F. Green, J. Chem. Phys., 2002, 116, 5801.

[71] D. Long, F. Lequeux, Eur. Phys. J. E, 2001, 4, 371.

[72] W.J. Orts, J.H. Van Zanten, W.L. Wu, S.K. Satija, Phys. Rev. Lett., 1993, 71, 867.

[73] G.B. DeMaggio, W.E. Frieze, D.W. Gidley, M. Zhu, H.A. Hristov, A.F. Yee, Phys. Rev. Lett., 1997, 78, 1524.

[74] J.A. Forrest, A.C. Rowai, K. Dalnoki-Veress, J.R. Stevens, J.R. Dutcher, J. Polym. Sci. B, 1996, 44, 3009.

[75] G. Reiter, Eur. Phys. J. E, 2002, 8, 251.

[76] P. O'Connell, G.B. McKenna, Science, 2005, 307, 1760.

[77] S.M. Aharoni, Polym. Adv. Tech., 1998, 9, 169.

[78] E. Laredo, M. Grimau, A. Muller, A. Bello, N. Suarez, J. Polym. Sci. B, 1998, 34, 2863.

[79] J. Dobbertin, A. Hensel, C. Schick, J. Therm. Anal., 1996, 47, 1027.

[80] S.Z.D. Cheng, Z.Q. Wu, B. Wunderlich, Macromolecules, 1987, 20, 2802.

[81] R. Y. F. Liu, Y. Jin, A. Hiltner, E. Baer, Macromol. Rapid Commun. 2003, 24, 943.

[82] J. Dubochet, M. Adrian, C.M. Teixeria Alba, R.K. Kadiyala, D.R. MacFarlane, C.A. Angell, J. Phys. Chem., 1984, 88, 6727.

[83] C.A. Angell, R.K. Kadiyala, D.R. MacFarlane, J. Phys.Chem., 1984, 88, 4593.

[84] D.R. MacFarlane, C.A. Angell, J. Phys. Chem., 1982, 86, 1927.

[85] F. Varnik, J. Baschnagel, K. Binder, Phys. Rev. E, 2002, 65, 021507.

[86] C. Mischler, J. Baschnagel, K. Binder, Adv. Colloid Interface Sci., 2001, 94, 197.

[87] P. Scheidler, W. Kob, K. Binder, Europhys. Lett., 2000, 52, 277.

[88] S.Wu, Polym. Eng.Sci., 1992, 32, 823.

[89] S. Wu, J.Polym.Sci., B Polym. Phys., 1989, 27, 723.

[90] P. E. Rouse, J. Chem. Phys., 1953, 21, 1272.

[91] F. Bueche, J. Chem. Phys., 1954, 22, 1570.

[92] W. L. Peticolas, Rubber Chem. Tech., 1963, 36, 1422.

[93] B. H. Zimm, J. Chem. Phys., 1956, 24, 269.

[94] P. G. de Gennes, J. Chem. Phys., 1971, 55, 572.

[95] M. Tirrell, Rubber Chem. Tech., 1984, 57, 523.

[96] M. Doi, S. F. Edwards, J. Chem. Soc. Faraday Trans., 1978, 2**,** 74**.**

[97] W.W.Graessley, Adv. Polym. Sci, 1982, 47, 67.

[98] M.Doi “Structure and Properties of Polymers”, R.W.Cahn, P.Haasen, E.J.Kramer (Eds.),“Materials Science and Technology”, VCH, Weinheim – New York – Basel – Cambridge - Tokyo 1993, 12, 9.

[99] P.G. de Gennes, “Scaling Concepts in Polymer Physics”, Cornell University Press, Ithaca and London 1979

[100] C.P. Slichter, Principles of Magnetic Resonance, Springer, Berlin, 1990.

[101] J. Schaefer, E.O. Stejskal, R.A. Mckay, W.T. Dixon, J. Magn. Reson., 1984, 57, 85.

[102] M. Hong, X.L. Yao, K. Jakes, D. Huster, J. Phys. Chem. B, 2002, 106, 7355.

[103] K. Schmidt-Rohr, H.W. Spiess, Multidimensional Solid-State NMR and Polymers, Academic Press, London, 1994.

[104] K. Schmidt-Rohr, J. Clauss, H.W. Spiess, Macromolecules, 1992, *25*, 3273.

[105] M. Hong, X. Yao, K. Jakes, D. Huster,J. Phys. Chem. B, 2002, 106, 7355.

[106] K. Zemke, K. Schmidt-Rohr, H.W. Spiess, Acta Polym., 1994, 45, 148.

[107] Z. Luz, H.W. Spiess, J.J. Titman, Isr. J. Chem., 1992, 32, 145.

[108] Z. Olender, D. Reichert, A. Muller, H. Zimmermann, R. Poupko, Z. Luz, J. Magn. Reson. A, 1996, 120, 31.

[109] A.A. Jones, J.F. O'Gara, P.T. Inglefield, J.T. Bendler, A.F. Yee, K. L. Ngai, Macromolecules, 1983, 16, 4, 658.

[110] J. Brus, J. Dybal, P. Schmidt, J. Kratochvıl, J. Baldrian, Macromolecules, 2000, 33,

6448.

[111] V. Lupasücu, S. J. Picken, M. Wubbenhorst, Macromolecules, 2006, 39, 5152.

[112] K. Fukao, S.Uno, Y. Miyamoto, A.Hoshino, H. Miyaji, Phys.Rev. E, 2001, 64, 051807.

[113] L. Hatmann, W. Gorbatschow, J.Hauwede, F. Kremer, Eur. Phys. J. E, 2002, 8, 145.

[114] M. Wubbenhorst, C.A. Murray, J.R. Dutcher, Eur. Phys. J. E, 2003, 12, S109.

[115] J. Jenczyk, M. Makrocka-Rydzyk, A. Wypych, S. Głowinkowski, S. Jurga, M. Radosz, Journal of Non-Crystalline Solids, 2010, 356, 582.

[116] V. Lupascu, H. Huth, Ch. Schick , M. Wubbenhorst, Thermochimica Acta, 2005, 432, 222.

[117] A. Galeski, e-Polymers, 2002, 026.

[118] R.F. Boyer, Midland Macromolecular Institute Symposium on “Molecular Basis of Transitions and Relaxations”, Midland, Michigan, Feb. 1975.

[119] C. Mueller, J. Kerns, T. Ebeling, S. Nazarenko, A. Hiltner, E. Baer, Polymer Process Engineering, Bradford, UK, July 1997, 137.

[120] W. Michaeli, Extrusion Dies for Plastics and Rubber : Design and Engineering Computations, Hanser Publishers, New York , 1992.

[121] W. J. Shrenk, D. S. Chisholm, K. J. Cleereman and T. Alfrey Jr, US Pat., 1971, 3576707.

[122] J. A. Radford, T. Alfrey Jr, W. J. Shrenk, Polym. Enging. Sci., 1973, 13, 216.

[123] T. Alfrey Jr, W. J. Shrenk, US Pat., 1973, 3711, 176.

[124] W. J. Shrenk, T. Alfrey Jr, Polym. Enging. Sci., 1969, 9, 393.

[125] M. Ma, K. Vijayan, A. Hiltner, E. Baer, Journal of Materials Science, 1990, 25, 2039.

[126] H. Wang, J. K. Keum, A. Hiltner, E. Baer, B. Freeman, A. Rozanski, A. Galeski, Science, 2009, 323, 757.

[127] M. Hong, X. Yao, K. Jakes, D. Huster, J Phys Chem B 2002, 106, 7355.

[128] J. Schaeffer, M.D. Sefcik, E.O. Stejskal, E.A. McKay, W.T. Dixon, R.E. Cais, Macromolecules, 1984, 17, 1107.

[129] A.A. Jones, Macromolecules, 1983, 16, 4.

[130] V. Lupaşcu, S.J. Picken, M. Wübbenhorst, Macromolecules, 2006,39, 5152.

[131] J. Weese, Computer Physics Communications, 1993, 77, 429.

[132] K. Osaki, T. Inoue, T. Uematsu, Y. Yamashita, Journal of Polymer Science: Part B: Polymer Physics, 2001, 39, 1704.

[133] L.J. Fetters, D.J. Lohse, R.H. Colby, Physical Properties of Polymers Handbook; J.E. Mark Ed., American Institute of Physics: Woodbury, NY, 1996.

[134] J.A. Forrest, K. Dalnoki-Veress, J.R. Dutcher, Phys. Rev. E ,1997, 56, 5705.

Role and properties of the confined amorphous phase of polymers

ABSTRACT: The aim of the thesis was to elucidate the effect of confinement of amorphous phase of a polymer above its glass transition temperature being in contact with another polymer in a rigid state. Confinement is unavoidably connected with surfaces enforcing confinement. It is very difficult to separate the effect of confinement from the effect of interfaces because both effects arise parallel and coincide. Multilayered films were chosen as the base material for the studies because they contain multifold number of confined layer and response from confinement and interfaces is multifold increased. Hoping that some of experimental techniques are more sensitive to interfaces while others to confinement we selected the following: microcalorimetry, SSNMR, direlectrical spectroscopy and dynamic shear rheology. We have searched for the influence of PS on dynamics of phenyl rings of PC for PC/PS film with ratio 70/30 in the temperature range from 296 K to 393 K employing PILGRIM pulse sequence. .We show that above the glass transition temperature of PS, the PC component became more flexible. It is at the first glance the effect of the interface because there is no significant confinement of thicker PC layers. Dielectric relaxation spectroscopy measurements in our study clearly provide evidence for deviations from a simple 2-phase structure in multilayered films PC/PS that is worth to be analyzed more in the future. The dielectric response of the multilayer samples was also modeled and compared with experimental results. We obtained again discrepancies between the simulated spectra and the measured spectra for multilayer films. Knowing the exact composition and viscoelastic behaviour of each component, the theoretical viscoelastic behavior of composites has been predicted numerically. Then, rheological tests have been made, and confronted with numerical predictions, to detect the confinement effect. The upper limit of thickness beyond which PS in confined layers at rubbery state becomes stiffer than in bulk is about 150/200 nm. It appeared that the shear modulus of the thinnest PS layers (10 nm) is nearly 2.5 times larger than that for bulk PS sample. We can note that T_g of PS layers also begins to increase beyond this upper limit of thickness.. None of the experiment could clearly deliver the information about the effect of confinement or interface on the behavior of PS layers alone. The results obtained here point out that separation of the effects of confinement and interfaces remains very difficult.

Keywords : confined amorphous phase, glass transition, dynamics at the interface, viscoelasticity, multilayered films

Rôle et propriétés de la phase amorphe confinée des polymères

RESUME : Le but de la thèse était de comprendre l'effet du confinement en épaisseur nanométrique sur les propriétés d'un polymère amorphe au-dessus de sa transition vitreuse. Le confinement est inévitablement lié aux effets de surface générant le confinement et on imagine immédiatement la difficulté qu'il y a à séparer les effets de confinement et d'interfaces. Des films multi-nanocouches alternées de PS et PC obtenus par un procédé spécifique d'extrusion ont été choisis pour l'étude car l'effet du confinement comme celui des interfaces sont multipliés et plus facilement détectable. En espérant que des techniques expérimentales soient plus sensibles à l'un des effets, nous avons plus particulièrement sélectionné la calorimétrie, la RMN, la spectroscopie diélectrique et la rhéologie dynamique en cisaillement. En RMN du solide, nous avons pu montrer que la mobilité des cycles phénoliques du PC augmente dans des films PC/PS en proportions respectives 70/30 pour des températures supérieures à la température de transition vitreuse du PS. Cet effet peut être plutôt attribué à l'interface sachant que l'épaisseur des couches de PC est plus importante. Les essais de relaxation diélectrique montre clairement un écart entre les réponses des films multi-couches et ceux pour les structures bi-composants. Ces résultats ont été confirmés par les écarts obtenus entre la réponse diélectrique simulée des films multi-couches obtenue à partir des réponses propres du PC et PS et celle mesurée. Ces résultats sont très prometteurs, mais demandent des études supplémentaires pour une analyse en profondeur. Connaissant le comportement rhéologique dynamique en cisaillement des matériaux PS et PC, celui des films multi-couches a été prédit. Il apparait que le module élastique du PS augmente significativement lorsque l'épaisseur des couches de PS descend en dessous d'un seuil plutôt élevée : 150 à 200 nm. En dessous de ce seuil, la transition vitreuse du PS mesurée par calorimétrie augmente également sensiblement. Aucune des modélisations proposées ne permet d'expliquer avec suffisamment de fidélité les résultats expérimentaux.

Mots clés : phase amorphe confinée, transition vitreuse, effet de surface, comportement viscoléastique, films multicouches

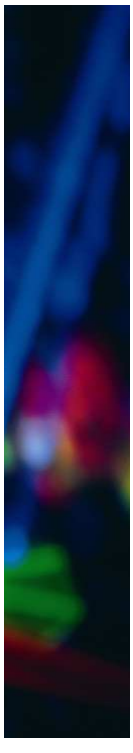

CMMS PAS, Lodz, Poland